Entangled photons in disordered media: from two-photon speckle patterns to Schmidt decomposition

Manutea Cande

UNIVERSITÉ DE GRENOBLE

THÈSE

Pour obtenir le grade de

DOCTEUR DE L'UNIVERSITÉ DE GRENOBLE

Spécialité : **Physique de la matière condensée et du rayonnement**

Arrêté ministériel : 7 août 2006

Présentée par

Manutea Candé

Thèse dirigée par **Sergey E. Skipetrov**

préparée au sein **Laboratoire de physique et modélisation des milieux condensés (CNRS/Université Joseph Fourier-Grenoble 1)**
et de **École doctorale de physique de Grenoble**

Entangled photons in disordered media:

From two-photon speckle patterns to Schmidt decomposition

Soutenance prévue le 11 décembre 2014 devant le jury composé de :

M. Rémi Carminati
Professeur à l'ESPCI (Institut Langevin), Rapporteur
M. Aurélien Drezet
Chargé de recherche au CNRS (Institut Néel), Examinateur
M. Christian Miniatura
Directeur de recheche au CNRS (Merlion Majulab, Singapour), Examinateur
M. Dominique Spehner
Maître de conférence à l'Université Joseph Fourier (Institut Fourier) , Examinateur
M. Thomas Wellens
Professeur-Assistant à Albert-Ludwigs University of Freiburg (Allemagne), Examinateur
M. Sergey E. Skipetrov
Directeur de recherche au CNRS (LPMMC), Directeur de thèse

M. Andreas Buchleitner
Professeur à Albert-Ludwigs University of Freiburg (Allemagne), Rapporteur extérieur

Contents

Introduction

This thesis deals with the transmission of high-dimensional bipartite entangled states of light through a random medium.

Random or disordered media refer to media with spatial heterogeneities, for instance, of the refractive index or of the positions of the scatterers in a cold atomic gas. Therefore, when light — or any type of wave — propagates through such complex media, multiple scattering takes place instead of ballistic propagation. Depending of the strength of disorder very interesting and quite surprising phenomena arise such as the coherent backscattering [1] or random lasing [2] when the disorder is weak, and Anderson localization [3] when the disorder is strong.

Most of the studies of the multiple scattering of light focus on classical phenomena that do not require quantization of the electromagnetic field to be understood [4, 1]. Light is even commonly categorized as a "classical wave" [1], in line with sound and elastic waves, as opposed to "quantum waves" describing electrons in disordered solids and matter waves in cold atomic systems. Meanwhile, even if states of light exist that mimic classical behavior very closely, light is probably the "most quantum" of all waves because it provides an unprecedented freedom in controlling and measuring its quantum state [5]. Indeed, the states of light that do not allow for a classical description (e.g., single and entangled photons, squeezed light, etc.) can nowadays be generated almost at will [6, 7], opening very promising perspectives for communication and information processing applications, including quantum computation [8]. Among the features of quantum states of light, quantum entanglement is probably the most important and intriguing aspect. Together with the wave-particle duality, entanglement is at the origin of the main differences between classical and quantum mechanics. One of the main challenges when dealing with quantum entanglement is its quantification, both theoretical and experimental.

Multiple scattering of non-classical light in random media attracts the attention of physicists since the pioneering paper by Beenakker [9] who introduced a convenient formalism of input-output relations in this field. In particular, propagation of pairs of entangled photons in random media has been studied both theoretically [10, 11] and experimentally [12, 13] in recent years. Experimentally, entanglement can be studied and characterized by coincidence measurements: one measures the coincidence photodetection rate $R_{\alpha\beta}$ of two photodetectors either placed behind the medium and counting photons in transmitted modes α and β [10, 14, 12, 15, 11] or embedded inside the medium at positions $\vec{r}_\alpha$ and $\vec{r}_\beta$ [16] leading to a two-photon speckle pattern. However, even if $R_{\alpha\beta}$ is sensitive to the entanglement of the incident state it is not an unambiguous measure of entanglement of scattered light. It is the purpose of this thesis, to study the impact of the quantum entanglement on $R_{\alpha\beta}$ and to present a way of quantifying the amount of entanglement present in the multiple scattered light.

The first chapter of the thesis provides the basic toolbox of quantum optics required to understand further work. After a presentation of the quantization of light in free space and in open media, we introduce the main quantum states of light that are studied in the thesis. Then, we discuss the most important properties of quantum states, the quantum entanglement. We first give a general introduction to the entanglement of bipartite states. Then, because in many experimental schemes quantum particles are identical, the still debated concept of entanglement between indistinguishable particles is presented and discussed.

Because of the randomness of the medium in which the light propagates, the observables considered in this thesis have to be treated statistically. Hence, in the second chapter, we present a statistical approach to the multiple scattering of light. We first consider a microscopic description of the multiple scattering based on the so-called Green's function formalism and then turn to a macroscopic description which uses the random S-matrix formalism.

In the third chapter, we extend and clarify the previous studies dealing with two-photon speckle patterns appearing in coincidence measurements. We first introduce the main properties of the two-photon state that we consider and discuss the coherence of the two-photon light. Then, we study in details the two-photon speckle pattern obtained with a broadband two-photon state incident on a disordered medium. We discuss whether or not signatures of non-classical light can be seen in coincidence measurements. Finally, we calculate the visibility of the one- and two-photon speckle patterns and show how the entanglement present in the incident state affects these visibilities.

The last chapter aims at providing a new theoretical approach to quantifying the average amount of entanglement in the scattered state. Using the random matrix theory, we derive the Schmidt decomposition of the scattered entangled state. We show how the statistics of the disorder impacts on the density of the Schmidt eigenvalues and quantify the entanglement through several measures of entanglement like the von Neumann entropy of Schmidt eigenvalues and the Schmidt number.

Chapter 1

Light as a quantum field

1.1 Quantum optics: a toolbox

1.1.1 Quantization of the electromagnetic field

In this thesis we are dealing with phenomena which can not be described by the classical theory of electromagnetic field. It is the case, for example, when only a few photons are present. Quantum theory is also required for a proper description of two-photon interferences [17, 18] and experiments with entangled photons like in the quantum teleportation and computation protocols [19, 20, 8]. It is the purpose of quantum electrodynamics to describe this quantum behavior of light [21]. Here we briefly present the quantization of electromagnetic field in free space and then in an open medium such as a chaotic cavity or a disordered medium.

Free space

In free space, we start from the well-known Maxwell equations to derive the wave equation satisfied by the vector potential $\mathbf{A}(\mathbf{r}, t)$ in the Coulomb gauge

$$\nabla^2 \mathbf{A}(\mathbf{r}, t) = \frac{1}{c^2} \frac{\partial^2 \mathbf{A}(\mathbf{r}, t)}{\partial t^2}. \tag{1.1}$$

It follows from Eq. 1.1 that the vector potential can be expressed as a superposition of plane waves in the form [22]

$$\mathbf{A}(\mathbf{r}, t) = \frac{1}{\epsilon_0^{1/2} L^{3/2}} \sum_{\mathbf{k}s} \left[c_{\mathbf{k}s} \epsilon_{\mathbf{k}s} e^{i(\mathbf{k}\cdot\mathbf{r} - \omega t)} + c.c. \right], \tag{1.2}$$

where ϵ_0, $\mathbf{k}$, ω, $\epsilon_{\mathbf{k}s}$ and $c_{\mathbf{k}s}$ are respectively the dielectric permitivity of the vacuum, the wave vector, the frequency, the vector of polarization and the complex amplitude of the plane wave. s is related to the two states of polarization of light. L does not have physical relevance because it is the size of the virtual cube used to introduce the Fourier series (1.2) and will tend to infinity at the end of derivation. In the following we will call a mode of the electromagnetic field the combination $\{\mathbf{k}, s\}$.

At this point, it is convenient to write the potential vector in terms of the so-called canonical variables $p_{\mathbf{k}s}(t)$ and $q_{\mathbf{k}s}(t)$

$$\begin{aligned} q_{\mathbf{k}s}(t) &= u_{\mathbf{k}s}(t) + u^*_{\mathbf{k}s}(t), \\ p_{\mathbf{k}s}(t) &= -i\omega\left(u_{\mathbf{k}s}(t) - u^*_{\mathbf{k}s}(t)\right), \end{aligned} \tag{1.3}$$

with $u_{\mathbf{k}s}(t) = c_{\mathbf{k}s}\mathrm{e}^{-\mathrm{i}\omega t}$. We have

$$\mathbf{A}(\mathbf{r},t) = \frac{1}{2\epsilon_0^{1/2}L^{3/2}}\sum_{\mathbf{k}s}\left[\left(q_{\mathbf{k}s}(t) + \frac{i}{\omega}p_{\mathbf{k}s}(t)\right)\epsilon_{\mathbf{k}s}e^{i\mathbf{k}\cdot\mathbf{r}} + c.c.\right]. \tag{1.4}$$

The quantization procedure is based on the correspondence principle between classical and quantum theory. A Hilbert space operator is associated to each canonical variable: $q_{\mathbf{k}s} \to \hat{q_{\mathbf{k}s}}$, $p_{\mathbf{k}s} \to \hat{p_{\mathbf{k}s}}$. Besides, in the case of light the analogy between the electromagnetic field and a group of quantum harmonic oscillators leads naturally to a "second" quantization framework. Instead of using the previous canonical variables we introduce the non Hermitian operator $\hat{a}_{\mathbf{k}s}(t)$ and its Hermitian conjugate $\hat{a}^\dagger_{\mathbf{k}s}(t)$ defined by

$$\hat{a}_{\mathbf{k}s}(t) = \frac{1}{(2\hbar\omega)^{1/2}}\left(\omega\hat{q}_{\mathbf{k}s}(t) + i\hat{p}_{\mathbf{k}s}(t)\right). \tag{1.5}$$

$\hat{a}_{\mathbf{k}s}(t)$ and $\hat{a}^\dagger_{\mathbf{k}s}(t)$ follow the bosonic commutation rules

$$\left[\hat{a}_{\mathbf{k}s}(t), \hat{a}^\dagger_{\mathbf{k}'s'}(t)\right] = \delta^3_{\mathbf{k}\mathbf{k}'}\delta_{ss'}, \tag{1.6}$$

$$\left[\hat{a}_{\mathbf{k}s}(t), \hat{a}_{\mathbf{k}'s'}(t)\right] = 0, \tag{1.7}$$

$$\left[\hat{a}^\dagger_{\mathbf{k}s}(t), \hat{a}^\dagger_{\mathbf{k}'s'}(t)\right] = 0. \tag{1.8}$$

Applying this quantization procedure to the vector potential and using the relation $\mathbf{E}(\mathbf{r},t) = -\frac{\partial\mathbf{A}(\mathbf{r},t)}{\partial t}$, we obtain the operator associated with the electric field

$$\hat{\mathbf{E}}(\mathbf{r},t) = \hat{\mathbf{E}}^{(+)}(\mathbf{r},t) + \hat{\mathbf{E}}^{(-)}(\mathbf{r},t), \tag{1.9}$$

where

$$\hat{\mathbf{E}}^{(+)}(\mathbf{r},t) = \frac{1}{L^{3/2}}\sum_{\mathbf{k}s}\left(\frac{\hbar\omega}{2\varepsilon_0}\right)^{\frac{1}{2}} i\hat{a}_{\mathbf{k}s}\epsilon_{\mathbf{k}s}e^{i(\mathbf{k}\cdot\mathbf{r}-\omega t)}, \tag{1.10}$$

with $\hat{a}_{\mathbf{k}s} = \hat{a}_{\mathbf{k}s}(0)$ ($\hat{a}^\dagger_{\mathbf{k}s} = \hat{a}^\dagger_{\mathbf{k}s}(0)$) the annihilation (creation) operator of a photon in the mode $\{\mathbf{k}, s\}$. The operator $\hat{\mathbf{E}}^{(+)}(\mathbf{r},t)$ and its Hermitian conjugate $\hat{\mathbf{E}}^{(-)}(\mathbf{r},t)$ are respectively the positive and negative frequency parts of the electric field.

Following the same procedure for the Hamiltonian of the electromagnetic field yields

$$\hat{H} = \sum_{\mathbf{k}s}\hbar\omega\left(\hat{a}^\dagger_{\mathbf{k}s}\hat{a}_{\mathbf{k}s} + \frac{1}{2}\right), \tag{1.11}$$

where the additional term $\hbar\omega/2$ corresponds to the energy of the vacuum and has no counter-part in classical physics. The evolution $\hat{a}_{\mathbf{k}s}(t)$ is given by the Heisenberg equations of motion

$$\frac{\mathrm{d}\hat{a}_{\mathbf{k}s}(t)}{\mathrm{d}t} = -\frac{i}{\hbar}\left[\hat{a}_{\mathbf{k}s}(t), \hat{H}\right]. \tag{1.12}$$

Provided that the commutation relations (1.6) are obeyed, these equations are quantum equivalents of Maxwell equations for classical fields.

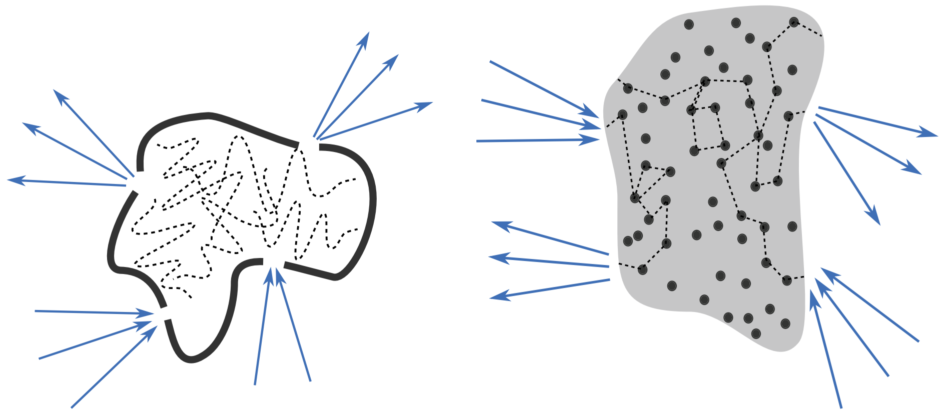

(a) (b)

Figure 1.1: Sketch of (a) an open chaotic cavity and (b) a random medium. Waves inside the cavity or the random medium are depicted by dotted lines and waves outside the cavity or the random medium by blue arrows.

Open media and input-output relations

An open media can be seen as an open optical cavity with a spatially nonuniform dielectric constant $\epsilon(\mathbf{r})$. The presence of a cavity modifies the density and the structure of the field modes inside the cavity compared to the one in free space. For instance the spontaneous emission rate of an atom embedded in a cavity is strongly affected by the cavity leading to the well known Purcell effect [23, 24]. The plane wave basis is not appropriate for describing the field inside the cavity. When dealing with open media, the leakage of energy outside the media change the dynamics of the field inside the cavity. Moreover in the case of an arbitrary shaped open cavity or a disordered medium with randomly varying dielectric constant, finding a suitable basis of modes describing the field inside the cavity is quite impossible due to their chaotic or random behavior. For these reasons the quantization of the field and the study of the light propagation in open random media is a challenging task [25, 26, 27, 28].

Using a Feshbach's projector framework, Hackenbroich *et al.* [27] perform a field quantization which takes fully into account the field modes inside the medium — denoted by λ and described by the operator $\hat{b}_\lambda$ — and the one outside the medium — denoted by $\{m, \omega\}$ and described by the operator $\hat{a}_m(\omega)$. Expanding the vector potential in these two sets of modes, we have the so-called system-and-bath Hamiltonian in the rotating wave approximation

$$
\begin{aligned}
\hat{H}_{\mathrm{S-B}} &= \overbrace{\sum_\lambda \hbar\omega_\lambda \hat{b}_\lambda^\dagger \hat{b}_\lambda}^{\text{Inside field term}} + \overbrace{\sum_m \int d\omega \hbar\omega \hat{a}_m^\dagger(\omega)\, \hat{a}_m(\omega)}^{\text{Outside field term}} \\
&+ \underbrace{\hbar \sum_\lambda \sum_m \int d\omega \left[W_{\lambda m}(\omega)\, \hat{b}_\lambda^\dagger \hat{a}_m(\omega) + \text{H.c.} \right]}_{\text{Coupling term}}
\end{aligned}
\tag{1.13}
$$

Using this Hamiltonian, one can obtain the Heisenberg equations of motion for operators describing the fields inside and outside the medium:

$$\frac{\mathrm{d}\hat{b}_{\lambda}(t)}{\mathrm{d}t} = -\mathrm{i}\omega_{\lambda}\hat{b}_{\lambda}(t) - \mathrm{i}\sum_{m}\int d\omega W_{\lambda m}(\omega)\,\hat{a}_{m}(t,\omega), \tag{1.14}$$

$$\frac{\mathrm{d}\hat{a}_{m}(t,\omega)}{\mathrm{d}t} = -\mathrm{i}\omega\hat{a}_{m}(t,\omega) - \mathrm{i}\sum_{\lambda}W^{*}_{\lambda m}(\omega)\,\hat{b}_{\lambda}(t). \tag{1.15}$$

The elements $W_{\lambda m}(\omega)$ couples the inside modes λ and the outside modes $\{m,\omega\}$ of the field taking into account the leakages in the cavity. We see that the dynamics of $\hat{b}_{\lambda}(t)$ is affected not only by the shape of the cavity, preventing the use of Fourier plane waves, but also by the presence of the external field $\hat{a}_{m}(\omega,t)$. Integrating the Eq. (1.15) for different time domains, a first time for $t_0 < t$ and another for $t_1 > t$, we obtain

$$\begin{aligned}\hat{a}_{m}(t,\omega) &= \mathrm{e}^{-\mathrm{i}\omega(t-t_0)}\hat{a}_{m}(t_0,\omega)\\ &\quad -\mathrm{i}\sum_{\lambda}W^{*}_{\lambda m}(\omega)\int_{t_0}^{t}dt'\mathrm{e}^{-\mathrm{i}\omega(t-t')}\hat{b}_{\lambda}(t'),\end{aligned} \tag{1.16}$$

$$\begin{aligned}\hat{a}_{m}(t,\omega) &= \mathrm{e}^{-\mathrm{i}\omega(t-t_1)}\hat{a}_{m}(t_1,\omega)\\ &\quad -\mathrm{i}\sum_{\lambda}W^{*}_{\lambda m}(\omega)\int_{t}^{t_1}dt'\mathrm{e}^{-\mathrm{i}\omega(t-t')}\hat{b}_{\lambda}(t').\end{aligned} \tag{1.17}$$

From Eqs. (1.16) and (1.17), defining the ingoing and outgoing modes operators by $\hat{a}^{\mathrm{in}}_{m}(\omega) = \mathrm{e}^{i\omega t_0}\hat{a}_{m}(\omega,t_0)$ $\hat{a}^{\mathrm{out}}_{m} = \mathrm{e}^{i\omega t_1}\hat{a}_{m}(\omega,t_1)$ and using the limits $t_0 \to -\infty$ and $t_1 \to \infty$, the input-output relations follow

$$\hat{a}^{\mathrm{out}}(\omega) - \hat{a}^{\mathrm{in}}(\omega) = -\mathrm{i}W^{\dagger}(\omega)\,\hat{b}(\omega), \tag{1.18}$$

where the $N \times M$ matrix W has elements $W_{\lambda m}$ and couples the M-component ingoing and outgoing vectors $\hat{a}^{\mathrm{in}}(\omega) = \{\hat{a}^{\mathrm{in}}_{m}(\omega)\}_m$ and $\hat{a}^{\mathrm{out}}(\omega) = \{\hat{a}^{\mathrm{out}}_{m}(\omega)\}_m$ with the N-component cavity vector $\hat{b}(\omega) = \{\hat{b}(\omega)_{\lambda}\}_{\lambda}$. If one is interested only in the field outside the medium, the operator $\hat{b}_{\lambda}$ can be expressed in term of $\hat{a}_{m}(\omega)$ through Eqs. (1.14) and (1.15). Therefore, the vector $\hat{b}(\omega)$ can be eliminated from Eq. (1.18) leading to the so-called input-output relations

$$\hat{a}^{\mathrm{out}}(\omega) = S(\omega)\,\hat{a}^{\mathrm{in}}(\omega), \tag{1.19}$$

where S is the $M \times M$ scattering matrix defined by

$$S(\omega) = 1 - 2\pi\mathrm{i}W^{\dagger}(\omega)\,D^{-1}(\omega)\,W(\omega). \tag{1.20}$$

with D a $N \times N$ matrix defined from the elements of W (see Eq.(63) in Ref [28]).

The scattering matrix relates the M input modes to the M output modes of the field. It contains all the information about the propagation of the field inside the cavity or the medium. Due to the commutation relations followed by $\hat{a}^{\mathrm{out}}(\omega)$ and $\hat{a}^{\mathrm{in}}(\omega)$ the scattering matrix is unitary and obeys $S^{\dagger}S = SS^{\dagger} = 1$. This relation ensures the conservation of energy in the absence of absorption and amplification in the cavity. Starting from Eq. (1.20) two different approaches can be adopted. The first one, called the Hamiltonian approach, considers the microscopic details of interaction between the medium and the field. The properties of the scattering matrix are then derived from the properties of the Hamiltonian using Eq. (1.20). The second approach is the random S-matrix approach where the microscopic details are disregarded. The matrix S is assumed to be a random matrix with a most general statistics restricted by fundamental symmetries only (unitarity, time-reversal symmetry, etc.).

When absorption and amplification are present in the medium, Eq. (1.18) has to be modified and becomes [9]

$$\hat{a}^{\text{out}}(\omega) = S(\omega)\,\hat{a}^{\text{in}}(\omega) + U(\omega)\,\hat{c}^{\text{in}}(\omega) + V(\omega)\,\hat{d}^{\dagger\text{in}}(\omega)\,, \tag{1.21}$$

where the operators $\hat{c}^{\text{in}}$ and $\hat{d}^{\text{in}}$ satisfy the usual bosonic commutation relations. The matrices U and V take into account the absorption and the amplification and are related to the scattering matrix by the relation

$$UU^{\dagger} - VV^{\dagger} = 1 - SS^{\dagger}, \tag{1.22}$$

which ensures the energy conservation.

In this thesis, we will mainly use the input-output relations and the random S-matrix framework in order to study the transmission of light through a random medium.

1.1.2 Pure and mixed states

Before introducing the usual and important states of light that appear in quantum optics let us present the notion of pure and mixed states. Considering a Hilbert space $\mathcal{H}$ of dimension N, a pure state is defined by a normalized vector $|\Psi\rangle$ belonging to $\mathcal{H}$, such that $\langle\Psi|\Psi\rangle = 1$. In an arbitrary basis $\{|\phi_k\rangle\}_k$ of $\mathcal{H}$, every pure state $|\Psi\rangle$ can be written as

$$|\Psi\rangle = \sum_k c_k\,|\phi_k\rangle\,, \tag{1.23}$$

where c_k are complex numbers that give the probability $|c_k|^2$ of finding the system in the state $|\phi_k\rangle$. The sum in Eq. (1.23) is a coherent superposition enables interference pattern. Indeed the expectation value of an operator is the square modulus of a sum of complex probability amplitudes c_k.

However when some classical uncertainty is introduced in the system, the state is no more a pure state and becomes mixed. This state, also called a statistical mixture, is described by a $N \times N$ Hermitian positive semidefinite density matrix $\hat{\rho} \in B(\mathcal{H})$, where $B(\mathcal{H})$ is the space of bounded operators acting on $\mathcal{H}$, which takes the general form

$$\hat{\rho} = \sum_k p_k\,|\psi_k\rangle\,\langle\psi_k|\,, \tag{1.24}$$

where $|\psi_k\rangle$ are pure states in which the system can be found with probabilities $p_k \geq 0$. The normalization of the state requires that $\text{Tr}\hat{\rho} = 1$. These states are generally encountered when the system of interest is in contact with an environment or is produced by a source which presents classical fluctuations like a heated filament producing thermal light. The sum in Eq. (1.24) is an incoherent superposition. No interferences appear because the expectation value of an operator is written as a sum of probabilities p_k.

Another important notion is the purity of a quantum state. The purity quantifies how close to a pure state is an arbitrary state and is defined by $\mathcal{P} = \text{Tr}\hat{\rho}^2$. Because the density matrix of a pure state is a projector ($\hat{\rho} = |\Psi\rangle\,\langle\Psi|$) its purity is equal to one. In contrast, for a mixed state we have $\mathcal{P} < 1$.

1.1.3 Fock space and second quantization

Fock states

Consider the hermitian operator $\hat{n}_{\mathbf{k}s} = \hat{a}^{\dagger}_{\mathbf{k}s}\hat{a}_{\mathbf{k}s}$ entering in the expression of the Hamiltonian (1.11). One can show that the eigenvalues of $\hat{n}_{\mathbf{k}s}$ are integers going from zero to infinity and related to the number of excitations in the mode $\{\mathbf{k}, s\}$. For this reason $\hat{n}_{\mathbf{k}s}$ is called the photon number operator, with "photon" denoting a quantum of the electromagnetic field.

The Fock states - sometimes also called number states - are defined as the eigenvectors of $\hat{n}_{\mathbf{k}s}$, they possess a well defined number of photons distributed over different modes of the electromagnetic field, i.e. with $\langle(\Delta\hat{n})^2\rangle = 0$, where $\Delta\hat{n} = \hat{n} - \langle\hat{n}\rangle$. A general Fock state is written as $|\{n\}\rangle = \prod_{\mathbf{k}s} |n_{\mathbf{k}s}\rangle$ with $\hat{n}_{\mathbf{k}s}|\{n\}\rangle = n_{\mathbf{k}s}|\{n\}\rangle$, and corresponds to an eigenstate of the Hamiltonian $\hat{H}$ in free space, such that $\hat{H}|\{n\}\rangle = E|\{n\}\rangle$, where E is the energy. The action of the creation and annihilation operators on Fock states follows from the relations

$$\begin{aligned} \hat{a}^{\dagger}_{\mathbf{k}s}|n_{\mathbf{k}s}\rangle &= \sqrt{n_{\mathbf{k}s}+1}\,|n_{\mathbf{k}s}+1\rangle \,, \\ \hat{a}_{\mathbf{k}s}|n_{\mathbf{k}s}\rangle &= \sqrt{n_{\mathbf{k}s}}\,|n_{\mathbf{k}s}-1\rangle \,. \end{aligned} \tag{1.25}$$

The equation $\hat{a}_{\mathbf{k}s}|1_{\mathbf{k}s}\rangle = |0\rangle$ introduces the vacuum state which has zero photons in every mode of the electromagnetic field.

From Eqs. (1.25), one can show that every Fock state can be constructed by repeatedly acting creation operators on the vacuum state such that

$$|\{n\}\rangle = \prod_{\mathbf{k}s} \frac{\left(\hat{a}^{\dagger}_{\mathbf{k}s}\right)^{n_{\mathbf{k}s}}}{\sqrt{(n_{\mathbf{k}s})!}}|0\rangle \,. \tag{1.26}$$

Besides the Fock states form an orthonormal basis in which an arbitrary state of light is written as

$$|\Psi\rangle = \sum_{\{n\}} c_{\{n\}}|\{n\}\rangle \,. \tag{1.27}$$

First and second quantization notations

Here we define the notations used in this thesis depending on whether the quantum state is written in first or in second quantization framework [29].

The Fock state basis is a natural basis used in the second quantization framework. For instance a state of two indistinguishable photons, one in the mode denoted by i and the other in the mode j ($i \neq j$) is written with the second quantization notations as

$$|\Psi\rangle = \hat{a}^{\dagger}_i\hat{a}^{\dagger}_j|0\rangle = |0, ...1_i, ...1_j, ...0\rangle = |1_i, 1_j\rangle \,. \tag{1.28}$$

When $i = j$, we have

$$|\Psi\rangle = \frac{1}{\sqrt{2}}\left(\hat{a}^{\dagger}_i\right)^2|0\rangle = |2_i\rangle \,. \tag{1.29}$$

This second quantization framework takes into account the symmetrization of the wave function.

Written with the first quantization notations the state in Eq. (1.28) becomes

$$|\Psi\rangle = \hat{S}_+ |1:i;2:j\rangle = |1:i;2:j\rangle_{\text{sym}} = \frac{1}{\sqrt{2}} \left(|1:i;2:j\rangle + |1:j;2:i\rangle \right), \qquad (1.30)$$

where $\hat{S}_+$ is the operator of symmetrization. Here 1 and 2 refer to the photons but they are unphysical labels because photons are indistinguishable. We also use the notation $|1:i;2:j\rangle = |i\rangle_1 \otimes |j\rangle_2$.

Obviously if one can attribute a physical label to distinguish the two photons these different notations still hold without the symmetrization constraint.

1.1.4 Coherent state

Coherent states of light are the states that are close to the field emitted by a coherent source like a laser far above the threshold or a classical current. They have been thoroughly studied by Glauber in the 60's [30, 31] leading to numerous important results in quantum optics and quantum mechanics in general. We focus here on very few properties of coherent states and we refer the reader to [32] for more details on these states.

A coherent state $|\{\nu\}\rangle$ is an eigenstate of the non-Hermitian annihilation operator $\hat{a}_{\mathbf{k}s}$. In a multi-mode representation, it is written as

$$|\{\nu\}\rangle = \prod_{\mathbf{k}s} |\nu_{\mathbf{k}s}\rangle , \qquad (1.31)$$

where $\nu_{\mathbf{k}s}$ are complex numbers satisfying

$$\hat{a}_{\mathbf{k}s} |\nu_{\mathbf{k}s}\rangle = \nu_{\mathbf{k}s} |\nu_{\mathbf{k}s}\rangle . \qquad (1.32)$$

In the Fock state basis, the single-mode coherent state has the form

$$|\nu_{\mathbf{k}s}\rangle = \mathrm{e}^{-\frac{|\nu_{\mathbf{k}s}|^2}{2}} \sum_{n_{\mathbf{k}s}} \frac{\nu_{\mathbf{k}s}^{n_{\mathbf{k}s}}}{\sqrt{n_{\mathbf{k}s}!}} |n_{\mathbf{k}s}\rangle , \qquad (1.33)$$

and defining the displacement operator $\hat{D}(\nu) = \mathrm{e}^{\nu \hat{a}^\dagger - \nu^* \hat{a}}$ one can show the relation

$$|\nu_{\mathbf{k}s}\rangle = \hat{D}(\nu_{\mathbf{k}s}) |0\rangle . \qquad (1.34)$$

The number of photons in such states is not well defined because $\langle (\Delta\hat{n})^2 \rangle = \langle \hat{n} \rangle$. However the phase of the state is well defined contrary to Fock states.

One can also use coherent states as a basis, however it is a non-orthogonal and over-complete basis.

1.1.5 Spontaneous parametric down converted light

Among the quantum states we will be interested in there are the spontaneous parametric down-converted (SPDC) two-photon states. These states are commonly used in quantum optics for a wide range of quantum experiments (e.g., quantum teleportation, two-photon interferences, etc.) because they are relatively easy to produce and due to the interesting correlations existing within the pairs of photons [17, 33, 34, 35].

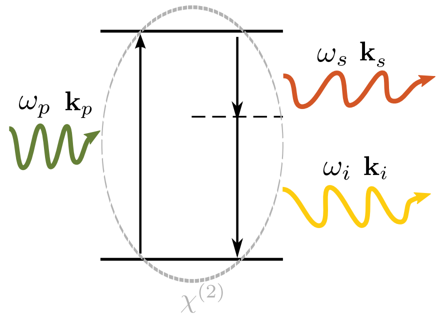

Figure 1.2: Energy level diagram of the spontaneous parametric down-conversion process. The black dashed line shows a virtual state.

SPDC two-photon states are generated by a $\chi^{(2)}$ non-linear process in which a pump field with frequency ω_p and wave vector $\mathbf{k}_p$ is sent in a non-linear crystal in order to create a "biphoton" [36] as shown in Fig. 1.2. Due to the conservation of energy and momentum the frequencies and wave vectors fulfill the following constraints

$$\omega_p = \omega_i + \omega_s, \tag{1.35}$$
$$\mathbf{k}_p\left(\omega_p\right) = \mathbf{k}_i\left(\omega_i\right) + \mathbf{k}_s\left(\omega_s\right), \tag{1.36}$$

where p stands for the pump and i, s for the down converted photons. For historical reasons the down-converted photons are called signal and idler photons. In parametric down-conversion the signal photons belong to the light beam that is sent into the medium along with the pump beam. However in SPDC, the down-converted photons are spontaneously generated from an initial vacuum state. Then from Eqs. (1.35) and (1.36), we see that the signal and idler photons can have a broad range of frequencies and wave vectors. This leads to the appearance of frequency and/or momentum correlations between the photons. We will see later in Sec. 1.3.4 how entanglement emerge from these correlations. The SPDC states are classified according to the polarization of the down-converted photons. In type I non-linear processes both photons have the same polarization. At the opposite, in Type II, they have orthogonal polarization, labeled o and e for ordinary and extraordinary polarizations. Because the non-linear crystals are generally birefringent, strong spectral differences appear between Type I and Type II biphoton states [37]. Besides, one can use continuous-wave or broadband pump, collinear or non-collinear propagation of the two photons according to the pump axis, leading to a wide variety of SPDC states. For more details on the zoology of SPDC two-photon states, we refer the reader to Refs. [38, 39].

In order to derive the two-photon state generated in a SPDC process one generally uses a first-order perturbation approach in an interaction picture. This method is valid only for a low gain regime in which the probability to generate more than two photons is very small. In Appendix A, we show an example of derivation of the two-photon state for type II SPDC. Let us present here the main features of these states. Whatever the experimental configuration, they can be written as

$$|\Psi\rangle = \sum_{ss'} \sum_{\mathbf{k}\mathbf{k}'} F\left(\mathbf{k}s, \mathbf{k}'s'\right) \hat{a}^\dagger_{\mathbf{k}s} \hat{a}^\dagger_{\mathbf{k}'s'} |0\rangle \, , \tag{1.37}$$

where $F\left(\mathbf{k}s, \mathbf{k}'s'\right)$ is the two-photon amplitude asociated with the probability of finding a pair with one photon in the mode $\{\mathbf{k}, s\}$ and the other one in $\{\mathbf{k}', s'\}$. In the general case it is given by

$$F\left(\mathbf{k}s, \mathbf{k}'s'\right) \propto \alpha_p\left(\omega, \omega'\right) h\left(\mathbf{k}, \mathbf{k}'\right), \tag{1.38}$$

where $h(\mathbf{k}, \mathbf{k}') = \int d^3\mathbf{r}\ e^{i\Delta\mathbf{k}\cdot\mathbf{r}}$ with $\Delta\mathbf{k} = \mathbf{k} - \mathbf{k}'$. $h(\mathbf{k}, \mathbf{k}')$ is the phase matching function which depends on the orientation and the length of the crystal, it ensures the momentum conservation. $\alpha_p(\omega, \omega')$ is the pump envelope function which ensures the conservation of energy.

1.1.6 Photodetection of light

Photodetection probabilities

We have at this point a description of the field operators and their dynamics, and we introduced some of the quantum states of light. Let us now present the theory of quantum photodetection of light [30, 40, 41]. The interaction between an electron of the detector and the electromagnetic field is described in the electric dipole approximation by the Hamiltonian $\hat{H}_{\text{int}} \approx -e\hat{\mathbf{r}}\cdot\hat{\mathbf{E}}(\mathbf{r}_0, t)$ with $\mathbf{r}_0$ the position of the electron and $e\hat{\mathbf{r}}$ its dipole moment. Then the probability of transition from the state $|d_I, \psi_I\rangle$ to $|d_F, \psi_F\rangle$ per unit of time, where d and ψ are respectively the states of the electron and the field, is given by

$$\mathrm{p}_1(\mathbf{r}_0, t) = \left| e\,\langle d_F, \psi_F|\,\hat{\mathbf{r}}.\hat{\mathbf{E}}(\mathbf{r}_0, t)\,|d_I, \psi_I\rangle \right|^2. \tag{1.39}$$

We now consider only the absorption of a photon, i.e. the term involving the operator $\hat{\mathbf{E}}^{(+)}(\mathbf{r}_0, t)$ and factorize out the expectation value associated with the electron by introducing a constant γ_D which contains the efficiency of the detector. This yields the probability

$$\mathrm{p}_1(\mathbf{r}_0, t) = \gamma_D \left| \langle\psi_F|\,\hat{\mathbf{E}}^{(+)}(\mathbf{r}_0, t)\,|\psi_I\rangle \right|^2. \tag{1.40}$$

Because we are not interested in the final state of the field, we trace over all the possible final states which form a complete set obeying the closure relation $\sum_F |\psi_F\rangle\ \langle\psi_F| = 1$. The probability of detection at time t becomes

$$\mathrm{p}_1(\mathbf{r}_0, t) = \gamma_D\ \langle\psi_I|\,\hat{\mathbf{E}}^{(-)}(\mathbf{r}_0, t)\,\hat{\mathbf{E}}^{(+)}(\mathbf{r}_0, t)\,|\psi_I\rangle\,. \tag{1.41}$$

If the input state contains a classical uncertainty, i.e. it is a mixed state described by $\hat{\rho}_I$, we obtain

$$\begin{aligned} \mathrm{p}_1(\mathbf{r}_0, t) &= \gamma_D \mathrm{Tr}\left[\hat{\rho}_I \hat{\mathbf{E}}^{(-)}(\mathbf{r}_0, t)\,\hat{\mathbf{E}}^{(+)}(\mathbf{r}_0, t)\right] \\ &= \gamma_D \langle\hat{\mathbf{E}}^{(-)}(\mathbf{r}_0, t)\,\hat{\mathbf{E}}^{(+)}(\mathbf{r}_0, t)\rangle, \end{aligned} \tag{1.42}$$

where $\langle ... \rangle$ stands for the quantum expectation value.
In a similar way, we define the two-photon detection probability per unit of time by

$$\mathrm{p}_2(\mathbf{r}_1, t_1, \mathbf{r}_2, t_2) = \gamma_D \langle\hat{\mathbf{E}}^{(-)}(\mathbf{r}_1, t_1)\,\hat{\mathbf{E}}^{(-)}(\mathbf{r}_2, t_2)\,\hat{\mathbf{E}}^{(+)}(\mathbf{r}_2, t_2)\,\hat{\mathbf{E}}^{(+)}(\mathbf{r}_1, t_1)\rangle. \tag{1.43}$$

It is equal to the photon coincidence counting rate of two detectors placed at $\mathbf{r}_1$ and $\mathbf{r}_2$, at times t_1 and t_2.

As we have seen in Sec. 1.1.1, observables of the field can be expressed in terms of creation and annihilation operators. Besides, we are mainly interested in the momentum representation when detection is taking place in the far field. Therefore, with lighten notations, we define the far field photodetection rate by

$$R_1\left(\mathbf{k},t\right) = \langle \hat{a}^{\dagger}_{\mathbf{k}}\left(t\right) \hat{a}_{\mathbf{k}}\left(t\right)\rangle, \tag{1.44}$$

and the coincidence counting rate by

$$R_2\left(\mathbf{k}_1,t_1,\mathbf{k}_2,t_2\right) = \langle \hat{a}^{\dagger}_{\mathbf{k}_1}\left(t_1\right) \hat{a}^{\dagger}_{\mathbf{k}_2}\left(t_2\right) \hat{a}_{\mathbf{k}_2}\left(t_2\right) \hat{a}_{\mathbf{k}_1}\left(t_1\right)\rangle. \tag{1.45}$$

First and second order correlation functions

Using the formalism introduced in the previous section, we can now introduce the correlation functions of the field studied by Glauber [30]. They are used to describe the coherence of the light. The first order correlation function is defined by

$$G_1\left(\mathbf{r}_{1,2},t_{1,2}\right) = \langle \hat{\mathbf{E}}^{(-)}\left(\mathbf{r}_1,t_1\right) \hat{\mathbf{E}}^{(+)}\left(\mathbf{r}_2,t_2\right)\rangle, \tag{1.46}$$

where $\mathbf{r}_{1,2}$ stands for $\mathbf{r}_1,\mathbf{r}_2$. We see that $G_1\left(\mathbf{r},t\right) \propto \mathrm{p}_1\left(\mathbf{r},t\right)$.
The second order correlation function is given by

$$G_2\left(\mathbf{r}_{1,2,3,4},t_{1,2,3,4}\right) = \langle \hat{\mathbf{E}}^{(-)}\left(\mathbf{r}_1,t_1\right) \hat{\mathbf{E}}^{(-)}\left(\mathbf{r}_2,t_2\right) \hat{\mathbf{E}}^{(+)}\left(\mathbf{r}_3,t_3\right) \hat{\mathbf{E}}^{(+)}\left(\mathbf{r}_4,t_4\right)\rangle, \tag{1.47}$$

and is related to the two-photon detection probability p_2. As for the photodetection and coincidence rates, the correlation functions can be expressed in momentum space and denoted by $G_1\left(\mathbf{k}_{1,2},t_{1,2}\right)$ and $G_2\left(\mathbf{k}_{1,2,3,4},t_{1,2,3,4}\right)$. The normalized correlation functions are defined by

$$g_1\left(x_1,x_2\right) = \frac{G_1\left(x_1,x_2\right)}{\left[G_1\left(x_1,x_1\right) G_1\left(x_2,x_2\right)\right]^{\frac{1}{2}}}, \tag{1.48}$$

and

$$g_2\left(x_1,x_2,x_3,x_4\right) = \frac{G_2\left(x_1,x_2,x_3,x_4\right)}{\left[G_1\left(x_1,x_1\right) G_1\left(x_2,x_2\right) G_1\left(x_3,x_3\right) G_1\left(x_4,x_4\right)\right]^{\frac{1}{2}}}, \tag{1.49}$$

where x stands for $\mathbf{r},t$ or equivalently for $\mathbf{k},t$. The generalization to higher order is then straightforward.

The coherence describes the property of a field to take correlated values at separated points in a "space" spanned by positions, times or momenta. The coherence is intimately related to the presence of randomness in the value taken at different position. A field is said to be coherent up to the order n when

$$\left|g_i\left(x_1,x_2,...,x_{2j}\right)\right| = 1, \forall j \leq n. \tag{1.50}$$

This is equivalent to the factorizability of correlation functions

$$G_i\left(x_1,...x_j,...,x_{2j}\right) = \mathcal{E}^*\left(x_1\right)...\mathcal{E}^*\left(x_j\right) \mathcal{E}\left(x_{j+1}\right)...\mathcal{E}\left(x_{2j}\right) \tag{1.51}$$

where $\mathcal{E}(x)$ is a complex function. This leads to an experimental point of view on the coherence. When a field is n-order coherent, its n-photon coincidence counting rate will be a product of single photon detection events.For example of coherent fields we have the classical plane wave and the coherent state, which in fact can be defined as the quantum state with the high order of coherence. At the opposite, the thermal radiation, which is stochastic, can not be coherent beyond the second order.

1.1.7 Signs of non-classicality

In this section we present physical quantities which characterize the non-classicality of a state.

The first one is based on the photon statistics of the state and is called the Mandel parameter Q:

$$Q = \frac{\langle (\Delta \hat{n})^2 \rangle - \langle \hat{n} \rangle}{\langle \hat{n} \rangle}, \tag{1.52}$$

where $\langle (\Delta \hat{n})^2 \rangle = \langle \hat{n}^2 \rangle - \langle \hat{n} \rangle^2$. This parameter is negative for sub-Poissonian distribution of the photon number, i.e. for states that can not be described by the classical theory, e.g., the Fock states. A coherent state will have a Poissonian distribution ($Q = 0$) meaning that the photon detection events are completely random, whereas a thermal state exhibits a super-Poissonian statistics with $Q > 0$. One also uses the Fano factor which is closely related to the Mandel parameter and defined by

$$F = \frac{\langle (\Delta \hat{n})^2 \rangle}{\langle \hat{n} \rangle}. \tag{1.53}$$

When the state allows for a classical description, the photocount statistics associated with it can b described by the so-called Mandel formula:

$$p(n) = \int_0^\infty \frac{I^n}{n!} \mathrm{e}^{-I} \mathcal{P}_{\mathrm{m}}(I)\, dI, \tag{1.54}$$

where I is the intensity of the field and $\mathcal{P}_{\mathrm{m}}(I) \geq 0$. Then a field is not classical if its photocount statistics can not be described by the Mandel formula (1.54).

Another way to characterize the quantumness of a state is to expand it in a specific basis of states. For instance the P-distribution $P(\alpha, \alpha^*)$, introduced by Sudarshan and Glauber [42, 31], characterizes a state in terms of coherent-state projectors such that its density matrix $\hat{\rho}$ is written as

$$\hat{\rho} = \int P(\alpha, \alpha^*) \left|\alpha\right\rangle \left\langle\alpha\right| d^2\alpha, \tag{1.55}$$

where

$$P(\alpha, \alpha^*) = \frac{\mathrm{e}^{|\alpha|^2}}{\pi^2} \int \left\langle -\beta \right| \hat{\rho} \left|\beta\right\rangle \mathrm{e}^{|\beta|^2} \mathrm{e}^{-\beta\alpha^* + \beta^*\alpha} d^2\beta, \tag{1.56}$$

with $d^2\beta = d(\mathrm{Re}\alpha)\, d(\mathrm{Im}\alpha)$. When this distribution is equivalent to a density of probability such that $P(\alpha, \alpha^*)$ is non-negative and not more singular than a delta function, the state possesses a classical description, otherwise it is a non-classical state.

To finish this section let us introduce the Wigner distribution quite similar to the P-distribution and defined by

$$W(\alpha, \alpha^*) = \frac{2e^{2|\alpha|^2}}{\pi^2} \int \langle -\beta| \hat{\rho} |\beta\rangle \, e^{-2(\beta\alpha^* - \beta^*\alpha)} d^2\beta. \tag{1.57}$$

As for the P-distribution, $W(\alpha, \alpha^*)$ is a quasi-probability density that can become negative for non-classical states.

1.2 Quantum entanglement in bipartite systems

1.2.1 Quantum entanglement in a nutshell

If no exception is pointed out, we discuss in the following sections only the case of pure bipartite quantum states. Given that different kinds of entanglement will be discussed, we mainly use at the beginning the term of "subsystem" without any reference to a particular physical system, e.g. particles or modes. Besides, in order to avoid any confusion, it is important to distinguish clearly the subsystems that are entangled and the physical observables that bear quantum correlations. For instance, one can say that two photons (subsystems) are entangled in polarization (observable).

Separable and entangled states

Consider a bipartite quantum system S divided in two subsystems S_1 and S_2. They are associated to the respective Hilbert spaces $\mathcal{H}$, $\mathcal{H}_1$ and $\mathcal{H}_2$ which satisfy the relation $\mathcal{H} = \mathcal{H}_1 \otimes \mathcal{H}_2$ where $\otimes$ stands for the tensor product that we sometimes omit. It follows that $N = N_1 \times N_2$ where $N_i = \dim\mathcal{H}_i$. Practically S can be an atom plus a photon in the case of the spontaneous emission process [43], an electron-hole pair in a two-dimensional electron gas [44], or a bimodal Bose-Einstein condensate [45]. In the case of pure states, the system S is described by a vector state $|\Psi\rangle \in \mathcal{H}$.

The state $|\Psi\rangle$ is a separable state if one can write it as a tensor product state

$$|\Psi\rangle = |\Phi_1\rangle \otimes |\Phi_2\rangle \, , \tag{1.58}$$

where $|\Phi_i\rangle \in \mathcal{H}_i$. Otherwise the state is said to be entangled which implies the existence of quantum correlations between the observables describing the state of the two subsystems S_1 and S_2. This definition of entanglement is negative in the sense that a state is entangled when it is not separable. Then a state can be very close to a separable state while being slightly entangled. This will lead naturally to the notion of entanglement quantification in Sec. 1.2.2, looking how far to the set of separable states is an entangled state.

One can also extend this criterion to systems of more than two parties like in entangled spin chains appearing in solid state or trapped ions systems [46, 47]. In the case of n-partite system, a state $|\Psi\rangle$ is fully separable (n-separable) when

$$|\Psi\rangle = |\Phi_1\rangle \otimes |\Phi_2\rangle \otimes ... \otimes |\Phi_n\rangle \, , \tag{1.59}$$

it is entangled otherwise. However the study of multipartite entanglement is quite more complex than the one of bipartite entanglement [48] and we will not deal with it in the rest of this thesis.

The definition of bipartite entanglement given above is rather formal and based on a mathematical separability criterion. However one can give to the separability of pure states a more practical meaning using the concept of physical reality. Indeed, looking to Eq. (1.58), the state $|\Psi\rangle$ can be prepared by manipulating each subsystem independently. One first prepares S_1 in $|\Phi_1\rangle$ and then S_2 in $|\Phi_2\rangle$. This means that a physical reality can be attributed to S_1 and S_2 independently. Whereas entanglement implies the impossibility to say with certainty in which state is S_1 independently of S_2, and reciprocally. One cannot assign a physical reality to one subsystem alone when entanglement is present. From the information theory point of view, it is said that when a state is entangled the amount of information contained in $|\Psi\rangle$ is greater than the sum of information contained in each subsystems independently. These features associated with entanglement are purely non-classical.

Reduced density matrix

Let us formalize the notion of entanglement using the reduced density matrix $\hat{\rho}_1$ associated to S_1

$$\hat{\rho}_1 = \mathrm{Tr}_2\ \hat{\rho}, \tag{1.60}$$

where Tr_2 stands for the partial trace over the subsystem S_2 and $\hat{\rho} = |\Psi\rangle\ \langle\Psi|$ is the density matrix of S. When $|\Psi\rangle$ is separable, i.e.can be written as a product state, the reduced density matrix of one subsystem – whatever the subsystem – describes a pure state with a purity, $\mathcal{P}_{\mathrm{sub}} = \mathrm{Tr}\left(\hat{\rho}_2^2\right) = \mathrm{Tr}\left(\hat{\rho}_1^2\right) = 1$, i.e. a state without classical uncertainty. On the contrary for an entangled state we have $\mathcal{P}_{\mathrm{sub}} \neq 1$ so that the subsystems are described by mixed states which implies a classical uncertainty in the outcome of a measurement performed on each subsystem independently.

We now illustrate these points using the so-called Bell states describing two distinguishable qubits and forming a basis of the two-qubit Hilbert space:

$$\left|\Psi^{\pm}\right\rangle = \frac{1}{\sqrt{2}}\left(|\uparrow\rangle_1 |\downarrow\rangle_2 \pm |\downarrow\rangle_1 |\uparrow\rangle_2\right), \tag{1.61}$$

$$\left|\Phi^{\pm}\right\rangle = \frac{1}{\sqrt{2}}\left(|\uparrow\rangle_1 |\uparrow\rangle_2 \pm |\downarrow\rangle_1 |\downarrow\rangle_2\right), \tag{1.62}$$

where the states $|\uparrow\rangle$ and $|\downarrow\rangle$ can correspond to polarizations of a photon or to spin projections of an electron. The density matrix of $|\Psi^+\rangle$ in the basis $\{|\uparrow\rangle_1 |\downarrow\rangle_2\}_{\uparrow,\downarrow}$ is

$$\hat{\rho}_{\mathrm{Bell}} = \frac{1}{2}\begin{pmatrix} 1 & 1 \\ 1 & 1 \end{pmatrix}, \tag{1.63}$$

which leads to the reduced density matrices

$$\hat{\rho}_1 = \hat{\rho}_2 = \frac{1}{2}\begin{pmatrix} 1 & 0 \\ 0 & 1 \end{pmatrix} = \frac{1}{2}\mathbb{1}. \tag{1.64}$$

The subsystems' states are here completely mixed. It is then impossible to attribute a physical reality, e.g. a state of polarization or a projection of the spin, to a subsystem alone.

These considerations lead to a different definition of separability and consequently of entanglement, introduced by Ghirardi *et al.* [49, 50] for systems of identical particles (see

Sec. 1.3). Two subsystems are said to be not entangled when both subsystems possess a complete set of properties. Formally, this is equivalent to the possibility of attributing to each subsystem a one-dimensional projection operator $\hat{P}_i \in B(\mathcal{H}_i)$ where $B(\mathcal{H}_i)$, is the space of bounded operators acting on $\mathcal{H}_i$, such that

$$\langle\Psi|\, \hat{P}_1 \otimes \mathbb{1}_2 \,|\Psi\rangle = 1. \tag{1.65}$$

When $|\Psi\rangle$ is separable, the reduced density matrix is a projector and necessarily with $\hat{P}_1 = \hat{\rho}_1$ we have $\langle\Psi|\, \hat{\rho}_1 \otimes \mathbb{1}_2 \,|\Psi\rangle = \mathrm{Tr}\left[|\Psi\rangle\, \langle\Psi|\, \hat{\rho}_1 \otimes \mathbb{1}_2\right] = \mathrm{Tr}_1\left[\hat{\rho}_1^2\right] = 1$. We will come back to this criterion of entanglement in Sec. 1.3.2.

Quantum correlations and non-locality

Until now we have only discussed the separability of a state and the possibility or not to attribute physical reality to one of the subsystems. However, the most striking consequence of entanglement are the non-local quantum correlations between measurement that two observers perform on a shared bipartite state.

Consider Alice and Bob who share the state $|\Psi^+\rangle$ given by Eq. (1.61). Alice possesses the qubit labeled 1 while the qubit 2 belongs to Bob. Suppose now that Alice performs a measurement in the orthonormal basis $\{|\uparrow\rangle_1, |\downarrow\rangle_1\}$. As explained in the previous section, the probabilities $p_1(\uparrow)$ and $p_1(\downarrow)$ of the two different outcomes of such a measurement reveal a complete uncertainty concerning the single particle state,

$$p_1(\uparrow) = p_1(\downarrow) = \frac{1}{2}, \tag{1.66}$$

and the same for Bob's measurement. However, when considering the joint probabilities, the outcomes of Alice and Bob's measurements appear to be strongly correlated. With $p_{1,2}(\uparrow,\downarrow) = \langle\Psi^+|\left(|\uparrow\rangle\, \langle\uparrow| \otimes |\downarrow\rangle\, \langle\downarrow|\right)|\Psi^+\rangle$, we obtain

$$\begin{aligned} p_{1,2}(\uparrow,\downarrow) &= p_{1,2}(\downarrow,\uparrow) = 1, \\ p_{1,2}(\uparrow,\uparrow) &= p_{1,2}(\downarrow,\downarrow) = 0, \end{aligned}$$

i.e. perfect anti-correlations. One would have obtained perfect correlations in the case of $|\Phi^+\rangle$ defined in Eq. (1.62). After her measurement Alice can predict with certainty the outcome of Bob's measurement. This is true whatever the distance between Alice and Bob. These non-local correlations strongly puzzled Einstein with coworkers who claim that quantum mechanics was incomplete and introduced the famous EPR paradox [51].

It is relevant to ask here why these correlations are quantum. Indeed one can obtain perfect correlations or anti-correlations with classical systems like colored socks [52], a red one and a blue one, sent randomly to Alice and Bob. In this case the system is a mixed state described by a density matrix

$$\hat{\rho}_{\text{socks}} = \frac{1}{2}$$
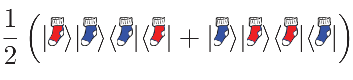
(1.67)

In this basis there are perfect anti-correlations. If Alice, opening her mail box, finds a blue sock, Bob will obviously find a red one. The measurement in the basis  is described by the operator

$$\hat{\sigma}_1 = \begin{pmatrix} 1 & 0 \\ 0 & -1 \end{pmatrix}. \tag{1.68}$$

The correlations between the outcomes of Alice and Bob's measurement are given by $\mathrm{Tr}\left[\hat{\rho}_{\mathrm{socks}}\hat{\sigma}_1 \otimes \hat{\sigma}_1\right] = -1$ which illustrates perfect anti-correlations. However, if they perform their measurements in another orthonormal basis like

$$\begin{aligned} |\,\rangle &= \frac{1}{\sqrt{2}}\left(|\,\rangle + |\,\rangle\right), \\ |\,\rangle &= \frac{1}{\sqrt{2}}\left(|\,\rangle - |\,\rangle\right), \end{aligned} \tag{1.69}$$

where the asociated operator written in the former basis is

$$\hat{\sigma}_2 = \begin{pmatrix} 0 & 1 \\ 1 & 0 \end{pmatrix}, \tag{1.70}$$

the outcome correlations vanish completely, as shown by $\mathrm{Tr}\left[\hat{\rho}_{\mathrm{socks}}\hat{\sigma}_2 \otimes \hat{\sigma}_2\right] = 0$. Consequently classical correlations are basis-dependent.

This is in strong contrast with quantum correlations which do not depend on the basis in which the measurement is performed. Indeed, in the basis of circular polarizations $\{|\circlearrowleft\rangle, |\circlearrowright\rangle\}$ defined by

$$\begin{aligned} |\circlearrowleft\rangle &= \frac{1}{\sqrt{2}}\left(|\uparrow\rangle + i\,|\downarrow\rangle\right), \\ |\circlearrowright\rangle &= \frac{1}{\sqrt{2}}\left(|\uparrow\rangle - i\,|\downarrow\rangle\right), \end{aligned} \tag{1.71}$$

the state $|\Psi^+\rangle$ given by Eq. (1.61) becomes

$$\left|\Psi^+\right\rangle = \frac{1}{\sqrt{2}}\left(|\circlearrowright\rangle_1 |\circlearrowright\rangle_2 - |\circlearrowleft\rangle_1 |\circlearrowleft\rangle_2\right). \tag{1.72}$$

The correlations are still present and perfect. Contrary to the classical correlations, the quantum correlations exhibited by $|\Psi^+\rangle$ are independent of the choice of basis.

A way to put in evidence such non-local quantum correlations is to verify if they violate or not the so-called Bell inequalities introduced many years after the EPR paradox [53] by John Bell. Violation of Bell inequalities have been demonstrated experimentally in 1981 by Aspect *et al.* [54] confirming that the non-locality is an essential and inevitable ingredient of quantum mechanics, and putting quantum entanglement into reality. Historically, entanglement and non-locality are intimately related, however, they are not equivalent properties. Indeed, some states can be entangled without violating the Bell inequalities [55] whereas non-locality always implies entanglement [48]. The situation becomes much simpler with pure bipartite quantum states because in this case entanglement is equivalent to the violation of the Bell inequalities [56].

1.2.2 Quantification of entanglement through the Schmidt decomposition

Schmidt decomposition

Up to now, we have only focused our attention on the existence or not of entanglement in a quantum state. We now introduce the Schmidt decomposition [57, 8, 58] in order to quantify bipartite entanglement in pure states. The Schmidt decomposition is a mere application of the singular value decomposition (SVD) of a quantum state which is particularly useful when dealing with high-dimensional states, i.e. beyond the qubit case. Here "high-dimensional" means that the correlated physical observables evolve in spaces of dimension much greater than two, e.g. frequency, momentum or photon number spaces.

Consider such a high-dimensional bipartite state $|\Psi\rangle$ written as

$$|\Psi\rangle = \sum_{ij}^{N\times N} C_{ij} |i\rangle_1 |j\rangle_2 , \tag{1.73}$$

where $\{|i\rangle_1\}_i$ and $\{|j\rangle_1\}_j$ are the respective N-dimensional bases of the subsystems S_1 and S_2 that we assume distinguishable. The elements C_{ij} form a complex $N\times N$ matrix C which contains all the information about the entanglement between the subsystems. By applying the SVD to the matrix C we can find new orthonormal bases $\{|u_k\rangle_1\}_k$ and $\{|v_k\rangle_2\}_k$ such that

$$|\Psi\rangle = \sum_{k=1}^{N} \sqrt{\lambda_k} |u_k\rangle_1 |v_k\rangle_2 , \tag{1.74}$$

where the λ_k's are the Schmidt eigenvalues. They are positive, real numbers and satisfy $\sum_{k=1}^{N} \lambda_k = 1$ because of the normalization $\langle\Psi|\,\Psi\rangle = 1$. The singular values d_k of C are linked to the eigenvalues λ_k of the square matrix $C^\dagger C$ by the relation $\lambda_k = |d_k|^2$.

It is important to point out the possibility of performing the Schmidt decomposition for continuous variable states as well [59], such as, e.g.,

$$|\Psi\rangle = \int_{-\infty}^{+\infty} d\Omega d\omega C(\Omega,\omega) |\Omega\rangle_1 |\omega\rangle_2 . \tag{1.75}$$

Actually, the single discrete sum appearing in Eq. (1.74) is independent of the initial representation of $ket\Psi$ in the form of a discrete sum (1.73) or in the form of an integral (1.75).

Let us discuss the consequences of Eq. (1.74). It contains only one sum over k so that the ambiguity in correlations disappear. Indeed, if a subsystem is in the state $|u_k\rangle_1$ the other one is with certainty in the state $|v_k\rangle_2$, with a joint probability λ_k.

The separability criterion can be transcribed using the Schmidt rank R_{Schmidt} defined as the number of non-null Schmidt eigenvalues. A state is separable iif $R_{\text{Schmidt}} = 1$ with the single eigenvalue $\lambda_1 = 1$. Consequently a state is entangled iif $R_{\text{Schmidt}} \geq 2$.

Physically, λ_k are the eigenvalues of the reduced density matrix of one subsystem. It is easy to show that the non-vanishing λ_k are the same whatever the choice of one subsystem. The Schmidt eigenvalues allow one to determinate if the states of subsystems are mixed and to calculate their purity. We have seen that separable states correspond to subsystems in pure states. On the contrary, entangled states correspond to subsystems in mixed states. However a state can be more or less mixed, hence an entangled state can be more or less entangled. The more mixed the subsystem, the more entangled is the whole system. This statement suggest a way of quantifying the amount of entanglement using Schmidt eigenvalues.

Local and global operation on a quantum system

In order to define entanglement measures, we first introduce the notion of local operations (LO). An operation is local if under its action on a bipartite state $|\Psi\rangle \in \mathcal{H}_1 \otimes \mathcal{H}_2$, the subsystems evolve independently from each other. Any LO can be written as

$$\hat{\mathcal{E}}_{\text{loc}} = \hat{A} \otimes \hat{B}, \tag{1.76}$$

where $\hat{A} \in B(\mathcal{H}_1)$ and $\hat{B} \in B(\mathcal{H}_2)$. A local operation is unitary when $A = A^\dagger$ and $B = B^\dagger$. The Schmidt decomposition is invariant under unitary local operations, i.e. λ_k remain unchanged. However, the Schmidt eigenvalues evolve when non-unitary local operations are performed but the entanglement can not increase under such local operations [8, 48]. The new set of eigenvalues will necessarily be associated with a smaller amount of entanglement. A more general and important class of operations frequently used in the quantum information theory is called "local operations and classical communications" (LOCC). Like LO, LOCC act independently on each subsystem but classical correlations can be created by an exchange of classical information. In practice, it means that Alice and Bob perform independent measurements on their subsystems but are allowed to communicate through a classical communication channel. An important axiom in quantum information is the monotonicity axiom [60]. It states that entanglement can not increase under LOCC. Actually an increase of entanglement is possible only with global operations, i.e. when interactions between the subsystems take place. The notions introduced above are important to define a good quantity to quantify entanglement as we will see in the next section.

Entanglement monotones and measures

Here we present the physical quantities that we will use in this thesis to quantify the entanglement of a state. First, an entanglement monotone is a function of the Schmidt eigenvalues that increases with the amount of entanglement but does not increase under LOCC. Then a measure of entanglement is a monotone which satisfy additional criteria like vanishing exactly for separable states, sub-additivity or convexity. Actually there is no unique consensus concerning the "perfect" entanglement measure. However, for pure bipartite states the following quantities are well accepted as good measures of entanglement.

- *Schmidt number*: It is defined by

  $$K(\Psi) = \frac{1}{\text{Tr}\left[\hat{\rho}_1^2\right]} = \frac{1}{\sum_k \lambda_k^2}, \tag{1.77}$$

  and it quantifies the number of significative terms in the Schmidt decomposition. Contrary to the Schmidt rank it takes into account the weight of the eigenvalues in addition to the number of non-vanishing ones. As discuss above, we see that the entanglement can be quantified through the purity of the subsystems. Actually, $K(\Psi) = 1/\mathcal{P}_{\text{sub}}$.

- *Concurrence*: Closely related to the Schmidt number, it is defined by

  $$C(\Psi) = \sqrt{2\left(1 - \text{Tr}\left[\hat{\rho}_1^2\right]\right)} = \sqrt{2\left(1 - \sum_k \lambda_k^2\right)}. \tag{1.78}$$

Separable state	Maximally entangled state
$\lambda_1 = 1$, $\lambda_k = 0$, for $k > 1$	$\lambda_k = \frac{1}{N}$, $\forall k$
$\vert\Psi_{\text{sep}}\rangle = \vert\Phi_1\rangle \otimes \vert\Phi_2\rangle$	$\vert\Psi_{\max}\rangle = \frac{1}{\sqrt{N}} \sum_{k=1}^{N} \vert u_k\rangle_1 \vert v_k\rangle_2$
$\hat{\rho}_1 = \vert\Phi_1\rangle \langle\Phi_1\vert$ (pure state)	$\hat{\rho}_1 = \mathbb{1}/N$ (completely mixed state)
....	....
$K(\Psi_{\text{sep}}) = 1$	$K(\Psi_{\max}) = N$
$C(\Psi_{\text{sep}}) = 0$	$C(\Psi_{\max}) = \sqrt{2\left(1 - \frac{1}{N}\right)}$
$D(\Psi_{\text{sep}}) = 0$	$D(\Psi_{\max}) = 2\left(1 - \sqrt{\frac{1}{N}}\right)$
$E(\Psi_{\text{sep}}) = 0$	$E(\Psi_{\max}) = \ln N$

Table 1.1: Properties of separable and maximally entangled states

It is a high-dimensional extension of the so-called Wootters concurrence [61] defined for two qubits.

- *Geometrical quantum discord*: It is a geometrical measure of entanglement based on the Bures distance which quantifies the distance in the Hilbert space between $|\Psi\rangle$ and the closest separable state [62, 63]. By definition,

$$D(\Psi) = 2\left(1 - \sqrt{\lambda_{\max}}\right), \tag{1.79}$$

where $\lambda_{\max} = \max_k (\lambda_k)$.

- *Von Neumann entropy*: It is defined by

$$E(\Psi) = -\text{Tr}\left[\hat{\rho}_1 \ln \hat{\rho}_1\right] = -\sum_k \lambda_k \ln\, \lambda_k. \tag{1.80}$$

The entropy quantifies the amount of information required to describe $|\Psi\rangle$.

Maximally entangled states

From the link between subsystem purity and entanglement, it appears that some states can be seen as maximally entangled because their associated subsystems are completely mixed whereas for separable states the subsystems are pure. Completely mixed states of dimension N are characterized by a density matrix spectrum $\{\frac{1}{N}, ..., \frac{1}{N}\}$ leading to the purity $\text{Tr}\hat{\rho}^2 = \frac{1}{N}$. Consequently, we can calculate the entanglement measures defined above for the two extremal states, the separable state and the maximally entangled state; their main properties are summarized in Table 1.1.

1.3 Entanglement with identical particles

We have seen in Sec. 1.2.1 that the notion of entanglement requires the possibility to distinguish two subsystems and, consequently, to construct a product Hilbert space according to which one can perform a partial trace and derive a Schmidt decomposition. Usually, in textbook examples, the subsystems are distinguishable and one considers, for instance, the entanglement between an atom and a photon which can be well distinguished one from another. Note that when subsystems are associated with particles, we refer to particle entanglement. In the case of photon entanglement for example, the correlated observables can be the polarization, the frequency, the angular momentum, etc. However, in real experiments one often deals with identical particles like, e.g., an electron gas, a Bose-Einstein condensate or a collection of photons. In such situations, is there any sense to speak of particle entanglement given that particles are identical?

Indeed, when dealing with identical particles it is no more possible to attribute a definite Hilbert space to each subsystems $S_{1,2}$ and so to construct a tensor product space describing the whole system S. Due to the (anti)symmetrization of the wave function for (fermions) bosons, a system of N particles evolves in a subspace $\mathcal{H}_+$ ("-" for fermions) of the whole N-fold product Hilbert space $\mathcal{H}^{\otimes N}$ where $\mathcal{H}$ is the one-particle Hilbert space. We have

$$\mathcal{H}_\pm = \{|\Psi\rangle \in \mathcal{H}^{\otimes N} : \hat{S}_\pm |\Psi\rangle = |\Psi\rangle\}, \tag{1.81}$$

where $\hat{S}_\pm$ is the operator of (anti)symmetrization. Then, if one wants to consider particle entanglement, several questions arise:

- As in the case of distinguishable[1] particles, is it still possible to perform a partial trace over one of the subsystems knowing that subsystems can not be distinguished one from another? Is it then possible to obtain the Schmidt decomposition of a system of two identical particles and use the previously introduced measures of entanglement?

- Besides, the (anti)symmetrization procedure leads to inevitable correlations, except in the case of two bosons occupying the same mode. Every state seems to be entangled after (anti)symmetrization of the wave function because they are no more separable, but is it really the case? Is this apparent entanglement useful, allowing one to perform quantum information tasks such as, for example, teleportation? This question is closely related to the impossibility of constructing a tensor product Hilbert space.

- Finally, in quantum information experiments, one usually uses identical particles like two photons as in the Orsay experiment [54]. However one does not care about the difficulties listed above and particles are treated as distinguishable. In fact, the indistingishability is suppressed through the measurement protocol. For instance, when particles can be well separated one from another without ambiguity, the notions introduced in Sec. 1.2 can be applied. How can we describe such experiments starting from the case of identical particles?

The goal of the present section is to clarify these points and answer these questions.

[1] We use here "distinguishable" instead of "non-identical" because as we will see later in Sec. 1.3.1, identical particles like photons can be distinguishable through operation on particular degree of freedom. Besides, distinguishable particles like two photons with orthogonal polarizations can become indistinguishable due to propagation through a medium which induces "losses" of the information about the polarization.

Another kind of entanglement can be considered when dealing with identical particles, it is called mode entanglement (or path entanglement) [64]. This entanglement is beared by the modes of a quantum field which constitute the entangled subsystems. One frequently encounters mode entanglement in optics when using a simple beam splitter [65] or any mode splitting devices like a disordered medium [14]. Indeed, one can create this type of entanglement using only linear optics [66] which is not possible with particle entanglement that imply particle interaction, i.e. non-linear optics. The mode entanglement can be defined only when particles are identical such that the number of particles populating each mode becomes the observable exhibiting quantum correlations. An example of a popular mode-entangled state is the $N00N$ state [67] defined by $|\Psi\rangle = 1/\sqrt{2}\left(|N_a, 0_b\rangle + \mathrm{e}^{i\phi}|0_a, N_b\rangle\right)$ where a and b are two modes of a quantum field. It has been shown that states presenting mode entanglement can violate the Bell inequality [68] so that this entanglement is useful for quantum computation and quantum information.

In the following we will study the particular case of two-photon states which allows clarifying the issues arising from the indistinguishability of particles. We will then discuss particle and mode entanglement based on the recent literature dealing with this quite debated subject. Actually, no real point of agreement has been found concerning this topic. For instance, some authors claim that the symmetrization leads to valuable and useful entanglement [29] while others consider that "*this entanglement is not a matter of concern*" [69, 49]. Besides, a wide range of proposals has been made to characterize and to quantify entanglement with identical particles and therefore depending on the authors and their particular entanglement measures [70, 71] the same state appear more or less entangled, or even entangled or not. We do not pretend here to close the debate but aim at giving a clear overview.

1.3.1 Two-photon state as an illustrating example

In order to illustrate the situation, let us consider a system of two photons evolving in a Hilbert space $\mathcal{H}_{\text{tot}}$. Because they are identical particles, the photons are *a priori* indistinguishable from each other. The one-particle Hilbert space is defined by $\mathcal{H} = \mathcal{H}_{\mathbf{k}} \otimes \mathcal{H}_s$ where $\mathcal{H}_{\mathbf{k}}$ is the infinite-dimensional Hilbert space associated with the wave vector degree of freedom and $\mathcal{H}_s$ is the two-dimensional one associated with the polarization of the photon. The postulate of symmetrization of the "wave function" describing the two-photon system implies that $\mathcal{H}_{\text{tot}}$ is a subspace of the tensor product $\mathcal{H} \otimes \mathcal{H}$ that contain only symmetric states. We write it as $\mathcal{H}_{\text{tot}} = \hat{S}_+[\mathcal{H}^{\otimes 2}]$ where S_+ is the operator of symmetrization. This symmetrization procedure strongly reduces the number of physical states compared to the case of distinguishable particles.

A general two-photon state belonging to $\mathcal{H}_{\text{tot}}$ is written as

$$|\Psi\rangle = \sum_{i,j}^{\infty}\sum_{a,b}^{2} \phi_{ij,ab}\hat{a}^{\dagger}_{\mathbf{k}_i s_a}\hat{a}^{\dagger}_{\mathbf{k}_j s_b}|0\rangle\ , \tag{1.82}$$

where $\hat{a}^{\dagger}_{\mathbf{k}s}$ is the photon creation operator which acting on the vacuum, $\hat{a}^{\dagger}_{\mathbf{k}s}|0\rangle = |1_{\mathbf{k},s}\rangle = |\mathbf{k}, s\rangle$, creates a photon in the mode $\{\mathbf{k}, s\}$ with s allowed to take two values corresponding to the two perpendicular polarizations $\uparrow$ and $\downarrow$ for linear polarization, or $\circlearrowleft$ and $\circlearrowright$ for circular ones. Given that the wave vector and polarization degrees of freedom are independent, the coefficient $\phi_{ij,ab}$ can be written as a product $\phi^{\mathbf{k}}_{ij}\phi^{s}_{ab}$. Due to the symmetrization, we have

$$\begin{aligned} \hat{a}^{\dagger}_{\mathbf{k}_i s_a}\hat{a}^{\dagger}_{\mathbf{k}_j s_b}\left|0\right\rangle &= \left|1_{\mathbf{k}_i,s_a}, 1_{\mathbf{k}_j,s_b}\right\rangle \\ &= \left|1:\mathbf{k}_i, s_a; 2:\mathbf{k}_j, s_b\right\rangle_{\mathrm{sym}} \\ &= \frac{1}{\sqrt{2}}\left(\left|1:\mathbf{k}_i, s_a; 2:\mathbf{k}_j, s_b\right\rangle + \left|1:\mathbf{k}_j, s_b; 2:\mathbf{k}_i, s_a\right\rangle\right), \end{aligned} \tag{1.83}$$

where 1 and 2 are unphysical labels. From Eq. (1.83), in terms of first quantization notations, the state $|\Psi\rangle$ becomes

$$|\Psi\rangle = \frac{1}{\sqrt{2}}\sum_{i,j}^{\infty}\sum_{a,b}^{2}\phi^{\mathbf{k}}_{ij}\phi^{s}_{s_a,s_b}\left(\left|1:\mathbf{k}_i, s_a; 2:\mathbf{k}_j, s_b\right\rangle + \left|1:\mathbf{k}_j, s_b; 2:\mathbf{k}_i, s_a\right\rangle\right). \tag{1.84}$$

Considering only one component of the wave vector that can be the frequency, the orbital angular momentum or its transverse part for instance, the state reduces to

$$|\Psi\rangle = \sum_{i,j}^{\infty}\sum_{a,b}^{2}\phi^{k}_{ij}\phi^{s}_{s_a,s_b}\hat{a}^{\dagger}_{k_i s_a}\hat{a}^{\dagger}_{k_j s_b}\left|0\right\rangle, \tag{1.85}$$

with k a component of $\mathbf{k}$. We now simplify the state $|\Psi\rangle$ even further in order to arrive at the usual quantum information qubit states, e.g. $|01\rangle + |10\rangle$. To this end, we consider $k \in \{k_\alpha, k_\beta\}$. In order to lighten the notations, we omit the symbols k and s, so that $|\alpha, a; \beta, b\rangle = |1 : k_\alpha, s_a; 2 : k_\beta, s_b\rangle$. The basis associated with the symmetric two-photon Hilbert space in this situation is given by

$$\underbrace{\begin{matrix} |\alpha,a;\beta,b\rangle_{\mathrm{sym}} & |\alpha,b;\beta,a\rangle_{\mathrm{sym}} \\ |\alpha,a;\beta,a\rangle_{\mathrm{sym}} & |\alpha,b;\beta,b\rangle_{\mathrm{sym}} \\ |\alpha,a;\alpha,b\rangle_{\mathrm{sym}} & |\beta,a;\beta,b\rangle_{\mathrm{sym}} \end{matrix}}_{\text{Not separable}} \qquad \underbrace{\begin{matrix} |\alpha,a;\alpha,a\rangle_{\mathrm{sym}} & |\alpha,b;\alpha,b\rangle_{\mathrm{sym}} \\ |\beta,a;\beta,a\rangle_{\mathrm{sym}} & |\beta,b;\beta,b\rangle_{\mathrm{sym}} \end{matrix}}_{\text{Separable (photons in the same mode)}} \tag{1.86}$$

We see that $\dim\mathcal{H}_{\mathrm{tot}} = 10$ whereas $\dim\mathcal{H}\otimes\mathcal{H} = 16$. This reduction of dimension due to the constraint imposed by symmetrization necessarily induces correlations between photons leading to non-separability of the state.

Separability as bad criterion for entanglement

The first remark that follows from Eq. (1.86) is that, with the exception of the four last basis states where the photons occupy the same mode, all the remaining basis states are not separable due to the symmetrization. Does that mean they are entangled?

Consider the state

$$|\alpha, a; \beta, b\rangle_{\mathrm{sym}} = \frac{1}{\sqrt{2}}\left(|1:\alpha, a; 2:\beta, b\rangle + |1:\beta, b; 2:\alpha, a\rangle\right). \tag{1.87}$$

Taking only the separability criterion, this state seems entangled. However when we consider the more physical criterion associated with the possibility to assign a physical reality to each particle independently [72], it appears that the state given by Eq. (1.87) is not entangled. It merely says that there is one particle with a definite set of properties $\{\alpha, a\}$ and, independently, another with properties $\{\beta, b\}$. However, one can not say which particle possesses which properties. The presence of uncertainty on the one particle state is due to the indistinguishability but it can not be used as a resource for quantum information, e.g. teleportation, dense coding, etc.

Another way to see this is to imagine that one can "capture" particles by putting them in two different cavities, one cavity, refereed to as $\mathcal{C}_1$, is associated with the polarization a whereas the other, $\mathcal{C}_2$, with b. Consequently, we add a dichotomic variable $\{\mathcal{C}_1, \mathcal{C}_2\}$ which serves as a physical label allowing to suppress the indistinguishability. Then the state can be written as

$$\begin{aligned} |\alpha, a; \beta, b\rangle_{\text{sym}} &\rightarrow |\mathcal{C}_1, \alpha, a; \mathcal{C}_2, \beta, b\rangle + |\mathcal{C}_1, \beta, b; \mathcal{C}_2, \alpha, a\rangle \\ &\rightarrow |\mathcal{C}_2, \beta, b; \mathcal{C}_1, \alpha, a\rangle \; . \end{aligned} \tag{1.88}$$

This demonstrates that the state is not entangled. If we used non-identical particles, with labels 1 and 2 associated with a physical property and hence still present after the capture of photons we would obtained a state which is entangled. Moreover, one can show [49] that the state of Eq. (1.87) can not violate any Bell inequality. Because for pure bipartite states non-locality and entanglement are equivalent, the state is not entangled. This leads us to a conclusion that not every (anti)symmetric state is entangled even if it is not separable. In Sec. 1.3.2 we will formalize the distinction between non-separability and entanglement for high-dimensional states, i.e. beyond the qubit case, and use a generalized Schmidt decomposition in order to quantify the particle and mode entanglement.

From identical particles to EPR states

Let us study the physical meaning of a state often used in quantum information textbooks [8], $1/\sqrt{2}\,(|01\rangle + |10\rangle)$ and generally related to the well-known EPR paradox [51]. In textbooks, nothing is said about the properties of entangled particles. In fact, from the quantum information point of view one just sees abstract subsystems as in Sec. 1.2. However, experiments have been done with this state in order to bring quantum information to the real world. It is the purpose of this section to show how this state can be prepared with identical particles.

Consider two photons with polarizations $0 = \uparrow$ and $1 = \downarrow$ produced by a cascade decay of an atom ($J = 0 \rightarrow J = 1 \rightarrow J = 0$) as in the Orsay experiment [54] that demonstrated the violation of Bell's inequality. Due to the conservation of momentum the two-photon state is written as

$$\begin{aligned} |\Psi\rangle &= |1:+k,\uparrow; 2:-k,\downarrow\rangle_{\text{sym}} + \mathrm{e}^{i\phi}\,|1:+k,\downarrow; 2:-k,\uparrow\rangle_{\text{sym}} \\ &= \frac{1}{2}\Big(|1:+k,\uparrow; 2:-k,\downarrow\rangle + |1:-k,\downarrow; 2:+k,\uparrow\rangle + \\ &\quad + \mathrm{e}^{i\phi}\,|1:+k,\downarrow; 2:-k,\uparrow\rangle + \mathrm{e}^{i\phi}\,|1:-k,\uparrow; 2:+k,\downarrow\rangle\Big) \, . \end{aligned} \tag{1.89}$$

This state is the EPR-Bohm entangled state [73]. How can one relate such a state to the one used in quantum information textbooks where particle indistinguishability does not matter? Let us rewrite $|\Psi\rangle$ as

$$\begin{aligned} |\Psi\rangle &= \frac{1}{2}\,|1:+k;2:-k\rangle \otimes \Big(\mathrm{e}^{i\phi}\,|1:\downarrow;2:\uparrow\rangle + |1:\uparrow;2:\downarrow\rangle\Big) \\ &+ \frac{1}{2}\,|1:-k;2:+k\rangle \otimes \Big(|1:\downarrow;2:\uparrow\rangle + \mathrm{e}^{i\phi}\,|1:\uparrow;2:\downarrow\rangle\Big)\,, \end{aligned} \tag{1.90}$$

which leads, in the case of $\phi = 0$, to

$$\begin{aligned} |\Psi\rangle &= \frac{1}{\sqrt{2}}\,(|1:+k;2:-k\rangle + |1:-k;2:+k\rangle\,) \otimes \\ &\otimes \frac{1}{\sqrt{2}}\,(|1:\downarrow;2:\uparrow\rangle + |1:\uparrow;2:\downarrow\rangle\,)\,. \end{aligned} \tag{1.91}$$

We have separated the two degrees of freedom. Actually, in the experiment one decides to associate Alice to a particular momentum, for instance, $+k$, and Bob to the other one, $-k$. Consequently, we get from Eq. (1.90)

$$|\Psi\rangle \to |{+k}\rangle_A\,|{-k}\rangle_B \otimes \Big(|\uparrow\rangle_A\,|\downarrow\rangle_B + \mathrm{e}^{i\phi}\,|\downarrow\rangle_A\,|\uparrow\rangle_B\Big)\,, \tag{1.92}$$

where we can now trace over the external degree of freedom $\pm k$ and obtain the well-known EPR state $1/\sqrt{2}\,(|01\rangle + |10\rangle\,)$. In fact, the observers chose one of the variables to become a physical label in order to obtain distinguished subsystems. Note that it is necessary to have two variables in order to "promote" one of them to a label.

It is possible to exchange the role of the observables k and $\uparrow$ leading to entanglement in momentum and not in polarization, such that the state becomes

$$|\Psi\rangle \to |\uparrow\rangle_A\,|\downarrow\rangle_B \otimes \Big(|{+k}\rangle_A\,|{-k}\rangle_B + \mathrm{e}^{i\phi}\,|{-k}\rangle_A\,|{+k}\rangle_B\Big)\,. \tag{1.93}$$

Therefore, there is a complete duality between the two observables. This duality cannot be exploited with non-identical particles. An even more interesting feature is that, for $\phi \neq 0$, there is a complementarity between these two forms of entanglement. As for conjugate operators for which expectation values can not be measured simultaneously, one cannot use simultaneously the entanglement in both variables [74]. It is not the case for $\phi = 0$ leading to Eq. (1.91) where both entanglement in polarization and in momentum are accessible simultaneously. Such a state is called double-entangled and can be used to increase the security of quantum communication [75]. One can also find states entangled in all degrees of freedom in the same time, they are called hyper-entangled [76, 77, 78].

1.3.2 Particle entanglement

As we have seen in the previous section, it is impossible to use the separability criterion when dealing with identical particles because the Hilbert space of the whole system is no more a tensor product of two one-particle Hilbert spaces and $\mathcal{H}_{\mathrm{tot}} = \hat{S}_+\left[\mathcal{H}^{\otimes 2}\right]$. Let us introduce a new criterion of entanglement which fully takes into account this impossibility to assign a physical label to the particles. Starting from the idea of a physical reality associated to each particle, Ghirardi and Marinatto [49, 50] define that

Two identical subsystems S_1 and S_2 are not entangled when both subsystems possess a complete set of properties.

This definition can also be applied to non-identical particles as seen in Sec. 1.2.1. When considering a state $|\Psi\rangle$ describing the two combined subsystems, one of the subsystems possesses a complete set of properties iif we can find a one dimensional projector $\hat{P} \in B(\mathcal{H})$ such that

$$\langle\Psi| \hat{\mathcal{E}}_P |\Psi\rangle = 1, \tag{1.94}$$

where

$$\hat{\mathcal{E}}_P = \hat{P} \otimes \left(\mathbb{1} - \hat{P}\right) + \left(\mathbb{1} - \hat{P}\right) \otimes \hat{P} + \hat{P} \otimes \hat{P}. \tag{1.95}$$

From this one can show [49, 79], for two bosons, the following criterion of entanglement:

Two identical bosons are not entangled iif the state $|\Psi\rangle$ is obtained from the symmetrization of a tensor product of two orthogonal states or if the two bosons occupy the same state.

Bosonic Schmidt decomposition

In order to quantify the entanglement between two indistinguishable bosons, let us now see how one can perform a Schmidt decomposition of a state. The case of fermions follows the same procedure with some subtle differences. Because in this thesis we are dealing with photons, we will not give details for fermionic systems and refer the interested reader to Refs. [80, 81].

Similarly to the high-dimensional state in Eq. (1.73), consider the general two-boson state written in first quantization

$$|\Psi\rangle = \sum_{ij}^{N\times N} C_{ij} |1:i; 2:j\rangle = \sum_{ij}^{N\times N} C_{ij} |i\rangle_1 |j\rangle_2 , \tag{1.96}$$

where the labels 1 and 2 have no physical meaning. Due to the symmetrization, $C_{ij} = C_{ji}$ so that the matrix C is symmetric ($C = C^T$). Using the SVD decomposition with symmetric matrices, one can show that

$$|\Psi\rangle = \sum_k \sqrt{\lambda_k} |u_k\rangle_1 |u_k\rangle_2 , \tag{1.97}$$

where $\{|u_k\rangle\}_k$ is an orthonormal basis associated with the one-boson Hilbert space. Note that we have a sum of terms where the two bosons are in the same state. As for the case of distinguishable particles, the Schmidt eigenvalues λ_k are positive and real numbers satisfying the normalization constraint $\sum_k \lambda_k = 1$. They also correspond to the eigenvalues of the reduced density matrix, but here we cannot associate this matrix with a specific particle. We still define the Schmidt rank R_{Schmidt} as the number of non-vanishing eigenvalues. However, contrary to the case of distinguishable particles, R_{Schmidt} is not enough to say if a state is entangled or not. Indeed, the following possibilities exist:

(a) $R_{\text{Schmidt}} = 1$ $(E(\Psi) = 0)$ $\Rightarrow |\Psi\rangle$ is not entangled.

(b) $R_{\text{Schmidt}} = 2$ and $E(\Psi) = \ln 2 \Rightarrow |\Psi\rangle$ is not entangled *because it is obtained from the symmetrization of the tensor product of two orthogonal states.*

(c) $R_{\text{Schmidt}} = 2$ and $0 < E(\Psi) < \ln 2 \Rightarrow |\Psi\rangle$ is entangled *because it is obtained from the symmetrization of the tensor product of two non-orthogonal states.*

(d) $R_{\text{Schmidt}} > 2 \Rightarrow |\Psi\rangle$ is entangled *because it is obtained from the symmetrization of a sum of product states.*

It appears that one needs to analyze a combination of both the Schmidt rank and a measure of entanglement to show the existence of entanglement in identical-particle states. Positive entropy does not necessary imply entanglement even if it is associated with an uncertainty in the one-particle state. Indeed, in the situation (b), positive entropy is due to the uncertainty implied by the symmetrization and not to entanglement.

In this thesis, we will mainly use second quantization framework. However, Eqs. (1.96) and (1.97) for which we introduced criteria of entanglement are written in the first quantization. In fact, both are equivalent when dealing with particle entanglement and the same conclusions hold for a state written as

$$|\Psi\rangle = \frac{1}{\sqrt{2}} \sum_{ij}^{N\times N} C_{ij} \hat{a}_i^\dagger \hat{a}_j^\dagger |0\rangle \,, \tag{1.98}$$

where the factor $\frac{1}{\sqrt{2}}$ allows to have, as for the first quantization, the normalization constraint $\mathrm{Tr} C^\dagger C = 1$. The Schmidt decomposition is then

$$|\Psi\rangle = \frac{1}{\sqrt{2}} \sum_k \sqrt{\lambda_k} \left(\hat{b}_k^\dagger\right)^2 |0\rangle \,, \tag{1.99}$$

where $\hat{b}_k^\dagger |0\rangle = |u_k\rangle$.

With these tools it is now possible to study particle entanglement. The main difference between distinguishable and indistinguishable particle entanglement lies at the lower bound of the entropy. A positive entropy implies entanglement for distinguishable particles but not for indistinguishable ones. The upper bound do not exhibit any difference; a maximally entangled state in the case of indistinguishable particles is

$$\begin{aligned} |\Psi_{\max}\rangle &= \frac{1}{\sqrt{N}} \sum_k^N |u_k\rangle_1 |u_k\rangle_2 \\ &= \frac{1}{\sqrt{2N}} \sum_k^N \left(\hat{b}_k^\dagger\right)^2 |0\rangle \,, \end{aligned} \tag{1.100}$$

in both first and second quantization, with an entropy $E(\Psi_{\max}) = \ln N$.

1.3.3 Mode entanglement

Hilbert space construction

We will now discuss what is called mode entanglement as introduced in the beginning of Sec. 1.3. Let us come back to the two-photon case introduced above. Instead of particles, modes are now the subsystems. Consider two different modes referred to as α and β. The Fock state basis of this system of two photons is

$$\{|1_\alpha, 1_\beta\rangle, |0_\alpha, 2_\beta\rangle, |2_\alpha, 0_\beta\rangle\}. \tag{1.101}$$

The system is constraint by a super-selection rule (SSR) [82, 83] on the total photon number operator $\hat{N} = \hat{n}_\alpha \otimes \mathbb{1}_\beta + \mathbb{1}_\alpha \otimes \hat{n}_\beta$, i.e. the number of photons can locally change but not globally, here fixed to $\langle \hat{N} \rangle = 2$. Due to this restriction, the total Hilbert space cannot be constructed as a simple tensor product and is given by $\mathcal{H}_{\rm tot} = \bigoplus_{n=0}^{2}(\mathcal{H}_n^\alpha \otimes \mathcal{H}_{2-n}^\beta)$ where $\mathcal{H}_n^\alpha$ is the one -dimensional Hilbert space associated to the basis $\{|n_\alpha\rangle\}$ [84]. The total photon number SSR strongly reduces the accessible Hilbert space compared to the one obtained with a tensor product $\mathcal{H}^\alpha \otimes \mathcal{H}^\beta$ where $\mathcal{H}^\alpha = \{|0_\alpha\rangle, |1_\alpha\rangle, |2_\alpha\rangle\}$. Here again, even if the subsystems – two different modes – are well distinguished the structure of the Hilbert space is not obvious and presents some constraints as in the case of subsystems made of identical particles.

One can extend this Hilbert construction to systems containing N photons. Then the total Hilbert space is defined by $\mathcal{H}_{\rm tot}^N = \bigoplus_{n=0}^{N}(\mathcal{H}_n^\alpha \otimes \mathcal{H}_{N-n}^\beta)$ with $\dim\mathcal{H}_{\rm tot} = N+1$.

Schmidt decomposition in the photon-number basis

A state $|\Psi\rangle \in \mathcal{H}_{\rm tot}^N$ can be written as

$$\begin{aligned} |\Psi\rangle &= \sum_{n=0}^{N} \frac{\sqrt{\lambda_n}}{\sqrt{n!\,(N-n)!}} \left(\hat{a}_\alpha^\dagger\right)^n \left(\hat{a}_\beta^\dagger\right)^{N-n} |0\rangle \\ &= \sum_{n=0}^{N} \sqrt{\lambda_n}\, |n_\alpha, (N-n)_\beta\rangle \\ &= \sum_{n=0}^{N} \sqrt{\lambda_n}\, |n\rangle_\alpha\, |(N-n)\rangle_\beta\,. \end{aligned} \tag{1.102}$$

We recognize a Schmidt decomposition in the photon-number basis with the Schmidt eigenvalues λ_n. The modes α and β are entangled; if one measures n photons in the mode α, the mode β is projected into the state $|N-n\rangle$. The absence of a double sum in the expression of the state is due to the fixed total number of photon. However, it is possible to write this state in basis different than the Fock state basis, e.g., in the basis of coherent states [82]:

$$|\Psi\rangle = \frac{1}{\pi^2}\int d^2\nu d^2\nu' c_{\nu\nu'}\, |\nu\rangle_\alpha\, |\nu'\rangle_\beta\,, \tag{1.103}$$

where $|\nu\rangle$ is a coherent state and $c_{\nu\nu'} = \sum_n^N \sqrt{\lambda_n}\langle \nu\,|n\rangle\,\langle \nu'\,|N-n\rangle$. Equation (1.103)is not a Schmidt decomposition but SSR are still present and constrain the moduli of ν and ν' which are not independent. As for particle entanglement where one can change the subsystem basis, for example, going from plane waves to Hermite-Gauss modes, in mode entanglement the subsystem basis can also be changed from Fock states to coherent states, for instance.

Actually the only states which do not exhibit mode entanglement have the form $|n_\alpha, (N-n)_\beta\rangle$ whereas the maximally entangled state is given by

$$|\Psi\rangle_{\rm max} = \frac{1}{\sqrt{N+1}}\sum_{n=0}^{N} |n\rangle_\alpha\, |(N-n)\rangle_\beta\,, \tag{1.104}$$

with an entropy of entanglement (see Eq. (1.80)) $E\left(\Psi_{\max}\right)=\ln\left(N+1\right)$.

The $N00N$ state

$$|\Psi\rangle_{N00N}=\frac{1}{\sqrt{2N!}}(\hat{a}_{\alpha}^{\dagger N}+\hat{a}_{\beta}^{\dagger N})\,|0\rangle \tag{1.105}$$

is sometimes referred to as a maximally entangled state. This seems to be in contradiction with what we said previously but one can reduce the space of N particles by considering only two possibilities 0 or N for the particle number. Then in this "qubit" space, the $N00N$ state is a Bell state of two qubits and, consequently, it is maximally entangled. These states are most interesting for quantum lithography and metrology rather than for quantum information because they can reach the Heisenberg limit in phase sensitive measurements [85, 86].

To summarize, as for particle entanglement, it is possible to extend the use of the Schmidt decomposition to characterize mode entanglement and to use entanglement measures like the entropy and the Schmidt number. It has been done, for example, in the case of two-mode Bose-Einstein condensates in Ref. [45].

Sub-algebra

Because the mode entanglement implies necessarily the second quantization, a quite recent approach has been put forward by the authors of Refs. [87, 79]. Using a sub-algebra bipartition based on the operators instead of the states, they describe the entanglement between two sets of modes in the following way.

Consider two sub-set of modes $I_1=\{i,...,j\}$ and $I_2=\{\alpha,...,\beta\}$ that partition the whole set of modes I. For instance, in the previous two-mode case, we have $I=\{\alpha,\beta\}$, $I_1=\{\alpha\}$ and $I_2=\{\beta\}$. Each set I_i is associated with a sub-algebra of operators $\mathcal{A}_i\subset\mathcal{A}$ generated by the operators of second quantization acting on the sub-set I_i, i.e. $\{\hat{a}_k,\hat{a}_k^\dagger\}_{k\in I_i}$, where $\mathcal{A}$ is the algebra generated by all the operators of second quantization. $(\mathcal{A}_1,\mathcal{A}_2)$ is a bipartition of $\mathcal{A}$ if any operators $\hat{A}_1\in\mathcal{A}_1$ and $\hat{A}_2\in\mathcal{A}_2$ commute. Note that $\hat{A}_i\in\mathcal{A}_i$ means that $\hat{A}_i$ can be any polynomial in creation and annihilation operators acting on the set of modes I_i.

A state $|\Psi\rangle$ is considered separable with respect to $(\mathcal{A}_1,\mathcal{A}_2)$ when

$$\langle\Psi|\,\hat{A}_1\hat{A}_2\,|\Psi\rangle\;=\;\langle\Psi|\,\hat{A}_1\,|\Psi\rangle\;\langle\Psi|\,\hat{A}_2\,|\Psi\rangle\;, \tag{1.106}$$

for all $\hat{A}_i\in\mathcal{A}_i$. From this it follows that $|\Psi\rangle$ is $(\mathcal{A}_1,\mathcal{A}_2)$-separable iif it is generated by a $(\mathcal{A}_1,\mathcal{A}_2)$-local operator $\hat{A}_1^\dagger\hat{A}_2^\dagger$, i.e.

$$|\Psi\rangle\;=\hat{A}_1^\dagger\hat{A}_2^\dagger\,|0\rangle\;, \tag{1.107}$$

where $\hat{A}^\dagger$ is a polynomial of creation operators only. Otherwise $|\Psi\rangle$ is entangled with an entanglement between the two sets of modes. It is straightforward to see that following this criterion, the mode entanglement depends on the set of modes considered. Indeed, entanglement present in a quantum system is strongly dependent on the choice of the subsystems [88].

1.3.4 Two-photon in quantum optics

Let us now illustrate the two forms of entanglement – entanglement of particles and of modes – with two-photon states frequently encountered in quantum optics.

- $|1_i, 1_j\rangle = \hat{a}_i^\dagger \hat{a}_j^\dagger |0\rangle$, $i \neq j$

  Applying the criterion of Ghirardi *et al* [49], this state is obviously obtained from the symmetrization of a product of two orthogonal states. Writing the state as in Eq. (1.96), its associated C matrix is

$$C = \begin{pmatrix} 0 & \frac{1}{\sqrt{2}} \\ \frac{1}{\sqrt{2}} & 0 \end{pmatrix}, \tag{1.108}$$

  which leads to $\lambda_k = \{1/\sqrt{2}, 1/\sqrt{2}\}$ and $R_{\text{Schmidt}} = 2$, $E(\Psi) = \ln 2$.
  Then it does not contain any particle entanglement even if there are correlations between the two particles due to the symmetrization.

  In terms of mode entanglement, this state does not exhibit any entanglement because it verifies Eq. (1.107). This is consistent with its Schmidt decomposition in the photon-number basis which contains a single Schmidt eigenvalue.

- $\frac{1}{\sqrt{2}}\left(|0_\alpha, 2_\beta\rangle + |2_\alpha, 0_\beta\rangle\right) = \frac{1}{\sqrt{2}}\left(\frac{\left(\hat{a}_\alpha^\dagger\right)^2}{\sqrt{2}} + \frac{\left(\hat{a}_\beta^\dagger\right)^2}{\sqrt{2}}\right)|0\rangle$

  This state is already written as a Schmidt decomposition in the mode basis following Eq. (1.99). Its Schmidt eigenvalues are $\lambda_k = \{1/\sqrt{2}, 1/\sqrt{2}\}$, meaning that it is not entangled in terms of particles according to Ghirardi *et al* [49].

  However, this state contains mode entanglement [64] because it cannot be written in the form of Eq. (1.107). In the photon-number basis, we also have $\lambda_k = \{1/\sqrt{2}, 1/\sqrt{2}\}$ but there it implies entanglement because the modes are two distinguishable subsystems.

The fact that for $|\phi_1\rangle = |1_i, 1_j\rangle$ and $|\phi_2\rangle = \frac{1}{\sqrt{2}}\left(|0_\alpha, 2_\beta\rangle + |2_\alpha, 0_\beta\rangle\right)$ the Schmidt eigenvalues are equal when considering particle entanglement is not surprising. Indeed, $|\phi_2\rangle$ can be obtain from $|\phi_1\rangle$ by a unitary local operation acting on the two photons, given by the relations

$$\begin{aligned} \hat{a}_i^\dagger &= \frac{1}{\sqrt{2}}\left(\hat{a}_\alpha^\dagger + i\hat{a}_\beta^\dagger\right) \\ \hat{a}_j^\dagger &= \frac{1}{\sqrt{2}}\left(\hat{a}_\alpha^\dagger - i\hat{a}_\beta^\dagger\right) \end{aligned} \tag{1.109}$$

This unitary transformation is frequently encountered when using a $50:50$ beam splitter with $|\phi_1\rangle$ in input and $|\phi_2\rangle$ in output. This also shows that a linear optical device can create mode entanglement. What appears to be a LOCC for particle entanglement can be non-local for modes, i.e. the mode splitting operation of Eq. (1.109) can create mode entanglement [65].

- $|\uparrow, \downarrow\rangle_{k_\alpha}$

  We can write this state as

$$|1_{k_\alpha\uparrow}, 1_{k_\alpha\downarrow}\rangle = 1/\sqrt{2}(|1:\uparrow; 2:\downarrow\rangle + |1:\downarrow; 2:\uparrow\rangle) \otimes |1:k_\alpha; 2:k_\alpha\rangle\,,$$

  thus it is quite similar to $|1_i, 1_j\rangle$. According to Plenio and coworkers [29], it is possible to extract useful entanglement from this state and thus the authors of [29] claim that symmetrization entanglement, i.e. entanglement between the pseudo-labels, is a resource for quantum information tasks. To justify that they consider a mode splitting operation $\hat{a}^\dagger_{k_\alpha s} \to r\hat{a}^\dagger_{k_i s} + t\hat{a}^\dagger_{k_j s}$, where s corresponds to $\uparrow$ or $\downarrow$ with $|r|^2 + |t|^2 = 1$. This operation transfers the pseudo-label entanglement into mode entanglement. Taking only the cross term rt, after this operation the state becomes $|\uparrow\rangle_i |\downarrow\rangle_j + |\downarrow\rangle_i |\uparrow\rangle_j$ which exhibits entanglement between the modes i and j. The authors of [29] state that there is no creation of entanglement in this operation even if it is an non-local operation. The entanglement of the output state – beared by modes – was already present before the operation in the pseudo-labels and consequently the state $|\uparrow, \downarrow\rangle_{k_\alpha}$ is entangled.

This situation is clearly different from the one where we go from $|1_i, 1_j\rangle$ to $\frac{1}{\sqrt{2}}\left(|0_\alpha, 2_\beta\rangle + |2_\alpha, 0_\beta\rangle\right)$ by the same type of mode splitting. Here we only have one degree of freedom per particles whereas in the Plenio and coworkers' case there are two degrees of freedom, one is splitted to be entangled – the modes k – and the other one – the polarizations – is the correlated variable. We find as for the EPR-Bohm entangled state in Sec. 1.3.1 the necessity to have two variables. Then there is no contradiction between the different conclusions concerning the entanglement of these states.

- $\frac{1}{\sqrt{2}}\left(|1_\alpha, 0_\beta\rangle + |0_\alpha, 1_\beta\rangle\right)$

  Finally, we introduce a $N00N$-state with only one particle, $N = 1$. This state can be prepared by sending a single photon in one arm of a beam splitter.

  Obviously there is no particle entanglement. However, there is a strong controversy concerning the mode entanglement [89, 90, 91, 92, 93]. Indeed this state presents some non-locality but, is it a classical-wave type of non-locality or a Bell non-locality? Several experiments where Bell inequality has been violated argue that this state is truly entangled [94, 95, 96, 97, 98].

The above examples shows that while the pure bipartite entanglement of distinguishable particles is well understood in textbooks, it is not at all the case when dealing with identical particles that often appear in real physical schemes.

Chapter 2

Statistical approach to the multiple scattering of light

2.1 Wave propagation in disordered media

2.1.1 Speckle pattern

When a coherent radiation propagates through or is reflected on a random medium, one observes a random interference pattern called a speckle pattern [99] as shown in Fig. 2.1a. Speckles may appear with various kind of waves, like sound waves, visible light or matter waves. In the following, we restrict our study to light. A speckle pattern is a succession of bright and dark spots in the detection plane which can be either in the far or in the near field of the random medium. These spots correspond respectively to constructive and destructive interferences of scattered waves (see Fig. 2.1b).

Formally, during the propagation, the radiation "follows" a lot of random paths as depicted in Fig. 2.1b leading to a scattered field E (in the scalar approximation) described by a coherent superposition of random complex amplitudes

$$E\left(x,y,t\right)=\sum_{n=1}^{N}a_n\left(x,y,t\right)\mathrm{e}^{i\phi_n\left(x,y,t\right)}, \tag{2.1}$$

where a_n and ϕ_n are random amplitudes and phases. Then interferences appear when measuring the intensity $I\left(x,y,t\right)=\left|E\left(x,y,t\right)\right|^2$ given by

$$I\left(x,y,t\right)=\sum_{i=1}^{N}\left|a_n\left(x,y,t\right)\right|^2+\underbrace{\sum_{i\neq j}a_i\left(x,y,t\right)a_j^*\left(x,y,t\right)\mathrm{e}^{i\left(\phi_i\left(x,y,t\right)-\phi_j\left(x,y,t\right)\right)}}_{\text{Interference term}}. \tag{2.2}$$

In the case of fully coherent radiation and large number of scatterers randomly distributed in space, the central limit theorem ensures that the probability density of intensity distribution is negative exponential

$$P\left(I\right)=\frac{1}{\bar{I}}\exp\left(-I/\bar{I}\right), \tag{2.3}$$

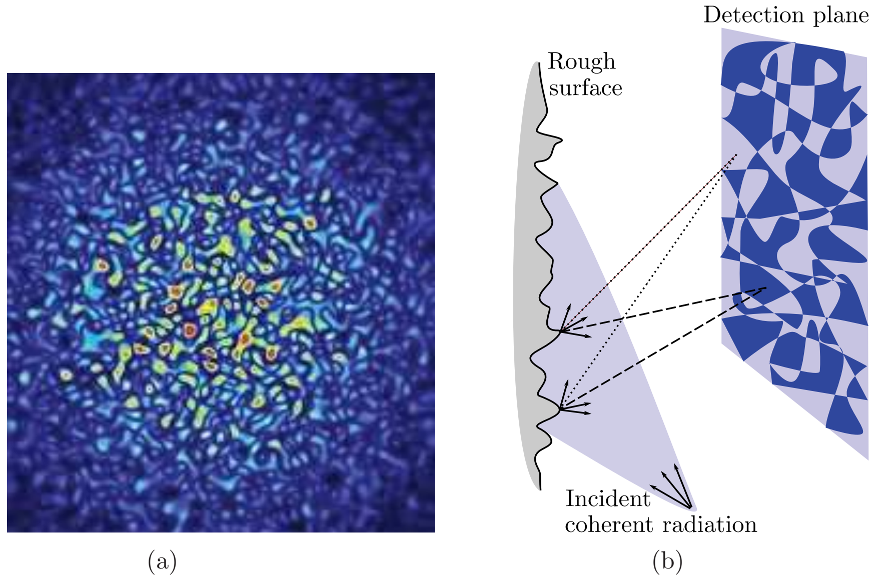

Figure 2.1: (a) Coherent light speckle pattern from Prof. Shpyrko's group [] (b) Sketch of a speckle experiment using the reflection of a coherent source on a rough surface. Two amplitudes involved in constructive interferences giving a bright spot of high intensity (dotted line). Two amplitudes which interfere destructively leading to a dark spot of low intensity (dashed line).

where $\overline{I}$ is the intensity averaged over different realizations of disorder. This distribution, also called the Rayleigh distribution, leads to a maximal visibility or contrast, defined by $\overline{I^2}/\overline{I} - 1$, equal to one. As we mentioned above, this distribution arises from the central limit theorem. Indeed, the scattered field in Eq. (2.1) can be seen as an infinite sum of independent random terms following the same statistics. Then its real and imaginary parts follow a Gaussian distribution which leads to the negative exponential distribution for intensity.

Generally one studies stationary speckle patterns but time-varying speckle patterns due to the motion of scatterers in the disordered medium or to a time dependent incident light can also take place and are used for dynamic imaging. Intensity speckle, also refereed to as one-photon speckle, has been widely studied [100, 99] during the past century and especially after the discovery of coherent laser light. It is seen either as a drawback or an advantage depending on the applications. For coherent imaging, the speckle pattern decreases the resolution and the contrast of images [101]. Then, one tries to suppress the speckles by various methods [99] like polarization or wavelength diversity, temporal averaging, etc. However speckle patterns are sometimes really helpful to obtain information either on the disorder media or on an object located behind the disorder, e.g. a star imaged from ground-based telescopes [102, 103]. Below we give a couple of examples of applications where speckles are used.

Astronomical speckle interferometry, introduced in 1970 by A. Labeyrie [104], is based on a Fourier analysis of several short exposure images of stars taken at different times from a ground-based telescope. Each image contains a unique speckle pattern as a consequence of the turbulent motion of the atmosphere which randomly modifies the wave front of the radiation coming from the space. Performing a Fourier transform on the images and adding the Fourier intensities, allows one to obtain the Fourier image of the object under study and obtain diffraction limited resolution. A lot of twins stars have been discovered using this method.

Another interesting application developed for bio-medical imaging is the laser speckle contrast imaging [105, 106]. The idea is to access the dynamics of the scatterers in a turbid medium through the contrast of the speckle. Because the exposure time is finite and the medium evolves during this time, the image is the sum of several slightly different speckle patterns. Then, the more blurred is the image the faster the dynamics of the scatterers. Biologists use this methods to observe the evolution of the blood flow in cortical vessels shining a coherent laser source through the skull.

One-photon speckle is related to the spatial or time fluctuations of intensity due to single-photon interferences. Besides, one introduces the two-photon speckle which corresponds to the random pattern of the coincidence counting rate and related to the so-called two-photon interferences. Since several years, this kind of speckle attracts more and more attention because it should contain information on the quantumness of the incident radiation. However, it is experimentally challenging to measure because two detectors have to scan the region of interest. We will study this kind of speckle pattern in Chapter 3.

2.1.2 Length scales and regimes of propagation

Length scales

Although very complex, the propagation of a wave in a random medium is well described by few simple parameters. The first one is obviously the size L of the medium in the direction of propagation. Then comes the central wavelength $\overline{\lambda}$ of the wave.

The most important length scale is the scattering mean free path ℓ which quantifies the average distance between two scattering events. For an ensemble of scatterers with a scattering cross-section σ and low number density n_i, the mean free path is given by

$$\ell = \frac{1}{n_i \sigma}. \tag{2.4}$$

In this thesis, we are not taking into account absorption, then the absorption length verifies $L_{\text{abs}} \gg L$. In the same way, the coherence of the wave is not affected by the propagation, i.e. the coherence length L_{coh} can be considered infinite.

Regimes of propagation

When a wave propagates through a three-dimensional disordered medium, depending on the relation between the length scales, different regimes of propagation appear.

When $\ell \gg L$, the propagation is ballistic and the wave does not "see" the medium. If ℓ is getting close to L, one enters in the single scattering regime where only one scattering event happens at most. In the opposite situation, $\ell \ll L$, the wave undergoes a lot of scattering events during the propagation. This regime is the one we are interested in and is called the multiple-scattering regime. Because of its inherent complexity, the multiple-scattering has to be treated statistically so that one is interested in quantities like the average intensity and its higher moments, for instance.

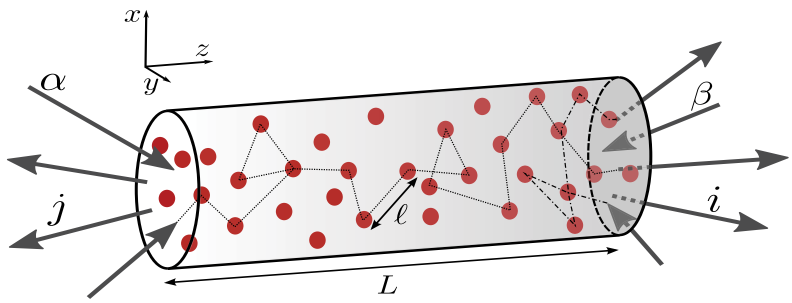

Figure 2.2: Sketch of a disordered waveguide of cross-section of area A and length $L \gg \sqrt{A}$ and $L \gg \ell$, where ℓ is the mean free path. The incoming and outgoing modes are respectively denoted by Greek and Roman lettering.

Considering the multiple-scattering regime $\ell \ll L$, one can compare the other length scales leading to the following situations:

- $\overline{\lambda} \ll \ell$: This situation corresponds to weak disorder and diffusive propagation. The propagation can be seen as a random walk of photons and the average intensity obeys a diffusion equation. This thesis mostly deals with this regime of propagation where one observes the coherent backscattering cone, the universal conductance fluctuations and the long-range correlations in the speckle pattern.
- $\overline{\lambda} \lesssim \ell$: The transport becomes coherent and the diffusion description of propagation starts to break down. Then, one observes sizable corrections to the random walk model of photon transport. It is the regime of weak localization.
- $\overline{\lambda} > \ell$: The disorder is strong and the diffusion vanishes. One enters into the regime of Anderson localization, first introduced in 1958 by P. W. Anderson for electrons in metals [3].

2.1.3 Scattering matrix

Here we present a description of scattering in terms of the scattering matrix S. For simplicity, until the end of this chapter, we deal with a quasi-one-dimensional (Q1D) geometry such as a waveguide. We consider a linear and elastically scattering disordered medium of length L and cross-section area A such that $L \gg \sqrt{A}$ as shown in Fig. 2.2. Similar to a cavity, this waveguide supports a certain number of transverse modes for a given central frequency $\overline{\omega}$ of the light. We recall that a transverse mode is the association $\{\mathbf{k}_\perp, s\}$ where $\mathbf{k}_\perp = \{k_x, k_y\}$ and s is the polarization of the light. The number of modes N is given by $N = N(\overline{\omega}) = 2 \times k(\overline{\omega})^2 A/2\pi$, where the factor 2 in the numerator takes into account the two orthogonal polarization of light. Then, we associate to the medium a $2N \times 2N$-dimensional scattering matrix S with elements $S_{i\alpha}$. It is convenient to write S as a block matrix

$$S = \begin{pmatrix} r & t' \\ t & r' \end{pmatrix}, \tag{2.5}$$

where the $N \times N$ matrices r (r') and t (t') are respectively the reflection matrix from left to left (right to right) and the transmission matrix from left to right (right to left), with elements $r_{i\alpha}$ ($r'_{i\alpha}$) and $t_{i\alpha}$ ($t'_{i\alpha}$). Because we are not considering absorption and amplification, the energy conservation implies that S is unitary, $S^\dagger S = SS^\dagger = \mathbb{1}$. Consequently the matrices $t^\dagger t$, $t'^\dagger t'$, $\mathbb{1} - r^\dagger r$ and $\mathbb{1} - r'^\dagger r'$ possess the same set of eigenvalues $\{\tau_1, \tau_2, ..., \tau_N\}$. These eigenvalues are called transmission eigenvalues. They are real numbers between 0 and 1. We will come back to this set of eigenvalues when dealing with the S-matrix approach in Sec. 2.3.

The scattering matrix S couples the $2N$ incoming modes to the $2N$ outgoing modes. In terms of field operators we have the input-output relation

$$\begin{aligned} \hat{a}_i(\omega) &= \sum_{\alpha=1}^{2N} S_{i\alpha}(\omega)\,\hat{a}_\alpha(\omega) \\ &= \sum_{\alpha=1}^{N} t_{i\alpha}(\omega)\,\hat{a}_\alpha(\omega) + \sum_{\beta=1}^{N} r'_{i\beta}(\omega)\,\hat{a}_\beta(\omega)\,, \end{aligned} \tag{2.6}$$

where the complex numbers $t_{i\alpha}$ and $r_{i\beta}$ are respectively the transmission and reflection coefficients. Introducing the vectors of operators $\hat{a}_{\text{out}} = (\hat{a}_i)_{i\in[1,2N]}$ and $\hat{a}_{\text{in}} = (\hat{a}_\alpha)_{\alpha\in[1,2N]}$ we have

$$\hat{a}_{\text{out}} = S\hat{a}_{\text{in}}. \tag{2.7}$$

The derivation of this relation has been explained in Sec. 1.1.1 where the quantization of the electromagnetic field in an open medium has been treated. From Eq. (2.6) and because the coefficients $t_{i\alpha}$ and $r_{i\beta}$ fluctuate from one realization to another, the disordered medium can be seen as a multi-port beam splitter. This feature allows using the disordered medium as a random interferometric system within which the light acquires random phase shifts.

The matrix S is extremely complex and sensitive to the particular realization of the disorder. It should be characterized by its statistical properties and view as a random matrix. In addition, it is often a large matrix ($N \gg 1$) so that standard methods of random matrix theory can be applied to it (see Sec. 2.3).

2.2 Diagrammatic approach

In this section we present a microscopic diagrammatic approach based on the Green's function formalism. It has the advantage of describing how the wave behaves in the medium and then gives a nice physical picture of the multiple scattering process. However it is a perturbative method and can rapidly lead to very tedious calculations. We refer the reader interested in to the very complete book of Akkermans and Montambaux [4] and references therein.

First, let us introduce some important notions and quantities used to describe the light propagation in a random medium.

2.2.1 Transmittances

According to the notations of Sec. 2.1.3 we define the following transmittances.

- *Intensity transmission coefficient* $T_{b\alpha}$: This coefficient is defined as the ratio between the energy carried away in the mode b by the scattered wave and the energy incoming in the mode α. It writes $T_{b\alpha} = |t_{b\alpha}|^2$.

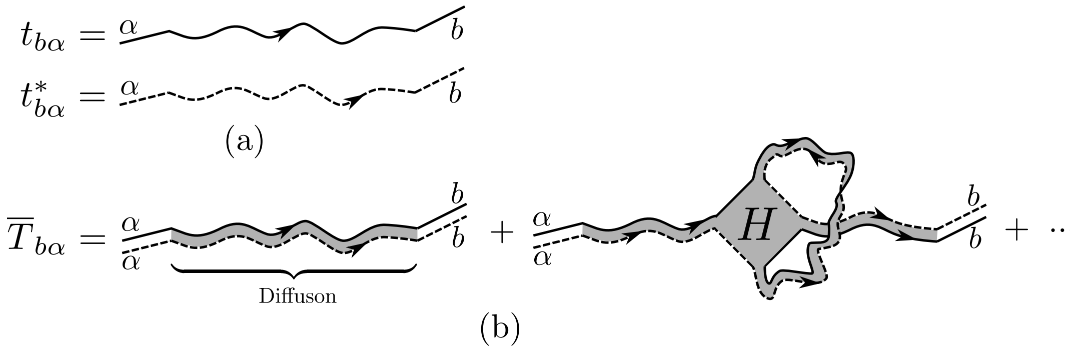

Figure 2.3: (a) Diagrams representing the transmission coefficient and its complex conjugate. (b) Diagrammatic expansion of the average intensity transmission coefficient. The first contribution is in r.h.s. of $\overline{T_{b\alpha}}$ is the product of three terms. The first one describes the entrance of the wave in the medium leading to the transition from ballistic to diffusive propagation. The second one, called diffuson, denoted by the gray part, describes the diffusive propagation. The third term is equivalent to the first and describes the exit from the medium. The second contribution in the r.h.s. is constructed similarly but contains a Hikami box describing interferences taking place in the medium. It leads to the first weak localization correction (see Ref. [4] for more details).

- *Total transmission coefficient* T_α: Defined by $T_\alpha = \sum_b T_{b\alpha}$, it corresponds to the situation where one measures all the outgoing modes using an integrating sphere. Note that the total transmission coefficients are the diagonal elements of the matrix $tt^\dagger$.

- *Conductance* T: It is defined by the sum of the intensity transmission over all the modes $T = \sum_\alpha T_\alpha = \sum_{\alpha b} T_{b\alpha}$. The term conductance comes from the electronic transport because in electronic systems T is equal to the conductance of the sample in units of e^2/h.

2.2.2 From the Green's function to the transmission coefficient

The starting point of the diagrammatic approach is the expression of the transmission coefficient $t_{\alpha b}$ in terms of the Green's function [4]:

$$t_{b\alpha} = i\sqrt{k_\alpha k_b} G^{\mathrm{R}}_{\alpha b}(0, L) \tag{2.8}$$

leading to

$$T_{b\alpha} = k_\alpha k_b |G^{\mathrm{R}}_{\alpha b}(0, L)|^2, \tag{2.9}$$

where k_α (k_b) is the projection of $\mathbf{k}_\alpha$ ($\mathbf{k}_b$) on the z-axis. $G^{\mathrm{R}}_{\alpha b}(0, L)$ is the retarded Green's function of the Helmholtz equation and it describes the propagation from the incident plane ($z = 0$) to the outgoing plane ($z = L$) for the modes α and b. For a wave propagating in a mode α, the Green's function is given by

$$G^R_\alpha(\mathbf{r}, \mathbf{r}') = -\frac{ik_\alpha}{4\pi} \exp\left(ik_\alpha |\mathbf{r} - \mathbf{r}'|\right), \text{ in } 1D, \tag{2.10}$$

$$G^R_\alpha(\mathbf{r}, \mathbf{r}') = -\frac{1}{4\pi|\mathbf{r} - \mathbf{r}'|} \exp\left(ik_\alpha |\mathbf{r} - \mathbf{r}'|\right), \text{ in } 3D. \tag{2.11}$$

Let us average Eq. (2.9) over disorder. It is convenient to represent this average with diagrams following the rules depicted in the Fig. 2.3. $\overline{T}_{b\alpha}$ is made of different contributions. The first diagram corresponds to the incoherent propagation of light, in the sense that no interferences are taking place in the medium. It can be written as

$$\int d\mathbf{r}_1 d\mathbf{r}_2 \left|\overline{G}_\alpha^R(0,\mathbf{r}_1)\right|^2 \Gamma_D(\mathbf{r}_1,\mathbf{r}_2) \left|\overline{G}_b^R(\mathbf{r}_2,L)\right|^2, \tag{2.12}$$

where the average Green's function is given by $\overline{G}_\alpha^R(\mathbf{r},\mathbf{r}') = G_\alpha^R(\mathbf{r},\mathbf{r}')\exp(-|\mathbf{r}-\mathbf{r}'|/2\ell)$ and $\Gamma_D(\mathbf{r}_1,\mathbf{r}_2)$ is the sum of ladder diagrams [1] and corresponds to the so-called diffuson [4]. The intensity given by this term satisfies the diffusion equation. The second diagram, smaller than the first one, arises from interferences surviving the average over the disorder and is described by the Hikami box. The weight of this term is related to the probability of having two diffusons crossing each other. This probability seen as the ratio between the "volume" of a diffuson $\lambda^2 L^2/\ell$ and the volume of the medium LA is approximately given by $L/N\ell$. Other terms involving several crossings follow but are not depicted in Fig. 2.3. In the diffusive regime, i.e., neglecting diagrams containing interferences, the average intensity transmission coefficient is $\overline{T_{b\alpha}} = \frac{l}{NL}$. It follows that $\overline{T_\alpha} = \frac{l}{L}$ and $\overline{T} = g = \frac{Nl}{L}$ where we introduced the average dimensionless conductance g.

We see that the weight of the second diagram containing the Hikami box is actually $1/g$. Therefore, considering the diffusive regime is equivalent to $g \gg 1$. As g is getting close to one, interferences become more and more important leading to the weak localization correction to transport. The regime of Anderson localization is reached when $g \simeq 1$, the wave being localized, the transport strongly reduced, and the dimensionless conductance being low.

2.2.3 Correlation function

We consider now the correlation function of the fluctuations of $T_{b\alpha}$ defined by

$$C_{\alpha b,\alpha' b'} = \frac{\overline{\delta T_{b\alpha}\delta T_{b'\alpha'}}}{\overline{T_{b\alpha}}\ \overline{T_{b'\alpha'}}}, \tag{2.13}$$

where $\delta T_{b\alpha} = T_{b\alpha} - \overline{T}_{b\alpha}$. It is usually decomposed as [4]

$$C_{\alpha b,\alpha' b'} = C^{(1)} + C^{(2)} + C^{(3)}. \tag{2.14}$$

In the case of a monochromatic incident wave, the correlation functions $C^{(1)}$, $C^{(2)}$ and $C^{(3)}$ are given by [4]

$$C^{(1)} = \delta_{\Delta\alpha\Delta b} F_1(\Delta\alpha L), \tag{2.15}$$

$$C^{(2)} = \frac{1}{g}\left(F_2(\Delta\alpha L) + F_2(\Delta b L)\right), \tag{2.16}$$

$$C^{(3)} = \frac{2}{15g^2}, \tag{2.17}$$

where $\Delta\alpha = |\mathbf{k}_{\alpha\perp} - \mathbf{k}_{\alpha'\perp}|$ and $\Delta b = |\mathbf{k}_{b\perp} - \mathbf{k}_{b'\perp}|$ and with

$$F_1(x) = \left|\frac{x}{\sinh x}\right|^2, \tag{2.18}$$

$$F_2(x) = \frac{\sinh(2x) - 2x}{2x\sinh(x)}. \tag{2.19}$$

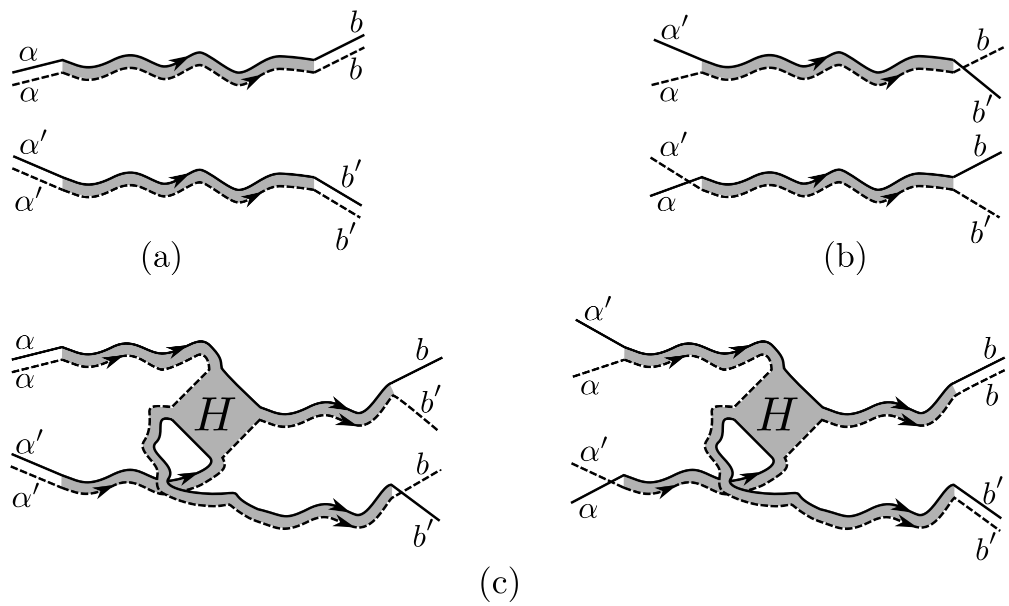

Figure 2.4: Diagrams contributing to the correlation function $C_{\alpha b,\alpha' b'}$. (a) Diagram associated to the product $\overline{T}_{b\alpha}\overline{T}_{b'\alpha'} = \overline{T}^2_{b\alpha}$ used in the definition of $C_{\alpha b,\alpha' b'}$. (b) Diagram leading to the correlation $C^{(1)}$. (c) The two diagrams involved in the correlation $C^{(2)}$ and containing an Hikami box. The diagrams linked to $C^{(3)}$ are obtained with using two Hikami boxes which yields four diagrammatic contributions. (see Ref. [4] for more details)

Note that these functions decay when $x \to \infty$ like $F_1(x) \sim \exp(-2x)$ and $F_2(x) \sim 1/x$.

2.2.4 Fluctuations of the scattered light

Intensity transmission fluctuations

The correlation function C_1 is a short-range contribution due to the exponential decay of F_1. It describes large fluctuations of the intensity transmission coefficient. Indeed in the diffusive regime when $g \gg 1$, we have at leading order the normalized fluctuations

$$\frac{\overline{\delta T_{b\alpha}^2}}{\overline{T}_{b\alpha}^2} = C_{\alpha b,\alpha' b'} \sim C^{(1)} = 1. \tag{2.20}$$

Large fluctuations of $\overline{T}_{b\alpha}$ at the origin of the granularity of the speckle pattern with a strong contrast between bright and dark spots. Taking into account the interferences, i.e. going to the first order in $1/g$, leads to the first weak localization correction

$$\frac{\overline{\delta T_{b\alpha}^2}}{\overline{T}_{b\alpha}^2} \sim 1 + \frac{4}{3g}. \tag{2.21}$$

Coming back to the order $\mathcal{O}(1)$, we consider the effect of a frequency shift $\Delta\omega$. Given the fast decay of F_1, we replace it by the Kronecker symbol. Physically, it means that each speckle spot is associated to a single transverse mode. It follows that [1]

$$C^{(1)} \simeq \delta_{\alpha\alpha'}\delta_{bb'} \left|C(\Delta\omega)\right|^2, \tag{2.22}$$

with

$$C(\Delta\omega) = \frac{\sqrt{-i\frac{\Delta\omega}{\Omega_{\mathrm{Th}}}}}{\sinh\left(\sqrt{-i\frac{\Delta\omega}{\Omega_{\mathrm{Th}}}}\right)}, \tag{2.23}$$

where Ω_{Th} is the Thouless frequency related to the Thouless time $\tau_{\mathrm{Th}} = 2\pi/\Omega_{\mathrm{Th}}$. The Thouless time corresponds to the average time the wave spends in the medium. It is given by $\tau_{\mathrm{Th}} = L^2/\mathcal{D}$ where $\mathcal{D}$ is the diffusion coefficient. In the following of the thesis, we will mostly encounter the equivalent way of writing Eq. (2.22):

$$\overline{T_{\alpha b}(\overline{\omega} - \Delta\omega)\, T_{\alpha' b'}(\overline{\omega} + \Delta\omega)} = \overline{T}_{\alpha b}^2(\overline{\omega}) \left(1 + C^{(1)}\right), \tag{2.24}$$

where we assume that $\overline{T}_{\alpha b}(\overline{\omega})$ and N are constant in the bandwidth of the incident light.

Total transmission fluctuations

Let us evaluate now the normalized fluctuations of the total transmission coefficient T_α. They are given by

$$\begin{aligned} \frac{\overline{\delta T_\alpha^2}}{\overline{T_\alpha}^2} &= \frac{\sum_{bb'}\left(\overline{T_{b\alpha}T_{b'\alpha}} - \overline{T}_{b\alpha}^2\right)}{\sum_{bb'}\overline{T}_{b\alpha}^2} \\ &= \frac{1}{N^2}\sum_{bb'} C_{\alpha b,\alpha b'}, \end{aligned} \tag{2.25}$$

where we use $\sum_{bb'}\overline{T}^2_{b\alpha} = N^2\overline{T}^2_{b\alpha}$. From the Eqs. (2.14), (2.15), (2.16) and (2.17) we have in the leading order

$$\begin{aligned}\sum_{bb'} C_{\alpha b,\alpha b'} &\simeq NC^{(1)} + N^2\left(C^{(2)} + C^{(3)}\right) \\ &\sim N^2 C^{(2)},\end{aligned} \tag{2.26}$$

due to the multiple scattering condition $l/L \ll 1$. Finally

$$\frac{\overline{\delta T^2_\alpha}}{\overline{T_\alpha}^2} \sim C^{(2)} = \frac{2}{3g}. \tag{2.27}$$

This result suggest a way to measure the long-range correlation $C^{(2)}$ without being disturbed by the much larger $C^{(1)}$: the integration over all the outgoing modes for a given incident mode and hence the measurement of the fluctuations of T_α.

Universal conductance fluctuations

In the same way, the normalized fluctuations of the conductance T are given by

$$\begin{aligned}\frac{\overline{\delta T^2}}{\overline{T}^2} &= \frac{1}{N^4}\sum_{\alpha\alpha' bb'} C_{\alpha b,\alpha' b'} \\ &= C^{(3)} \sim \frac{2}{15g^2}.\end{aligned} \tag{2.28}$$

This result has a more striking form

$$\overline{\delta T^2} \sim \frac{2}{15}. \tag{2.29}$$

This shows that the fluctuations of the conductance are independent of any parameters of the disordered medium like, e.g, the mean free path ℓ. This phenomenon is called universal conductance fluctuations. This universality of the multiple scattering hints toward the use of random matrix theory to describe wave propagation in disordered media. Indeed, this universality means that it might be possible to describe multiple scattering independently of the microscopic details of the medium, only considering the statistical properties of some random matrices like, for example, the scattering and transmission matrices. It is the purpose of the following section to introduce the random S-matrix approach.

2.3 Random S-matrix approach

This section is devoted to a presentation of the statistical properties of the scattering and transmission matrices encountered in the propagation of light in a disordered medium. Ideally, one wants to find an ensemble of random matrices to which the scattering or transmission matrices belong. For instance, in a chaotic cavity with point contact coupling the random Hamiltonian belongs to the Wigner-Dyson ensemble. Hence the associated scattering matrix is in the circular ensemble of uniformly distributed unitary matrices. For simplicity, we will consider in the following the case of a disordered wire, i.e. a disordered region in a quasi one-dimensional waveguide (see Fig. 2.2).

2.3.1 Random matrices: a brief introduction

The random matrix theory (RMT) consists in the study of the statistical properties of large matrices with random elements, for instance the probability distribution of the eigenvalues or the eigenvectors. In physics RMT has been introduced by the pioneering work of Wigner in 1951 in order to study the statistics of energy levels of heavy nuclei [107]. The idea was to conjecture that the spectral properties of the Hamiltonian of a nuclei are the same as those of a large random matrix. It has been found that the spacing between energy levels is given by the spacing between the eigenvalues of a random matrix. After that, the theory has been extended to a lot of fields, like mesoscopic physics, wireless communications or financial market analysis [108, 109, 110]. In the past decades, a strong effort has been made to study the quantum transport of electrons and light in chaotic cavities and open random media using RMT [111, 112, 9, 113].

In order to study a statistical problem using RMT, the first step is to relate its properties to the one of a particular ensemble of random matrices. For instance, one shows that the energy level statistics of chaotic systems is well described by the so-called Wigner-Dyson ensemble [114, 115]. Consider a particular ensemble of $N \times N$ Hermitian random matrices H described by the probability distribution $p(H)$. The joint probability distribution of the N real eigenvalues $p(\{\lambda_i\})$ are obtained by calculating the Jacobian between the elements and the eigenvalues and eigenvectors. Then by integration of the joint probability distribution, one infers the eigenvalue density $p(\lambda)$

$$p(\lambda) = \frac{1}{N}\left\langle \sum_{n=1}^{N} \delta(\lambda - \lambda_n) \right\rangle \tag{2.30}$$

$$= \frac{1}{N}\int_{-\infty}^{\infty} \prod d\lambda_n p(\{\lambda_n\}) \sum_{n}^{N} \delta(\lambda - \lambda_n) \tag{2.31}$$

$$= \int_{-\infty}^{\infty} \prod_{n=1}^{N-1} d\lambda_n p(\{\lambda_n\}), \tag{2.32}$$

where $\langle ... \rangle$ refers here to the average over the ensemble of random matrices H. $p(\lambda)\, d\lambda$ is the probability of finding an eigenvalue in the segment $[\lambda, \lambda + d\lambda]$.

Unfortunately, the above steps are not always possible. For instance, in the case of the Euclidean random matrices (ERM) ensemble encountered in random laser theory [116], the probability distribution $p(H)$ is not known and one has to determine the eigenvalue density using methods like diagrammatic expansions or the free probability theory. This situation will be ours when we will study the ensemble of random matrices used to described the amount of bipartite entanglement contained in some scattered states of light.

Let us introduce two important ensembles of random matrices for which the statistical properties are well known.

Gaussian ensemble

The first ensemble of interest is the so-called Gaussian ensemble. Consider the Wigner-Dyson ensemble of $N \times N$ Hermitian matrices H with the probability distribution

$$p(H) \propto \exp\left(-\beta N \mathrm{Tr}\left[V(H)\right]\right), \tag{2.33}$$

where V is a particular potential and β the symmetry index. The Gaussian ensemble appears when taking $V(H) \propto H^2$ leading to independent Gaussian random elements in the matrix H. According to Dyson, three classes of matrices come out depending of the symmetries obeyed by the system, i.e. depending on the degrees of freedom contained in the matrix elements.

- *Gaussian unitary ensemble* (GUE): Because no particular symmetry is imposed, $p(H)$ is invariant under any transformation $H \to UHU^\dagger$ with U unitary and $\beta = 2$.
- *Gaussian orthogonal ensemble* (GOE): In this case, there is time-reversal symmetry, then $p(H)$ is invariant under any transformation $H \to UHU^\dagger$ with U an orthogonal matrix and $\beta = 1$. Consequently, the elements are real numbers and H is a real symmetric matrix $H = H^T$.
- *Gaussian sympletic ensemble* (GSE): This ensemble takes into account the spin degree of freedom and is necessary when spin-orbit coupling cannot be neglected in a system. With time-reversal symmetry, $p(H)$ is invariant under any transformation $H \to UHU^\dagger$ with U sympletic, i.e. unitary with real quaternion elements, and $\beta = 4$.

For the GOE, we have

$$\langle H_{ij} H_{kl} \rangle = \frac{1}{N} \left(\delta_{il}\delta_{jk} + \delta_{ik}\delta_{jl} \right), \tag{2.34}$$

where $\langle ... \rangle$ corresponds to the average over the GOE, i.e. average over $p(H)$. In the limit $N \to \infty$, the eigenvalue density obeys the so-called semi-circle law

$$p(\lambda) = \begin{cases} \frac{1}{2\pi}\sqrt{4-\lambda^2}, & \forall \lambda \in [-2,2], \\ 0, & \forall |\lambda| > 0. \end{cases} \tag{2.35}$$

Wishart ensemble

The second important ensemble is the Wishart ensemble. It is frequently encountered when dealing with covariant matrices used in data analysis, e.g. in the method of principal component analysis frequently used in image processing [117]. The Wishart ensemble also appears in statistical physics, in wireless communication and in random entangled state problems [109, 118].

A $N \times N$ Wishart matrix is given by

$$W = H^\dagger H, \tag{2.36}$$

where H is a $M \times N$ Gaussian random matrix with elements independent and identically distributed (i.i.d.) according to a Gaussian distribution. Considering here only the case of complex elements with zero mean the probability distribution is

$$p(H) \propto \mathrm{e}^{N \mathrm{Tr}\left(H^\dagger H\right)}, \tag{2.37}$$

and

$$\langle H_{i\alpha} H^\dagger_{\beta j} \rangle = \frac{1}{N} \delta_{ij} \delta_{\alpha\beta}. \tag{2.38}$$

In the limit of large matrices, $N \to \infty$ and $M \to \infty$, the Wishart ensemble leads to the Marchenko-Pastur law [119]

$$p(\lambda) = \left(1 - \frac{1}{c}\right)^{+} \delta(\lambda) + \frac{1}{2\pi\lambda}\sqrt{(\lambda_{+} - \lambda)^{+}(\lambda - \lambda_{-})^{+}}, \tag{2.39}$$

where

$$\lambda_{\pm} = \left(\frac{1}{\sqrt{c}} \pm 1\right)^{2}, \tag{2.40}$$

and $c = \frac{N}{M}$, $x^{+} = \max(x, 0)$.

2.3.2 Polar decomposition of the scattering matrix

Let us now apply RMT to the scattering matrix S. According to the block representation of the S-matrix given by Eq. (2.5) one can perform a polar decomposition

$$S = \begin{pmatrix} U & 0 \\ 0 & V \end{pmatrix} \begin{pmatrix} -\sqrt{1-\tau} & \sqrt{\tau} \\ \sqrt{\tau} & \sqrt{1-\tau} \end{pmatrix} \begin{pmatrix} U' & 0 \\ 0 & V' \end{pmatrix}, \tag{2.41}$$

where $\tau = \mathrm{diag}(\tau_1, \tau_2, ..., \tau_N)$, with $\{\tau_n\}_n$ the transmission eigenvalues of the matrix $t^{\dagger}t$, and U, V, U' and V' are $N \times N$ unitary matrices.[1] Then the transmission matrix from the left to the right side of the medium is written as

$$t = V\sqrt{\tau}U', \tag{2.42}$$

leading to the transmission coefficient,

$$t_{b\alpha} = \sum_{k}^{N} v_{bk}\sqrt{\tau_k}u'_{k\alpha}, \tag{2.43}$$

where v_{bk} and $u'_{k\alpha}$ are the elements of the unitary matrices V and U'. The physical meaning of Eq. (2.42) is the following. The matrix U' ensures the transition from the incoming modes on the left to the eigenmodes of $t^{\dagger}t$ associated with the transmission eigenvalues τ_n. The eigenmodes are connected to the outgoing modes on the right of the medium by the matrix V. The same picture holds for the reflection.

2.3.3 DMPK equation

The idea is now to infer the statistics of the transmission matrix given the statistics of V, U' and $\sqrt{\tau_n}$. For this purpose one makes the isotropy approximation. It assumes a perfect mode mixing, i.e., when entering into the medium, the wave loses instantaneously the information about its direction of incidence. This assumption holds only for a quasi-one-dimensional geometry such as a waveguide with large number of modes $N \gg 1$. Then it follows that averaging over realizations of disorder is performed using the measure

$$dp(t) = p(\{\tau_n\}) \prod_{n}^{N} d\tau_n d\mu(U') d\mu(V), \tag{2.44}$$

[1] If time reversal symmetry is present ($\beta = 1$), in addition to the unitarity condition, the S-matrix has to be symmetric, $S = S^T$. Then $U' = U^T$ and $V = V^T$.

where $p(\{\tau_n\})$ is the joint probability distribution of the transmission eigenvalues and $d\mu(U')$ $(d\mu(V))$ is the Haar measure, i.e. the invariant measure of the unitary group $\mathcal{U}(N)$. Eq. (2.44) says that averaging over the ensemble of transmission matrices is done independently over $\{\tau_n\}$, U' and V.

At this point, one needs to evaluate $p(\{\tau_n\})$ in order to perform the averaging. The first step has been done in the 1980's by Dorokhov [120] and independently by Mello, Pereira and Kumar [121] who derived a N-dimensional Fokker-Planck equation called the DMPK equation. We do not give its derivation here and refer to the complete review of Beenakker [108] for more details. In few words, the procedure is to describe the evolution of $p(\{\tau_n\})$ according to a scaling approach, i.e., to follow its evolution while increasing the length L of the medium. The scaling approach allows to cross over from one regime of propagation to another by considering only one parameter, here L, which is equivalent to vary g. Using the random transfer matrix[2] M which is constructed from the S-matrix and connects all the left modes (either incoming or outgoing) to the right modes, an increase of L, $L \to L+\delta L$, is equivalent to $M \to M\delta M$. The multiplicative properties of M and the expression for the variation of $p(\{\tau_n\})$ with respect to δL yield the DMPK equation

$$\frac{\partial p(\{x_n\})}{\partial s} = \frac{1}{2\gamma}\sum_{n=1}^{N}\frac{\partial}{\partial x_n}\left(\frac{\partial p(\{x_n\})}{\partial x_n} + p(\{x_n\})\frac{\partial \Omega}{\partial x_n}\right), \tag{2.45}$$

where

$$\Omega = -\sum_{i<j} U(x_i, x_j) - \sum_{i=1}^{N} V(x_i), \tag{2.46}$$

$s = L/l$, $\gamma = \beta N + 2 - \beta$ and $x_n \geq 0$ is defined by the relation $\tau_n = 1/\cosh^2 x_n$. Eq. (2.45) describes the Brownian motion of the variables x_n seen as N particles evolving in one dimension in an external potential

$$V(x) = \ln|\sinh(2x)|, \tag{2.47}$$

with a two-particle interaction potential

$$U(x_i, x_j) = \ln\left|\sinh^2(x_j) - \sinh^2(x_i)\right|. \tag{2.48}$$

In the diffusive regime $N \gg s \gg 1$, and thus the solution of the DMPK equation is stationary so that the joint distribution takes the form of a Gibbs distribution[3]

$$p(\{x_n\}) \propto \mathrm{e}^{-H_{\mathrm{diff}}(\{x_n\})}, \tag{2.49}$$

[2]

$$M = \begin{pmatrix} V & 0 \\ 0 & V'^{\dagger} \end{pmatrix}\begin{pmatrix} \sqrt{\tau^{-1}} & \sqrt{\tau^{-1}-1} \\ \sqrt{\tau^{-1}-1} & \sqrt{\tau^{-1}} \end{pmatrix}\begin{pmatrix} U' & 0 \\ 0 & U^{\dagger} \end{pmatrix},$$

[3] Deeply in the localized regime, when $s \gg N \gg 1$, it is also possible to put $p(\{x_n\})$ into the form of a Gibbs distribution but the external and internal potentials are slightly different. However, the crossover from diffusive to localized regime is not contained in such a Gibbs distribution [122]. In the case of $\beta = 2$ an exact solution valid both in the diffusive and the localized regime has been found by Beenakker and Rejaei [123, 124], so that the crossover can be well described.

where the Hamiltonian is given by

$$H_{\mathrm{diff}}\left(\{x_n\}\right)=\sum_{i<j}^{N}u\left(x_i,x_j\right)+N\sum_{i=1}^{N}v\left(x_i\right), \tag{2.50}$$

with

$$\begin{aligned} v\left(x\right) &= \frac{\gamma}{2Ns\beta}x^2-\frac{1}{2N\beta}\ln\left|x\sinh\left(2x\right)\right|, && (2.51)\\ u\left(x_i,x_j\right) &= -\frac{1}{2}\ln\left|\sinh^2\left(x_j\right)-\sinh^2\left(x_i\right)\right|-\frac{1}{2}\ln\left|x_i^2-x_j^2\right|. && (2.52)\end{aligned}$$

This form of solution is convenient for numerical simulations using Monte-Carlo techniques [125] and we will also use it for comparison with analytical results in Chapter 4.

The next step is now to derive the eigenvalue density $p_{t^\dagger t}\left(\tau\right)$ (given $p\left(x\right)$). One way is to minimize the Hamiltonian using the method of steepest descent. This has been used, for instance, to find the eigenvalue density of the Gaussian and Wishart ensembles. For these canonical ensembles, the minimization procedure leads to an integral equation

$$⨍_{-\infty}^{\infty}dx'\,\frac{p\left(x'\right)}{x-x'}=\frac{\partial v_{\mathrm{ext}}\left(x\right)}{\partial x} \tag{2.53}$$

associated with the normalization constraint $\int dxp\left(x\right)=1$ where $⨍$ stands for the Cauchy principal value and v_{ext} is the external potential seen by the eigenvalues. Generally Eq. (2.53) can be solved by using the Tricomi theorem [126]. However, in the case of transmission eigenvalues, the form of the two-body potential $u\left(x_i,x_j\right)$ involves non-logarithmic eigenvalue repulsion [108]. Then the minimization does not lead to an integral equation like Eq. (2.53) where the denominator is associated with the logarithmic eigenvalue repulsion. One can skirt this difficulty by using a different approach based on the spectral rigidity [127, 128]. Indeed, the eigenvalues strongly repeal each other due to the interaction potential $u\left(x_i,x_j\right)$ and hence form a lattice-like structure with small fluctuations around mean positions. In the limit $N\to\infty$, the length of the lattice is given by the typical range s of the external potential. Then putting N "particles" equally spaced by a mean spacing $L/\ell N$ yields the following homogeneous density $p\left(x\right)$

$$p\left(x\right)=\left\{\begin{array}{ll}\frac{1}{s}, & \forall x\leq s,\\ 0, & \forall x\geq s.\end{array}\right. \tag{2.54}$$

From Eq. (2.54) and using the relation $\tau=1/\cosh^2\left(x\right)$, one obtains the so-called bimodal distribution

$$p_{t^\dagger t}\left(\tau\right)=\frac{1}{2s}\frac{1}{\tau\sqrt{1-\tau}},\quad\text{for}\quad\frac{1}{\cosh^2\left(s\right)}\leq\tau<1. \tag{2.55}$$

This distribution tells us that the propagation of the wave is dominated by some "open" channels[4] related to transmission eigenvalues close to one, all the others being close to

[4] By channel we mean an eigenvector of the matrix $tt^\dagger$.

zero as shown in Fig. 2.5. The bimodal distribution of transmission coefficients was shown to hold for arbitrary geometry [129] and not only for Q1D waveguides.

Let us say a few words about the statistical distributions of the three transmittances introduced in Sec 2.2.1. Using the expression of $t_{b\alpha}$ obtained from the polar decomposition, they can be written as

$$T_{b\alpha} = \sum_{k=1}^{N}\sum_{l=1}^{N} v_{bk} v_{bl}^{*} \sqrt{\tau_k \tau_l}\, u_{k\alpha}'^{*} u_{l\alpha}'^{*}, \tag{2.56}$$

$$T_{\alpha} = \sum_{k=1}^{N} \tau_k \left| u_{k\alpha}'^{*} \right|^2, \tag{2.57}$$

$$T = \sum_{k=1}^{N} \tau_k = \mathrm{Tr}\left(t^{\dagger} t\right), \tag{2.58}$$

where we use the unitarity of the matrices V and U' such that $\left(VV^{\dagger}\right)_{ij} = \sum_k^N v_{ik} v_{jk}^{*} = \delta_{ij}$. Eq (2.58) is the so-called Landauer formula first introduced for disordered conductors [130]. From this relation we see that in the diffusive regime when the transmission eigenvalues follow the bimodal distribution, g quantifies the effective number N_{eff} of channels that contribute to propagation.

From Eqs. (2.56) and (2.57) and in the leading order in $1/N$, we obtain the moments of $T_{b\alpha}$ by averaging over the elements of V

$$\overline{T_{b\alpha}^{n}} = \frac{n!}{N^n} \overline{T_{\alpha}^{n}}, \tag{2.59}$$

which leads to a relation between the distribution of $T_{b\alpha}$ and T_α [131]

$$p\left(T_{b\alpha}\right) = \frac{\overline{T_\alpha}}{\overline{T_{b\alpha}}} \int_0^{\infty} dT_\alpha \frac{p\left(T_\alpha\right)}{T_\alpha} \exp\left(-\frac{T_{b\alpha}}{T_\alpha} \frac{\overline{T_\alpha}}{\overline{T_{b\alpha}}}\right). \tag{2.60}$$

This equation allows calculating the distribution of the intensity transmission coefficient from a known distribution of total transmission. From Eq. (2.57), T_α appears to be a sum of random independent terms following the same probability distribution. In the diffusive regime, according to the bimodal distribution of τ_n's, this sum can be considered infinite because $N_{\text{eff}} = g \gg 1$. It follows from the central limit theorem that $p\left(T_\alpha\right)$ is a Gaussian distribution with a variance of the order $1/g$. Taking the limit of $g \to \infty$ and considering Eq. (2.60) leads to the Rayleigh distribution of $T_{b\alpha}$. Small deviations from the Rayleigh ($T_{b\alpha}$) and Gaussian (T_α) distributions come in when taking g finite, i.e., when taking into account weak localization corrections. The same argument can be used to show the Gaussian statistics of conductance in the diffusive regime.

The above results are known both from perturbative diagrammatic [132] and random matrix [131] theories and are not qualitatively different from one geometry to another. Non-perturbative results are obtained using a solution of the DMPK equation valid in both diffusive and localized regimes [123] from which one can study the transition from Rayleigh and Gaussian statistics to log-normal statistics when the wave is getting localized as L increases [133]. However the later result is valid only for the wire geometry and particular symmetry constraints ($\beta = 2$).

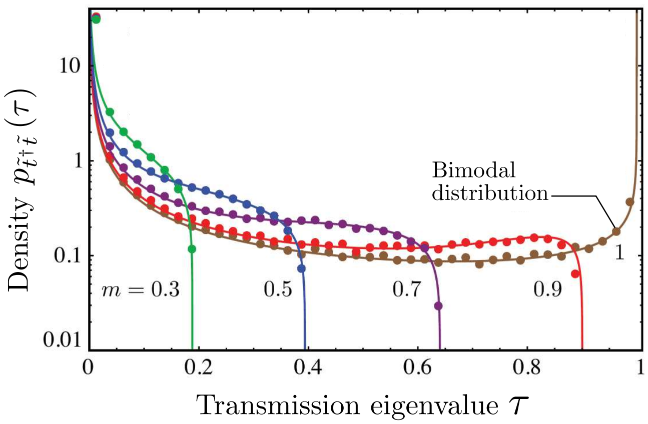

Figure 2.5: Transmission eigenvalue density of a disordered slab placed in a waveguide with N channels for different fractions of controlled channels $m = M/N$, from [134]. Analytical results obtained from the free probability theory (solid line). Numerical results from solving the wave equation (dots).

2.3.4 Transmission eigenvalues: From bimodal to Marchenko-Pastur law

In this section, we present another type of transition which affects the transmission eigenvalue density. In the diffusive regime, using spatial light modulator and interferometric methods one is able to measure the transmission matrix t and obtain the density of its singular values $\sqrt{\tau_n}$ [135]. This has also been done previously with acoustic waves [113]. In both situations, the singular value density is close to the quarter-circle law that one obtains with uncorrelated Gaussian random matrices and corresponding to a Marchenko-Pastur law for the transmission eigenvalues τ_n. This experimental observation differs from the bimodal distribution predicted by the theory.

Recently, Goetschy and Stone [134] have shown that this discrepancy comes from an incomplete control of the input and output modes. Indeed, in all current experimental setups, fractions of controlled modes m_1 (input) and m_2 (output) cannot reach exactly one, the value associated to the whole transmission matrix t. So that the measurements have access to a truncated transmission matrix $\tilde{t}$ that is often a small part of t. Using the free probability theory, Goetschy and Stone calculate the eigenvalue density of $\tilde{t}^\dagger \tilde{t}$ taking into account this experimental constraint. The main result is shown in Fig. 2.5. One can see that taking $m_1 = m_2 = m \leq 1$ suppresses the peak corresponding to the open channels. Moreover, when $m \leq \overline{T_\alpha}$ which is equivalent to $M \leq g$, $p(\tau)$ approaches the Marchenko-Pastur law. It means that the truncated matrix $\tilde{t}$ becomes statistically similar to random matrix with uncorrelated Gaussian distributed elements. We will use this result to derive the Schmidt eigenvalue density of a scattered quantum state in Sec. 4.2.6.

Chapter 3

Two-photon speckle

3.1 Quantum optics with disorder: an overview

Multiple scattering of non-classical light in disordered media attracts the attention of physicists since the pioneering paper by Beenakker [9] who studied the statistics of the spontaneous emission in a disordered slab. The author associated the random matrix theory which successfully describes the multiple scattering of light (see Chapter 2) with the input-output theory that allows to describes the dynamics of quantum operators in open random systems (see Sec. 1.1.1). The same framework has been applied by Beenakker and coworkers to study the multiple scattering of squeezed light [136] and to characterize the channel capacity of a disordered medium taking into account the quantum nature of the radiation that carries the information [137]. One can view behind this procedure a way to study the interplay between the statistics of the random medium and the statistics of the quantum light that propagates inside it. The main idea is then to study how the two combine in the scattered state.

3.1.1 Correlations in speckle pattern

In this spirit, several groups have studied both theoretically and experimentally the quantum fluctuations present in the scattered light for different types of monochromatic quantum incident states in the diffusive regime [138, 139, 140, 141, 142, 143]. Both for stationary and fluctuating disordered media, Lodahl *et al.* [138] and Skipetrov [141] showed that the normalized variance of the photon number in an outgoing mode is given by

$$\frac{\overline{\langle \hat{n}_i^2 \rangle}}{\overline{\langle \hat{n}_i \rangle}^2} - 1 = \frac{1}{\overline{\langle \hat{n}_i \rangle}} + \delta^2_{\text{class}} + \frac{Q_\alpha}{\langle \hat{n}_\alpha \rangle} \left(1 + \delta^2_{\text{class}}\right), \tag{3.1}$$

where the horizontal bar $\overline{\cdots}$ denotes the ensemble average over random realizations of disorder in the medium. It should be distinguished from the quantum-mechanical expectation value denoted by $\langle \cdots \rangle$. Q_α is the Mandel parameter of the incident state introduced in Sec 1.1.7 and δ^2_{class} is the normalized variance of the scattered intensity obtained when one disregards the quantum nature of light. For a static disorder, in the diffusive regime, $\delta^2_{\text{class}} = 1 + 8/3g$ [138]. The first term in Eq. (3.1), corresponds to the so-called shot noise which takes into account the granularity of the light field made

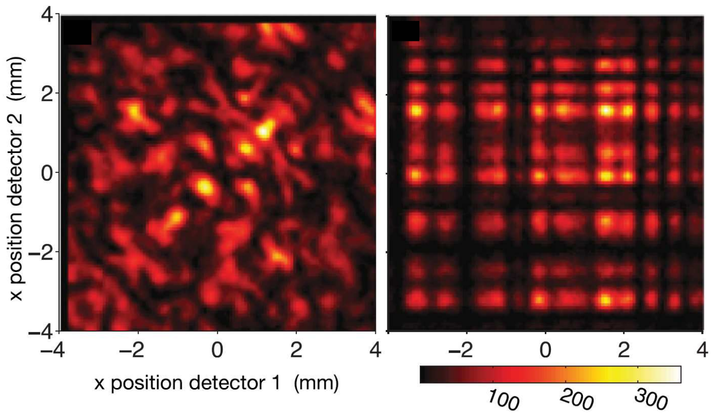

(a) (b)

Figure 3.1: Two-photon speckle patterns observed in far field after multiple scattering of a two-photon incident state. (a) Nonlocal speckle obtained from an highly entangled state. (b) Separable speckle obtained from a two-photon state with very small amount of entanglement, $K \simeq 1$. From Ref. [144].

up of photons that arrive at a detector one by one so that it is an intrinsic quantum noise. From Eq. (3.1), one sees that the statistics of the disordered medium and the one of the quantum incident state are combined in a way that can not be predicted without calculation. For the coherent state, $Q_\alpha = 0$ so that only the sum of shot noise and classical noise remains. However, for a quantum state like the Fock state, $Q_\alpha = -1$, and if $\langle \hat{n}_\alpha \rangle = 1$ the variance becomes independent of the classical noise meaning that the quantum fluctuations dominate largely over the classical ones. The same type of results and conclusions are obtained for the correlation of the photon number in two different outgoing modes except that the shot noise is absent and that the correlations are decreased by a factor 2. These theoretical predictions have been verified experimentally in Refs. [142, 143].

3.1.2 Two-photon speckle

Even if the observables involved in the works presented above imply more than one photon, the incident states did not bear any quantum correlations. More recently, the possibility of finding signatures of quantum correlations, i.e. the entanglement present in the incident state, in the two-photon speckle pattern has been investigating [10, 14, 12, 11, 13, 144].

In Ref. [10], the authors showed the link between one and two-photon speckle patterns through the relation $\mathcal{P} = \mathcal{V}^{(2)} - 2\mathcal{V}^{(1)}$ where $\mathcal{P}$ is the purity of the incident state and $\mathcal{V}^{(1,2)}$ are visibilities of the one and two-photon speckle patterns. Then, for a pure state, $\mathcal{V}^{(1)}$ gives information on $\mathcal{V}^{(2)}$, and vice versa. The above relation has its origin in the so-called complementarity observed in one and two-photon interferences [145, 146]. Besides, the authors of Ref. [10] showed that the distribution of the two-photon intensity $\langle : \hat{n}_i \hat{n}_j : \rangle$ is non-exponential unless the amount of entanglement becomes maximal.

The two-photon speckle pattern and statistical distributions of two-photon intensities have then been observed quite recently [12, 144]. We show in Fig. 3.1 a two-photon speckle pattern measured in van Exter's group for a far field configuration.

Another interesting feature of multiple scattering of quantum states is the survival of quantum interferences after the average over the disorder realizations. It has been predicted in Ref. [14] and then observed for spatial two-photon interferences [13].

All the work presented above deal with monochromatic light with two photons entangled in transverse momentum. In Ref. [11], Cherroret and Buchleitner studied the propagation of a frequency entangled state which is non-stationary. By considering the coincidence rate between two outgoing modes, they showed the survival of temporal two-photon interferences and the possibility of accessing either the entanglement spectrum of the incident state or the properties of the disordered medium via the Thouless frequency.

3.2 Two-photon entangled states

In this section, we discuss the properties of the two-photon incident state that we will use in this chapter. We consider a frequency entangled state which belongs to the family of so-called continuous variable entangled states [147]. These types of states are frequently encountered when dealing with high dimensional entanglement experiments and were used by Einstein and coworkers to introduce their paradox about quantum non-locality considering the momentum and position as continuous variables [51].

3.2.1 Bi-Gaussian and SPDC biphoton states

The expression of the SPDC two-photon state given in Chapter 1.1.5 is rather complex and does not always allow obtaining simple analytical expression for observables like the coincidence rate especially when interferences occur in a disordered medium. The purpose of this section is thus to study the conditions that allow to approximate the SPDC two-photon state by a bi-Gaussian state. We are interested only in the spectral and time properties and consider that the mean frequencies of the down-converted photons are equal, i.e., $\overline{\omega}_s = \overline{\omega}_i = \overline{\omega}$. Then, considering a collinear propagation of the two photons along the pump axis, the SPDC state can be written as

$$|\Psi\rangle_{\mathrm{SPDC}} = \iint_{-\infty}^{\infty} d\omega_1 d\omega_2 \; \phi_{\mathrm{SPDC}}\left(\omega_1, \omega_2\right) \hat{a}^{\dagger}_{\alpha_1}\left(\omega_1\right) \hat{a}^{\dagger}_{\alpha_2}\left(\omega_2\right) |0\rangle \, , \tag{3.2}$$

where $\phi_{\mathrm{SPDC}}\left(\omega_1, \omega_2\right) = \mathcal{N} \alpha\left(\omega_1, \omega_2\right) h\left(\omega_1, \omega_2\right)$ is the two-photon amplitude with $\mathcal{N}$ a constant fixed by the normalization of the state, and $\alpha_1, 2$ the polarization state. Considering a Gaussian pump spectrum, we have

$$\alpha\left(\omega_1, \omega_2\right) = \exp\left(-\frac{\left(\omega_1 + \omega_2 - 2\overline{\omega}\right)^2}{2\sigma^2}\right), \tag{3.3}$$

where σ is the frequency bandwidth of the pump and $2\overline{\omega}$ its central frequency. The phase-matching function $h\left(\omega_1, \omega_2\right)$ is given by

$$h\left(\omega_1, \omega_2\right) = \mathrm{sinc}\left(\frac{\Delta k\left(\omega_1, \omega_2\right) L_{\mathrm{crys}}}{2}\right), \tag{3.4}$$

where $\mathrm{sinc}(x) = \sin(x)/x$ and $L_{\mathrm{crys.}}$ is the length of the non-linear crystal. All the phase-matching properties are contained in $\Delta k\,(\omega_1, \omega_2)$ which writes as

$$\Delta k\,(\omega_1, \omega_2) = k_p\,(\omega_1 + \omega_2) - k_s\,(\omega_1) - k_i\,(\omega_2)\,, \tag{3.5}$$

where p, i and s denote the pump, idler and signal photons, respectively (see Sec. 1.1.5) and where $k_j(\omega) = \omega n_j(\omega)/c$ is the wave number associated with the photon j, c the celerity of light in the vacuum, and $n(\omega)$ the refractive index.

Let us now determine the conditions under which the SPDC state described by Eq. (3.2) can be approximate by $|\Psi\rangle_{\mathrm{Gauss}} = \iint_{-\infty}^{\infty} d\omega_1 d\omega_2\, \phi_{\mathrm{Gauss}}\,(\omega_1, \omega_2)\, \hat{a}^{\dagger}_{\alpha_1}\,(\omega_1)\, \hat{a}^{\dagger}_{\alpha_2}\,(\omega_2)\,|0\rangle$ where ϕ_{Gauss} is given by

$$\phi_{\mathrm{Gauss}}\,(\omega_1, \omega_2) = \sqrt{\frac{2}{\pi ab}}\, \exp\left[-\left(\frac{(\omega_1 + \omega_2 - 2\overline{\omega})^2}{2a^2} + \frac{(\omega_1 - \omega_2)^2}{2b^2}\right)\right]. \tag{3.6}$$

Here a and b are the frequency bandwidths that constraint the sum and the difference of the frequencies of the two photons, respectively. The normalization of the state is ensured by $\iint d\omega_1 d\omega_2 |\phi_{\mathrm{Gauss}}\,(\omega_1, \omega_2)\,|^2 = 1$. It is *a priori* not obvious if the SPDC two-photon amplitude ϕ_{SPDC} can be approximated by ϕ_{Gauss}. It depends on the argument of the phase-matching function. A convenient way of studying this argument is to perform a Taylor expansion of the wave number $k_j(\omega)$ around the central frequency $\overline{\omega}$ for the signal and idler photons and around $2\overline{\omega}$ for the pump. To the second order, we obtain

$$\begin{aligned} k_p\,(\omega) &= k_p\,(2\overline{\omega}) + (\omega - 2\overline{\omega})\, k'_p + (\omega - 2\overline{\omega})^2\, k''_p/2, & (3.7)\\ k_j\,(\omega) &= k_j\,(\overline{\omega}) + (\omega - \overline{\omega})\, k'_j + (\omega - \overline{\omega})^2\, k''_j/2, & (3.8) \end{aligned}$$

where $j = i$ or s, $k'_p = \partial k_p\,(\omega)\,/\partial\omega|_{\omega=2\overline{\omega}}$ and $k'_j = \partial k_j\,(\omega)\,/\partial\omega|_{\omega=\overline{\omega}}$, and similarly for k''_p and k''_j. Assuming a perfect phase-matching at the central frequency, i.e. $k_p\,(2\overline{\omega}) - k_s\,(\overline{\omega}) - k_i\,(\overline{\omega}) = 0$, and considering the variables $\Omega_{1,2} = \omega_{1,2} - \overline{\omega}$, Δk can be written as

$$\begin{aligned} \Delta k\,(\omega_1, \omega_2) &\simeq (\Omega_1 + \Omega_2)\, k'_p - \Omega_1 k'_s - \Omega_2 k'_i + \\ &+ (\Omega_1 + \Omega_2)^2\, k''_p/2 - \Omega_1^2 k''_s/2 - \Omega_2^2 k''_i/2. \end{aligned} \tag{3.9}$$

It turns out that Δk is strongly different between type-I and type-II SPDC states and when the pump is monochromatic (cw pump) or not. Let us discuss these different possibilities.

Type-I SPDC state

In this case, the polarizations of the down-converted photons are the same and $k_s\,(\omega) = k_i\,(\omega)$.

- *cw pump*

  Due to the energy conservation, $\Omega_1 = -\Omega_2 = \Omega$ and $\omega_s + \omega_i = 2\overline{\omega}$. Therefore, we have $\Delta k \simeq -k''_s \Omega^2$. The minus sign is not relevant because the sinc function is even. Therefore, the case of a cw pump can be described by a bi-Gaussian in the limit $a \to 0$.

- *Broadband pump*

  Here, the sum $\omega_s + \omega_i$ is no more constraint to a fixed value. We have $\Delta k \simeq (\Omega_1 + \Omega_2)\left(k'_p - k'_s\right) + (\Omega_1 + \Omega_2)^2 k''_p/2 - \left(\Omega_1^2 + \Omega_2^2\right) k''_s/2$. Taking only the first order term in the previous expression allows to perform the transformation $\mathrm{sinc}(x) \rightarrow \exp(-\gamma x^2)$ with γ a fitting parameter such that the Gaussian function has the same width at half maximum as the sinc function. However, this is valid only if $\alpha(\omega_1, \omega_2)$ is wider than the sinc function. Otherwise, $\Omega_1 + \Omega_2$ becomes much smaller than $\Omega_1 - \Omega_2$ and one has to take into account the second order terms.

  When considering both first and second order terms, Δk contains both linear and quadratic contributions and one cannot directly approximate $\mathrm{sinc}(x)$ by $\exp(-\gamma x^2)$. However, assuming a perfect group velocity matching at the central frequency, one can drop the linear term in Δk. The group velocity matching condition is given by $k'_p - (k'_s - k'_i)/2 = 0$. The association of phase-matching and group velocity matching conditions is called the extended phase-matching [148, 149]. Under these assumptions and using the relation $x^2 + y^2 = 1/2[(x+y)^2 + (x-y)^2]$, Δk becomes

  $$\Delta k \simeq (\Omega_1 + \Omega_2)^2 \left(k''_p/2 - k''_s/4\right) - (\Omega_1 - \Omega_2)^2 k''_s/4. \tag{3.10}$$

  Unless $k''_p - k''_s/2 = 0$, the bi-Gaussian representation cannot match the SPDC state without strong and not experimentally relevant assumptions.

To conclude, for the type-I SPDC state, the use of a bi-Gaussian representation implies distinguishing different regimes depending on the bandwidth of the pump compared to the one of the phase matching function, as it has been done in Ref. [150], for example.

Type-II SPDC state

For type-II SPDC states, the down-converted photons have orthogonal polarizations so that their group velocities are different because the non-linear crystal is birefringent. Then it is not necessary to go beyond the first order and therefore the bi-Gaussian approximation implies less physical constraints than for the type-I SPDC as we will see below.

- *cw pump*

  In this situation, the same arguments as those used for the type-I case, yield the phase-matching condition as $\Delta k \simeq -\left(k'_s - k'_i\right)\Omega$.

- *Broadband pump*

  In the first order, $\Delta k \simeq \left(k'_p - k'_s\right)\Omega_1 + \left(k'_p - k'_i\right)\Omega_2$. Here, contrary to the type-I case, the argument is not symmetric with respect to Ω_1 and Ω_2 because of the difference of the group velocities. Consequently, the spectra of the two photons are different, hence the photons are distinguishable by their frequencies. We will see in Sec. 3.5.1 that this reduces the visibility of the two-photon speckle pattern. From this consideration of symmetry, it is *a priori* impossible to approximate the phase-matching function by a Gaussian function which is symmetric with respect to the frequencies. However, assuming the extended phase-matching condition introduced above implies that $k'_p - k'_s = -\left(k'_p - k'_i\right)$. Then, one obtains

$$\Delta k \simeq \left(k'_p - k'_s\right)\left(\Omega_1 - \Omega_2\right). \tag{3.11}$$

The phase-matching function is now symmetric with respect to the frequencies which allows replacing the sinc function by a Gaussian whatever the sign of $\left(k'_p - k'_s\right)$. It means that when the group velocity matching condition is satisfied the two photons have necessary the same spectrum and become indistinguishable by frequency.

It follows from the foregoing discussion that for type-II SPDC states, one can use the bi-Gaussian approximation after the transformation $\mathrm{sinc}(x) \to \exp(-\gamma_2 x^2/2)$ with the parameters

$$\begin{aligned} a &= \sigma, \\ b &= \frac{2}{\sqrt{\gamma_2} L_{\text{crys.}} |k'_p - k'_s|}. \end{aligned} \tag{3.12}$$

In the following, we will consider only type-II SPDC states and therefore we will exploit the above approximation which relies on the extended phase-matching condition. It has been shown that such a condition can be fulfilled experimentally using a periodically poled $\chi^{(2)}$ material [151] or with usual non-linear materials for long wavelengths $\lambda_{\text{pump}} \simeq 1\ \mu$m [152].

3.2.2 Spectral and temporal coherence properties of two-photon states

Frequency correlations

We now consider the bi-Gaussian two-photon amplitude given by Eq. (3.6) with the bandwidths a and b given by Eq. (3.12) for the type-II phase-matching. Because the two-photon amplitude $\phi_{\text{Gauss}}(\omega_1, \omega_2)$ is *a priori* not separable the two photons are entangled in frequency. From the expressions of a and b, one sees that the correlations in frequency are different depending on the physical situation, i.e., depending on the length of the crystal and the spectral width of the pump pulse. When $a/b > 1$, the two photons are correlated in frequency whereas when $a/b < 1$, they are anti-correlated. Let us consider, two limiting cases in order to illustrate this behavior:

- $a/b \ll 1$:

  The first term in the argument of the Gaussian in Eq. (3.6) leads to a very narrow function. Then $|\phi_{\text{Gauss}}(\omega_1, \omega_2)|^2 \to 2/(\sqrt{\pi} b)\delta(\omega_1 + \omega_2 - 2\overline{\omega}) \exp[-(\omega_1 - \omega_2)^2/b^2]$ so that the frequencies of the two photons are perfectly anti-correlated. This situation appears when one uses a cw pump. It leads to the state

  $$|\Psi\rangle_{\text{cw}} = \sqrt{\frac{2}{\sqrt{\pi} b}} \int_{-\infty}^{\infty} d\omega\, \exp\left[-2\frac{\omega^2}{b^2}\right] |\overline{\omega} + \omega\rangle_i\, |\overline{\omega} - \omega\rangle_s. \tag{3.13}$$

  Although perfect anti-correlations are present, the corresponding state is not maximally entangled.

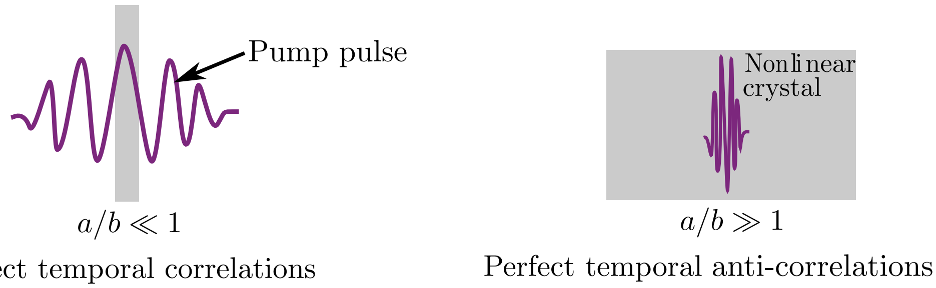

Figure 3.2: Sketch of the physical situations corresponding to the different limits $a/b \ll 1$ and $a/b \gg 1$ giving a nice insight of the relation between temporal correlations and the experimental situations.

- $a/b \gg 1$:

  We are here in the situation where the second term in the argument of the Gaussian in Eq. (3.6) leads to a very narrow function and $|\phi_{\text{Gauss}}(\omega_1, \omega_2)|^2 \to 2/(\sqrt{\pi}a)$ $\delta(\omega_1 - \omega_2)\exp[-(\omega_1 + \omega_2 - 2\overline{\omega})^2/a^2]$ so that the frequencies of the two photons are perfectly correlated. Because $b \propto 1/L_{\text{crys.}}$, such correlations correspond to the limit of a very long crystal:

$$|\Psi\rangle_{\text{Long crys}} = \sqrt{\frac{2}{\sqrt{\pi}a}} \int_{-\infty}^{\infty} d\omega \, \exp\left[-2\frac{\omega^2}{a^2}\right] |\overline{\omega} + \omega\rangle_i \, |\overline{\omega} + \omega\rangle_s \, . \tag{3.14}$$

If $a/b = 1$ the frequency correlations vanish and the two-photon amplitude can be written as $\phi_{\text{Gauss}}(\omega_1, \omega_2) = \varphi_{\text{Gauss}}(\omega_1)\, \varphi_{\text{Gauss}}(\omega_2)$. Moreover, if $a \to 0$ the separable state tends to the Fock state $|\overline{\omega}\rangle_s \, |\overline{\omega}\rangle_i$.

We will now see what happens in the time domain and calculate the coherence times of SPDC states in the Gaussian approximation.

Temporal correlations

The Fourier transform $\tilde{\phi}_{\text{Gauss}}$ of ϕ_{Gauss} is given by

$$\tilde{\phi}_{\text{Gauss}}(t_1, t_2) = \sqrt{\frac{ab}{2\pi}} \exp\left[-i\,(t_1 + t_2)\,\omega_0\right] \exp\left[-\frac{1}{8}\left((t_1 - t_2)^2\, b^2 + (t_1 + t_2)^2\, a^2\right)\right] \tag{3.15}$$

Temporal correlations are constrained by b whereas temporal anti-correlations are constrained by a. The state is correlated in time when $a/b < 1$ and anti-correlated when $a/b > 1$. As for frequency correlations, perfect time correlations are obtained in the limit $a/b \ll 1$ and perfect anti-correlation in the in the limit $a/b \gg 1$. One can understand physically these behaviors by looking at the sketches in Fig. 3.2. Time correlations are related to the uncertainty of the relative time of emission[1] of the two photons, and when $b \to \infty$, $L_{\text{crys.}} \to 0$ is very small so that there is no uncertainty in the relative time. In the same way, time anti-correlations are related to the absolute

[1] The relative time of emission is the difference between the times at which the two photon exit the non-linear crystal.

time[2] of emission, and for a pump very short in time ($a \to \infty$) there is no uncertainty in the absolute time because the photons are generated within the duration of the pump pulse.

One cannot have perfect correlations in time and in frequency "simultaneously" because $\omega_1 - \omega_2$ and $t_1 - t_2$ are Fourier conjugate variables. The same statement holds for anti-correlations with the variables $\omega_1 + \omega_2$ and $t_1 + t_2$. However, the variables $\omega_1 - \omega_2$ and $t_1 + t_2$, and then their uncertainties are independent so that a state can have well defined $\omega_1 - \omega_2$ and "simultaneously" $t_1 + t_2$. Here again, it also applies to $\omega_1 - \omega_2$ and $t_1 + t_2$. This feature is intimately linked to the entanglement in time and in frequency of the photons. Actually, it comes from the basis independence properties of entanglement introduced in Sec. 1.2. Here entanglement, seen through the correlations[3], is independent of the choice of time or frequency representation. Moreover, when the state is maximally entangled in frequency, i.e., when $a \to 0$ and $b \to \infty$ or $a \to \infty$ and $b \to 0$, it is necessary maximally entangled in time. This is in strong contrast with the case of a separable state with $a = b$. In the case $a \to \infty$ leading to $|\overline{\omega}\rangle_s |\overline{\omega}\rangle_i$, there is no uncertainty in frequency but the price to pay in the time domain is a necessarily infinite uncertainty in time.

Single and two-photon coherence

In the case of non-stationary states of light, the single-photon coherence time is defined by

$$\Delta t_{\mathrm{c}} = \left(\frac{\int_{-\infty}^{\infty} d\tau \; \tau^2 \left| \tilde{G}_1(\tau) \right|^2}{\int_{-\infty}^{\infty} d\tau \; \left| \tilde{G}_1(\tau) \right|^2} \right)^{\frac{1}{2}}, \tag{3.16}$$

where

$$\tilde{G}_1(\tau) = \int_{-\infty}^{\infty} dt \; \tilde{G}_1(t, t+\tau), \tag{3.17}$$

with $\tilde{G}_1(t_1, t_2)$ the first-order correlation function introduced in Sec. 1.1.6: $\tilde{G}_1(t_1, t_2) = \langle \hat{a}_i^\dagger(t_1)\, \hat{a}_i(t_2) \rangle$. Using the Fourier transform of the two-photon amplitude, we have[4]

$$\tilde{G}_1(t, t+\tau) = \int_{-\infty}^{\infty} dt_2 \; \tilde{\phi}^*_{\mathrm{Gauss}}(t, t_2)\, \tilde{\phi}_{\mathrm{Gauss}}(t+\tau, t_2). \tag{3.18}$$

Using the expression of $\tilde{\phi}_{\mathrm{Gauss}}$, Eq. (3.15), we obtain

$$\tilde{G}_1(\tau) = \exp\left[-i\tau\overline{\omega}\right] \exp\left[-\frac{1}{16}\left(a^2 + b^2\right)\tau^2\right]. \tag{3.19}$$

[2]The absolute time of emission is two times the time at which the center of momentum of the two photons exits the crystal [153].

[3]We recall that for pure bipartite entangled states, non-local correlations, i.e., correlations that violate Bell's inequalities, are equivalent to entanglement.

[4]It would be similar to work with t_1 instead of t_2 because $\tilde{\phi}_{\mathrm{Gauss}}(t+\tau, t_2)$ is symmetric with respect to its two arguments.

Then the single-photon coherence time is

$$\Delta t_{\mathrm{c}} = \frac{2}{\sqrt{a^2+b^2}}. \tag{3.20}$$

From (3.20) and the discussion above one can see that Δt_{c} tends to zero for a maximally entangled state ($a, b \to \infty$). This is not surprising because a maximally entangled state implies a complete lack of information about the single photon state which is then a maximally mixed state. Therefore, the single-photon state is an incoherent sum of an infinite number of terms, hence it has no coherence at all. To be more general, let us consider how the single-photon time coherence changes with the amount of entanglement quantified by the Schmidt number $K = \mathrm{Tr}\left(\hat{\rho}_1^2\right)$. For the bi-Gaussian state, we find

$$K = \frac{a^2+b^2}{2ab}, \tag{3.21}$$

so that the amount of entanglement depends only on the ratio a/b. Therefore, $\Delta t_{\mathrm{c}} = \mu/\sqrt{K}$ where $\mu = \sqrt{2/ab}$ and the more entangled the state is, the more the single-photon coherence decreases.

Similarly the single-photon spectral bandwidth is

$$\Delta\omega_{\mathrm{c}} = \left(\frac{\int_{-\infty}^{\infty} d\omega\ (\omega-\overline{\omega})^2 \left|G_1(\omega)\right|^2}{\int_{-\infty}^{\infty} d\omega\ \left|G_1(\omega)\right|^2}\right)^{\frac{1}{2}}, \tag{3.22}$$

where

$$G_1(\omega) = \frac{1}{\sqrt{2\pi}} \int_{-\infty}^{\infty} d\omega\ \tilde{G}_1(t)\, \mathrm{e}^{i\omega t}. \tag{3.23}$$

The spectral bandwidth is then

$$\Delta\omega_{\mathrm{c}} = \frac{\sqrt{a^2+b^2}}{4}, \tag{3.24}$$

such that the coherence time and the bandwidth satisfy the uncertainty relation

$$t_{\mathrm{c}}\Delta\omega_{\mathrm{c}} = \frac{1}{2}. \tag{3.25}$$

In the case of non-Gaussian two-photon amplitude, we have the inequality

$$t_{\mathrm{c}}\Delta\omega_{\mathrm{c}} \geq \frac{1}{2}. \tag{3.26}$$

We now consider the two-photon coherence properties. Similarly, one can define the two-photon coherence times by

$$\Delta t_{\pm} = \left(\frac{\int_{-\infty}^{\infty} d\tau\ \tau^2 \left|\tilde{G}_2(\tau, \pm\tau)\right|^2}{\int_{-\infty}^{\infty} d\tau\ \left|\tilde{G}_2(\tau, \pm\tau)\right|^2}\right)^{\frac{1}{2}}, \tag{3.27}$$

where

$$\tilde{G}_2\left(\tau,\tau'\right)=\int_{-\infty}^{\infty}dtdt'\;\tilde{G}_2\left(t,t',t+\tau,t'+\tau'\right), \tag{3.28}$$

with $\tilde{G}_2\left(t_1,t_2,t_3,t_4\right)$ the second-order correlation function introduced in Sec. 1.1.6. Applying it to the Gaussian two-photon state leads to

$$\tilde{G}_2\left(t,t',t+\tau,t'+\tau'\right)=\tilde{\phi}^*_{\mathrm{Gauss}}\left(t,t'\right)\tilde{\phi}_{\mathrm{Gauss}}\left(t+\tau,t'+\tau'\right), \tag{3.29}$$

so that

$$\tilde{G}_2\left(\tau,\tau'\right)=\exp\left[-i\overline{\omega}\left(\tau+\tau'\right)\right]\exp\left[-\frac{1}{16}\left(a^2\left(\tau+\tau'\right)^2+b^2\left(\tau-\tau'\right)^2\right)\right]. \tag{3.30}$$

We see that taking $\tau=\tau'$ gives the uncertainty in the absolute time whereas $\tau=-\tau'$ gives the uncertainty in the relative time between the two photons. Finally the two-photon coherence times are

$$\Delta t_+ = \frac{1}{a}, \tag{3.31}$$

$$\Delta t_- = \frac{1}{b}. \tag{3.32}$$

In the same way, one can calculate the spectral bandwidths of the two photons, $\Delta\omega_+$ and $\Delta\omega_-$, which correspond, respectively, to the uncertainty in the frequency sum $\omega_1+\omega_2$ and frequency difference $\omega_1-\omega_2$. We obtain

$$\Delta\omega_+ = \frac{a}{4}, \tag{3.33}$$

$$\Delta\omega_- = \frac{b}{4}. \tag{3.34}$$

We thus have the following uncertainty relations

$$\Delta t_+\Delta\omega_+ = \frac{1}{4}, \tag{3.35}$$

$$\Delta t_-\Delta\omega_- = \frac{1}{4}, \tag{3.36}$$

which become inequalities for non-Gaussian two-photon state. Moreover, two other relations arise due to the entanglement of the two photons:

$$\Delta t_+\Delta\omega_- = \frac{b}{4a}, \tag{3.37}$$

$$\Delta t_-\Delta\omega_+ = \frac{a}{4b}. \tag{3.38}$$

Actually, any separable state ($a=b$) satisfies the inequalities

$$\Delta t_+\Delta\omega_- \geq \frac{1}{4}, \tag{3.39}$$

$$\Delta t_-\Delta\omega_+ \geq \frac{1}{4}, \tag{3.40}$$

with equalities for Gaussian states. Equations (3.39) and (3.40) are equivalent to Bell's inequalities for continuous variable entanglement. Any entangled two-photon state will violate one of these two inequalities. For instance, if we consider the time correlated entangled state with $a/b < 1$ then the inequality (3.40) is violated. And vice versa, the time anti-correlated state violates Eq. (3.39).

From the above discussion, we see that the coherence bandwidths of a two-photon state give information about the presence or not of entanglement through the inequalities (3.39) and (3.40). A similar properties exists for position/momentum entanglement, with similar inequalities. Using far field — for the momentum — and near field — for the position — coincidence imaging schemes, one can access the different coherence lengths and angles and then verify if the state violates or not the Bell inequalities [154, 155, 156].

3.3 Two-photon interferences

In practice it is not possible to measure directly the coherence time and the spectral bandwidth, especially when dealing with two-photon entangled states for which both can be quite small. For instance, the uncertainty of the relative time of emission is subpicosecond [17] whereas the time resolution of photodetectors is of the order of 10 to 100 picoseconds. For that reason one uses two-photon interferometric schemes to achieve high precision measurements. In the following, we present two types of interferometers. Each of them allows to access a particular width, either a or b, and therefore to test Bell's inequalities (3.39) and (3.40). Besides, interferometric schemes allow to evidence non-local effects due to the presence of entanglement in the two-photon state. It is the case of the postponed compensation scheme that we present at the end of this section.

3.3.1 Hong-Ou-Mandel interferometer

The first important example to discuss two-photon interferences is the so-called Hong-Ou-Mandel (HOM) interferometer [17] that uses a beam splitter (BS) as depicted in Fig. 3.3.a. In order to describe the interferences, we consider the coincidence rate R_{34} at the output ports 3 and 4 with an incident state given by the Gaussian two-photon amplitude (3.6). This interference scheme can be realized both with type-I and type-II SPDC. For the type-II case, one has to suppress the polarization distinguishability using a half-wave plate which rotates the polarization of one of the photon so that the two photons end up in the same polarization state. Another possibility is to send the two photons in the same input port of the BS and consider that each polarization constitutes an input mode of the BS. These two situations are physically equivalent. The coincidence rate is defined by

$$R_{34} = \int_{-\Delta T/2}^{\Delta T/2} dt dt' \ \langle : \hat{n}_3 (t) \, \hat{n}_4 \left(t'\right) : \rangle, \tag{3.41}$$

where ΔT is the sampling time and $\hat{n}_i (t)$ is the photon number operator of the mode i. We assume in the following that the sampling time is much larger than all other time scales of the problem, i.e. $\Delta T \gg t_c \gg 1/\overline{\omega}$, such that the domain of time integration

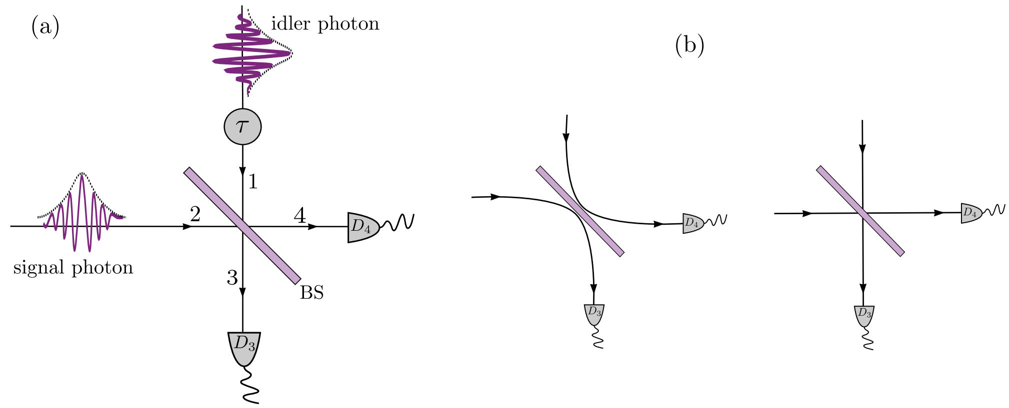

Figure 3.3: (a) Sketch of the Hong-Ou-Mandel interferometer. Two photons arrive at the input arms 1 and 2 of a beam splitter. Then they are either reflected or transmitted with probabilities 1/2 for a symmetric beam splitter before being absorbed by the two photodetectors D_3 and D_4. In order to observe the interferences, a delay line, placed in the arm 1, introduces a phase shift of one of the two photons only. (b) Sketch of the two interfering paths.

can be extended to infinity in Eq. (3.41). The operator $\hat{a}_i(t)$ is a Fourier transform of $\hat{a}_i(\omega)$:

$$\hat{a}_i(t) = \frac{1}{\sqrt{2\pi}} \int_{-\infty}^{+\infty} d\omega \ \hat{a}_i(\omega) \mathrm{e}^{-i\omega t}. \tag{3.42}$$

The BS is assumed to be lossless and symmetric, i.e. its transmission and reflection coefficients are equal in absolute value. Hence the output and input modes are related by the following unitary transformation which ensures energy conservation [40]:

$$\begin{aligned} \hat{a}_3(\omega) &= \frac{1}{\sqrt{2}} \left(\hat{a}_1(\omega) + i\hat{a}_2(\omega) \right), \\ \hat{a}_4(\omega) &= \frac{1}{\sqrt{2}} \left(\hat{a}_2(\omega) + i\hat{a}_1(\omega) \right). \end{aligned} \tag{3.43}$$

Then taking into account the time delay τ in the input arm 1, one obtains

$$R_{34} = \frac{1}{2} - \frac{1}{2} \int_{-\infty}^{\infty} d\omega d\omega' \ \phi\left(\omega, \omega'\right) \phi^*\left(\omega', \omega\right) \mathrm{e}^{-i\tau(\omega - \omega')}, \tag{3.44}$$

which can be express in the following convenient form

$$R_{34} = \frac{1}{2} - \frac{1}{2} \int_{-\infty}^{\infty} dt dt' \ \tilde{\phi}\left(t+\tau, t'-\tau\right) \tilde{\phi}^*\left(t', t\right) \tag{3.45}$$

$$= \frac{1}{2} - \frac{\tilde{G}_2(\tau, -\tau)}{2}. \tag{3.46}$$

Using the expression of $\tilde{G}_2(\tau, \tau')$ given in Eq. (3.29) for the bi-Gaussian two-photon state, we can write the coincidence rate as

$$R_{34} = \frac{1}{2} \left(1 - \exp\left(-\frac{(b\tau)^2}{4} \right) \right), \tag{3.47}$$

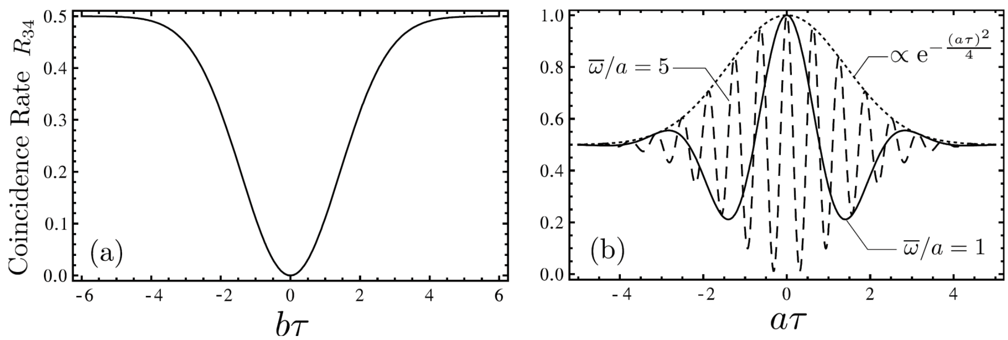

Figure 3.4: Coincidence photocount rate at the output of (a) the Hong-Ou-Mandel interferometer and (b) the Mach-Zender interferometer.

which yields the so-called HOM dip with absence of coincidence at $\tau = 0$ as shown in Fig. 3.4.a where the coincidence rate is plotted as a function of the dimensionless parameter $b\tau$. The absence of coincidences is related to perfectly destructive interferences between the two paths that lead to the same result, as shown in Fig. 3.3.b. The HOM interferometer allows measuring Δt_- and then $\Delta\omega_-$, i.e. it measures the time delay between the two photons at the output surface of the non-linear crystal [17].

It is important to note that entanglement is not necessary to obtain such quantum interferences[5]. Complete absence of coincidence can be achieved with a separable state $\left|\overline{\Omega}\right\rangle_1 \left|\overline{\Omega}\right\rangle_2$. In Eq. (3.47), the visibility,

$$\mathcal{V} = \max(R_{34}) - \min(R_{34}) / (\max(R_{34}) + \min(R_{34})), \tag{3.48}$$

equals one because the two photons are perfectly indistinguishable, so that the two path are indistinguishable too. Moreover, one can still obtain interferences even with distinguishable photons but with less visibility. It is the case, for instance, if the central frequency $\overline{\omega}$ is different for the two photons. The more distant the two central frequencies, the more lower the visibility.

One can see that for a fixed single-photon coherence time Δt_c, the interference pattern is sensitive to the correlations present in the incident state. When the state is perfectly anti-correlated in frequency, $b \to 0$ such that $\Delta t_- \to \infty$, $R_{34} = 0$, i.e. one obtains the same result as for the monochromatic case with $|\Psi\rangle = |\overline{\omega}\rangle_i |\overline{\omega}\rangle_s$. At the opposite, when the state is perfectly correlated in time, $\Delta t_- \to 0$ and $R_{34} = 1/2$ which is the result obtained with Bernoulli trials, for instance, when flipping a coin.

3.3.2 Mach-Zender interferometer

We now consider another type of interferometer, the so-called Mach-Zender (MZ) interferometer depicted in Fig. 3.5. The derivation of the coincidence rate is similar to the case of the HOM interferometer and leads to

$$R_{34} = \frac{1}{2} + \frac{1}{2}\int_{-\infty}^{\infty} d\omega d\omega' \cos\left((\omega + \omega')\tau\right) \phi\left(\omega, \omega'\right) \phi^*\left(\omega', \omega\right). \tag{3.49}$$

[5] By quantum interference we mean the interference that cannot be reproduced with classical waves with maximal visibility.

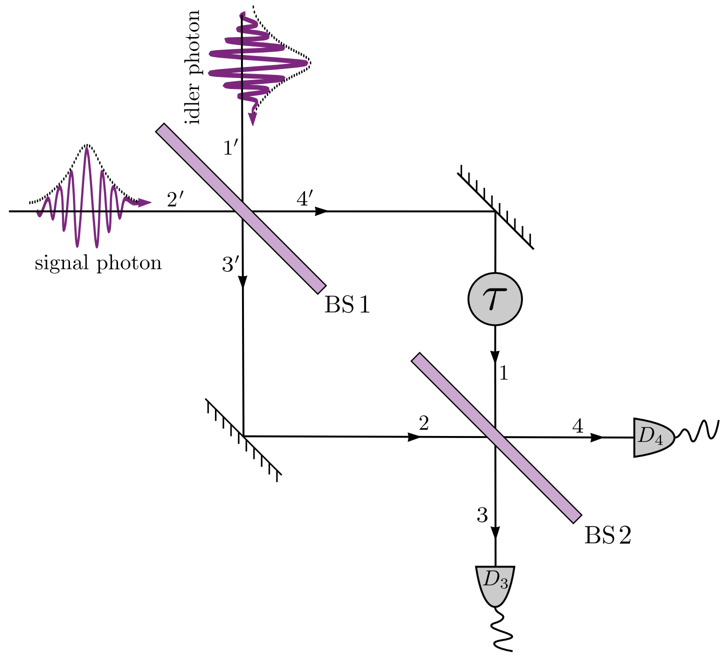

Figure 3.5: Sketch of the Mach-Zender interferometer.

Using the Fourier transform of $\phi\left(\omega,\omega'\right)$ we obtain

$$R_{34} = \frac{1}{2}+\frac{1}{2}\mathrm{Re}\left[\int_{-\infty}^{\infty} dtdt'\ \tilde{\phi}\left(t+\tau,t'+\tau\right)\tilde{\phi}^{*}\left(t',t\right)\right] \tag{3.50}$$

$$= \frac{1}{2}+\frac{\mathrm{Re}\left[\tilde{G}_2\left(\tau,\tau\right)\right]}{2}. \tag{3.51}$$

Then for a bi-Gaussian two-photon state, using Eq. (3.29), we have

$$R_{34} = \frac{1}{2}\left(1+\cos\left(2\tau\overline{\omega}\right)\exp\left[-\frac{\left(a\tau\right)^2}{4}\right]\right). \tag{3.52}$$

The situation is quite similar to the HOM interferometer except the existence of oscillations at the central frequency $\overline{\omega}$. The MZ interferometer allows one to measure Δt_+ and $\Delta\omega_+$. We show in Fig. 3.4.b the coincidence rate as a function of the dimensionless parameter $a\tau$.

Here again, the interferences do not require any entanglement in the incident state. Besides, when the state is perfectly correlated in frequency, $a\to 0$, then $\Delta t_+\to\infty$ and interferences are present whatever the value of τ. In the opposite case, when $a\to\infty$, the interferences disappear leading to the classical result $R_{34}=\frac{1}{2}$.

We see from the above discussion that HOM *or* MZ interferometers cannot distinguish a separable state from an entangled state. However, the combined measurement of the coincidence rates in MZ *and* HOM interferometers allows obtaining both Δt_+ and Δt_- and then checking if one of the inequalities (3.39) or (3.40) is violated.

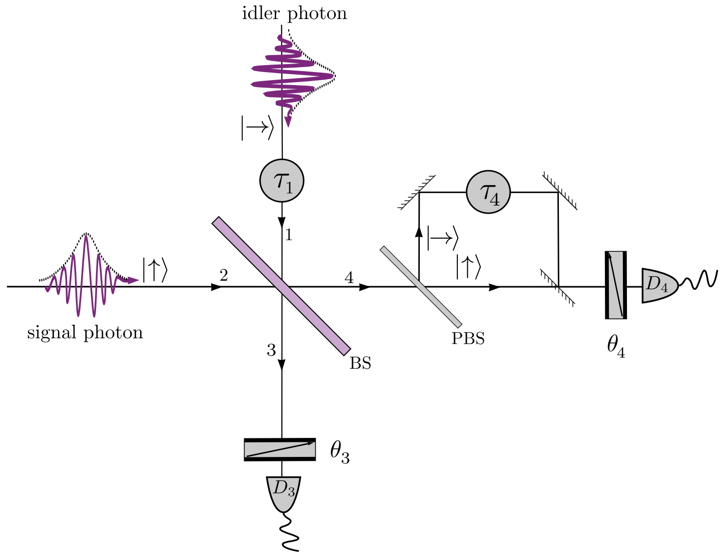

Figure 3.6: Sketch of the HOM interferometer with postponed compensation.

3.3.3 Non-local interferences with postponed compensation

As we have seen in the previous section concerning HOM and MZ interferometers, the entanglement between the two photons is not necessary for obtaining quantum interferences. Here, we present a type of interference scheme where interferences can only be obtained if the incident state is entangled.

The idea is the following. Two wave packets with orthogonal polarizations arrive at the input ports of a BS with a large time delay τ_1 imposed on the photon of polarization $\rightarrow$ such that the two photons do not overlap at the beam splitter. Thus the photons are well distinguishable in time. Then the first time delay can be compensated by applying a second time delay τ_4 in one of the output arms of the BS for the photon of polarization $\uparrow$. Before reaching the photodetectors, the polarization distinguishability is suppressed by two polarizers such that the polarization state of each photon after the polarizers is given by $|\theta\rangle = \cos\theta|\uparrow\rangle + \sin\theta|\rightarrow\rangle$.

Applying the same procedure than as the HOM and MZ interferometers, the coincidence rate at the two detectors D_3 and D_4 is given by

$$\begin{aligned} R_{34} &= \frac{1}{8}\left(\sin^2(\theta_3+\theta_4)+\sin^2(\theta_3-\theta_4)\right)+ \\ &+\frac{1}{8}\left(\cos^2(\theta_3+\theta_4)-\cos^2(\theta_3-\theta_4)\right)\times \\ &\times\mathrm{Re}\left[\int_{-\infty}^{\infty} d\omega d\omega'\ \phi(\omega,\omega')\,\phi^*(\omega',\omega)\exp\left[-i\left(\omega(\tau_4-\tau_1)+\omega'\tau_1\right)\right]\right] \end{aligned} \tag{3.53}$$

Then using the Fourier transform of $\phi_{\text{Gauss}}(\omega, \omega')$ we obtain

$$\begin{aligned}
&\int_{-\infty}^{\infty} d\omega d\omega' \; \phi(\omega, \omega') \, \phi^*(\omega', \omega) \exp\left[-i\left(\omega(\tau_4 - \tau_1) + \omega'\tau_1\right)\right] = \\
&= \int_{-\infty}^{\infty} dt dt' \; \tilde{\phi}(t - \tau_1, t' + \tau_1 - \tau_4) \, \tilde{\phi}^*(t', t) \\
&= \tilde{G}_2(-\tau_1, \tau_1 - \tau_4) \, .
\end{aligned}$$

For the Gaussian two-photon state, using Eq. (3.29), we have

$$\begin{aligned}
R_{34} &= \frac{1}{8}\left(\sin^2(\theta_3 + \theta_4) + \sin^2(\theta_3 - \theta_4)\right) + \\
&+ \frac{1}{8}\left(\cos^2(\theta_3 + \theta_4) - \cos^2(\theta_3 - \theta_4)\right) \exp\left[-\frac{1}{16}\left(a^2\tau_4^2 + b^2(\tau_4 - 2\tau_1)^2\right)\right] .
\end{aligned} \tag{3.54}$$

From Eq. (3.54) we see that interferences appear with time delay variations similarly to HOM interferometer but also with the variations of the polarizer angles, leading to an oscillatory behavior. Let us consider only the time interferences by fixing the angles at $\theta_3 = \theta_4 = \pm\pi/4$. The coincidence rate becomes

$$R_{34} = \frac{1}{8}\left(1 - \exp\left[-\frac{1}{16}\left(a^2\tau_4^2 + b^2(\tau_4 - 2\tau_1)^2\right)\right]\right) .$$

When $\tau_1 \gg \Delta t_-$, i.e., when the two photons are well separated in time the interferences no longer exist if there is no postponed compensation, i.e., if $\tau_4 = 0$. This situation corresponds to $b\tau \gg 1$ in HOM with distinguishable events. However, if $\tau_4 \neq 0$ interferences can be restored if the argument in the exponential function is set to zero. This is not possible for all kinds of two-photon states and depends on the correlations existing in the incident state. Indeed, the discriminant Δ of the quadratic equation for τ_4 obtained by requiring the argument to be zero, is $\Delta = -(ab\tau_1)^2$, so that a physical solution is possible only if a or/and $b = 0$. The case $a = b = 0$ implies $\Delta t_c = \infty$ and obviously any time delay is meaningless for such an incident state.

The situation is more interesting when Δt_c has a finite value. In this situation, interferences are not possible if the incident state is separable. However, if the state is entangled one can observe a perfect interference with maximal visibility. It corresponds to the situation of $a = 0$ or $b = 0$. If the state is perfectly anti-correlated in frequency ($a = 0$), perfect interferences occur for $\tau_4 = 2\tau_1$. If the state is perfectly correlated in frequency ($b = 0$), the time delay τ_1 has no effect and perfect interferences are obtained for $\tau_4 = 0$. Because, the photons cannot overlap at the BS, these interferences require time "non-locality" which is present only in entangled states.

We conclude this section on two-photon interferences by insisting on the fact that two-photon interferences are called quantum interferences because the results discussed above cannot be obtained with maximal visibility with classical states of light such as coherent states. However, the only prerequisite for perfect visibility is the indistinguishability of the photons so that the propagation paths are also indistinguishable. Therefore, the entanglement is not needed unless in situations where non-locality is involved as it is the case in the postponed compensation experiment.

However, when the incident photons are indistinguishable the output state becomes entangled whatever the incident state, but it is an entanglement between modes and not between particles (photons). Actually, the BS transformation is local for the photons but is nonlocal for the modes leading to the creation of mode entanglement. Then, quantum correlations appear and are beared by the modes which leads to quantum interferences. Historically, such two-photon interferences have been realized first with entangled two-photon states because SPDC was the easiest way to obtain photon pairs.

We will see in the next section how these results and behaviors can be transposed in the case where a disordered medium takes the place of the deterministic interferometer.

3.4 Two-photon speckle with bi-Gaussian two-photon states

We now consider the transmission of a two-photon state through a disordered medium. In order to obtain analytical results, we first consider the bi-Gaussian state introduced above and compare the results with the one obtained with a two-mode coherent state [22] defined by

$$|\psi_{\mathrm{coh}}\rangle = |\{\alpha(\omega)\}\rangle_{\alpha_1} |\{\alpha(\omega)\}\rangle_{\alpha_2}, \tag{3.55}$$

with

$$\alpha(\omega) = \frac{1}{(\sqrt{\pi}\Delta)^{1/2}} \exp\left(-(\omega-\overline{\omega})^2/2\Delta^2\right). \tag{3.56}$$

This state describes two pulses with orthogonal polarizations and a frequency bandwidth Δ around the central frequency $\overline{\omega}$. The fundamental difference between the coherent state (3.55) and the previously introduced two-photon states is that the former is not an eigenstate of the photon number operator $\hat{n}$. The number of photons is therefore not a good quantum number in this state. However, similarly to the Fock state, the photons in the state (3.55) have the same spectral properties and hence cannot be distinguished after being transmitted through a disordered medium.

3.4.1 Stationary random medium

Let us consider a three-dimensional slab of elastically scattering random medium (no absorption or gain), perpendicular to the z axis and having thickness L and cross-section $A \gg L^2$ (see Fig. 3.7). The incident light is multiply scattered by the random heterogeneities of the medium before reaching one of the two detectors located in the far field. In the multiple scattering regime, the mean free path ℓ due to disorder is much shorter than the slab thickness L, $\ell \ll L$. On the other hand, the disorder is considered to be weak, so that $\ell \gg \lambda_0$, with λ_0 being the central wavelength of the incoming light. This corresponds to the diffusive regime of propagation introduced in Sec. 2.1.2.

Monochromatic light at a frequency ω incident on the slab can be decomposed over the basis of plane waves having wave vectors $\mathbf{k}(\omega) = \{\mathbf{k}_\perp, k_z\}$, with $\mathbf{k}_\perp = \{k_x, k_y\}$, in one of two orthogonal polarization states that we will denote by 'α_1' and 'α_2'. We recall that for a slab of surface A, the number of modes in this basis is $2 \times N(\omega) = 2 \times k(\omega)^2 A/2\pi$. The same representation is valid for the light leaving the slab. From here on we will assume that N can be assumed constant (i.e., independent of ω) within the frequency bandwidth of the incident light. Input-output relations give the photon annihilation operators $\hat{a}_i(\omega)$ associated with the outgoing modes i in terms of the

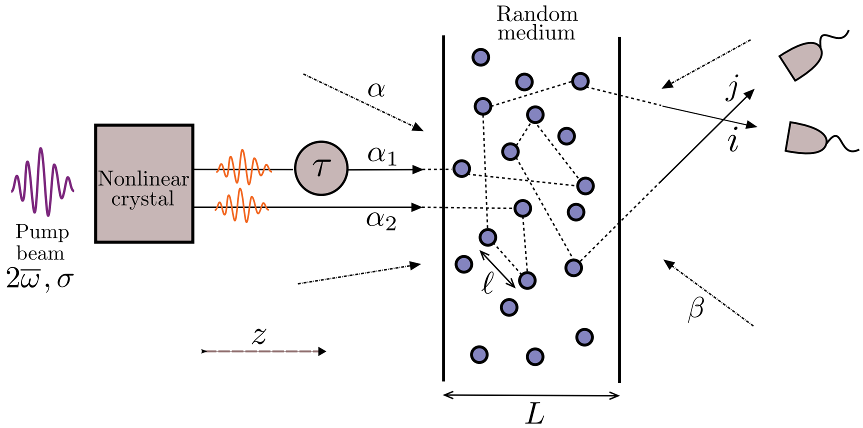

Figure 3.7: Sketch of the experimental situation considered to measure the coincidence rate of two-photon light transmitted through a disordered slab. A birefringent non-linear crystal is pumped by laser pulses of central frequency $2\bar{\omega}$ and bandwidth σ. Two collinear beams of orthogonal polarizations 'α_1' and 'α_2' and frequencies ω_1 and ω_2, are obtained as a result of spontaneous parametric down-conversion in the crystal. These beams are incident on a slab of disordered medium, with the 'α_1' beam delayed by a time τ. Light is multiply scattered inside the slab and the transmitted light in modes i and j is detected by two photodetectors in the far field. The multiple scattering regime is ensured by the requirement $\ell \ll L$, with ℓ the mean free path due to disorder and L the thickness of the slab.

annihilation operators $\hat{a}_\alpha(\omega)$ associated with the incoming modes α [9]:

$$\hat{a}_i(\omega) = \sum_{\alpha=1}^{N} t_{i\alpha}(\omega)\, \hat{a}_\alpha(\omega) + \sum_{\beta=N+1}^{2N} r_{i\beta}(\omega)\, \hat{a}_\beta(\omega)\,. \tag{3.57}$$

For the outgoing mode i on the right of the slab (as in Fig. 3.7), the first sum runs over the incoming modes α incident from the left and transmitted through the slab with transmission coefficients $t_{i\alpha}(\omega)$, whereas the second sum runs over the incoming modes β incident from the right and reflected with reflection coefficients $r_{i\beta}(\omega)$. As explain in Chapter 2 the coefficients $t_{i\alpha}(\omega)$ and $r_{i\beta}(\omega)$ form the (unitary) scattering matrix S of the slab. Operators $\hat{a}_i$ and $\hat{a}_\alpha$ obey the usual bosonic commutation relations: $[\hat{a}_i(\omega_1), \hat{a}_j(\omega_2)] = 0$ and $[\hat{a}_i(\omega_1), \hat{a}_j(\omega_2)^\dagger] = \delta_{ij}\delta(\omega_1 - \omega_2)$, and the same for $\hat{a}_\alpha$ and $\hat{a}_\beta$.

As far as $L \gg \ell$, $N \gg 1$, and we are not interested in quantities that involve summations over all input or output modes (like, e.g., the conductance or the total transmission), the unitary constraint on the matrix S can be relaxed. Then, in the diffuse regime of scattering, the transmission coefficients $t_{i\alpha}(\omega)$ can be assumed to be independent identically distributed random variables with circular Gaussian statistics, zero mean, and some frequency correlation function $C(\Delta\omega)$: $\overline{t_{i\alpha}(\omega)t_{j\alpha'}(\omega')^*} = \overline{T}_{\alpha b}\delta_{\alpha\alpha'}\delta_{ij}C(\omega-\omega')$ (see Sec. 2.2.3). Here $\overline{T}_{\alpha b} = \overline{|t(\omega)|^2}$ is the frequency-independent, average intensity transmission coefficient. Note that the average intensity transmission coefficient is assumed independent of the incoming and outgoing modes considered.

In the following, we will use two different models for the frequency correlation function $C(\Delta\omega)$. A simple model I, $C(\Delta\omega) = \exp(-|\Delta\omega|/\Omega_0)$, with Ω_0 the correlation frequency, will facilitate integrations all along the chapter and thus will allow for a number of analytic results. A more realistic model II, introduced in Sec. 2.2.3, $C(\Delta\omega) = \sqrt{-i\Delta\omega/\Omega_{\text{Th}}}/\sinh(\sqrt{-i\Delta\omega/\Omega_{\text{Th}}})$ [157], with Ω_{Th} the Thouless frequency, will be used to obtain predictions that can be experimentally verified in a diffusely scattering disordered medium. We note, however, that both correlation functions given above decay fast with $\Delta\omega$ and hence the results will be similar for both models.

3.4.2 Average photocount rate

All states that we are considering have on average one photon in each polarization state. This can be confirmed by calculating the quantum expectation value $\langle \hat{n}_{\alpha_1,\alpha_2} \rangle$ of the photon number operator [22]

$$\hat{n}_{\alpha_1,\alpha_2} = \int_{-\Delta T/2}^{\Delta T/2} dt\; \hat{a}^\dagger_{\alpha_1,\alpha_2}(t)\hat{a}_{\alpha_1,\alpha_2}(t), \tag{3.58}$$

where $\hat{a}_i(t)$ is the inverse Fourier transform of $\hat{a}_i(\omega)$. This quantity can be measured in an experiment by counting photons arriving at a polarization-discriminating photodetector placed in front of the photon source during a sufficiently long time ΔT.

To start with and to illustrate our general calculation scheme, let us compute the average number of photons transmitted into a mode i, also called the one-photon intensity. The operator corresponding to this quantity is [22]

$$\hat{n}_i = \int_{-\Delta T/2}^{\Delta T/2} dt\; \hat{a}^\dagger_i(t)\hat{a}_i(t). \tag{3.59}$$

To perform the calculation, we express the operator $\hat{a}_i(t)$ through the operators $\hat{a}_\alpha(t)$ and $\hat{a}_\beta(t)$ using the input-output relations (3.57), use commutation relations to compute the quantum expectation values and the Gaussian statistics of $t_{i\alpha}$ to average over realizations of disorder. The result is the same for both coherent and two-photon entangled states:

$$\overline{\langle \hat{n}_i \rangle} = (\langle \hat{n}_{\alpha_1} \rangle + \langle \hat{n}_{\alpha_2} \rangle)\overline{T}_{\alpha b} = 2\overline{T}_{\alpha b}. \tag{3.60}$$

We thus observe that the average photon number is not sensitive to the quantum state of light, — a well-known and quite general fact in quantum optics. It is not surprising indeed that the entanglement between two photons is not accessible from one-photon observables such as the one-photon intensity. One has to consider two-photon observables to expect manifestation of entanglement.

Given the normalization of the input state and the fact that $\overline{T}_{\alpha b} \ll 1$ in the diffusive regime, $\overline{\langle \hat{n}_i \rangle}$ is equal to the ensemble-averaged probability $\overline{P_1}$ that a photodetector measures a photon in the outgoing mode i. It also gives the photon counting rate (in units of photons per pulse) if a sequence of independent and separated in time pulses is sent through the random medium.

3.4.3 Coincidence rate and photon correlations

We now turn to the study of the two-photon speckle. Two different but related quantities can be used to characterize correlations between numbers of photons transmitted into two modes i and j: the photon number correlation function $C_{ij} = \langle \hat{n}_i \hat{n}_j \rangle$ and the probability $P_2(i,j)$ to detect a photon in each of the modes i and j. The later also corresponds to the rate of photon coincidence counts if a sequence of pulses in the same quantum state is sent into the medium. The two quantities are related through a relation that we derive in Appendix B:

$$P_2(i,j) = \frac{1}{1+\delta_{ij}} \langle : \hat{n}_i \hat{n}_j : \rangle = \frac{C_{ij} - \delta_{ij} \langle \hat{n}_i \rangle}{1+\delta_{ij}}, \tag{3.61}$$

where $: \cdots :$ denotes the normal ordering of operators. It is worthwhile to note that $P_2(i,j)$ was identified with $\langle : \hat{n}_i \hat{n}_j : \rangle$ in some of the recent literature [11] without distinguishing the cases $i \neq j$ and $i = j$.

For two independent[6] photons, P_2 factorizes: $P_2(i,j) = P_1(i)P_1(j)$, where $P_1(i)$ is the probability to detect a photon in the outgoing mode i. It describes the usual, one-photon speckle pattern and it is proportional to the intensity of light in the mode i. Actually, when a separable state is sent in only *one* mode of the disordered medium, P_2 factorizes too, as shown by van Exter's group in Refs. [12, 144] (see Fig. 3.1). However, when a separable state is sent in two different modes, i.e., one photon in each mode, P_2 does not factorize. The latter situation is similar to the HOM interferometer discussed in Sec. 3.3.1.

It is important to realize that P_2 defined above corresponds to a single realization of the random medium. It is therefore a random quantity and fluctuates from one realization of disorder to another. To obtain a deterministic quantity, it is therefore natural to average P_2 over an ensemble of realizations of the random medium.[7] This ensemble-averaged quantity was studied in Refs. [10, 11, 12, 13]. Note that even for two independent photons, $\overline{P_2(i,j)} = \overline{P_1(i)P_1(j)}$ does not factorize into a product of $\overline{P_1}$'s (in contrast to the unaveraged P_2) because $P_1(i)$ can have nontrivial (classical) correlations in both space and time [4, 1]. Therefore, the ensemble-averaged two-photon speckle $\overline{P_2(i,j)}$ combines properties due to the quantum nature of the incident light and those arising from the classical correlations between photons in two different modes.

As we see from Eq. (3.61), both $P_2(i,j)$ and C_{ij} can be found from the normally ordered correlation function $\langle : \hat{n}_i \hat{n}_j : \rangle$. The average of the latter over disorder is derived in Appendix C.1 for any kind of quantum state and reads

$$\begin{aligned}
\overline{\langle : \hat{n}_i \hat{n}_j : \rangle} \;&=\; \overline{T}^2_{\alpha b} \iint_{-\infty}^{\infty} d\omega d\omega' \sum_{\alpha,\beta} \left(\left\langle \hat{a}^\dagger_\beta\left(\omega'\right) \hat{a}^\dagger_\alpha\left(\omega\right) \hat{a}_\alpha\left(\omega\right) \hat{a}_\beta\left(\omega'\right) \right\rangle + \right. \\
&+\; \left. \delta_{ij} \left\langle \hat{a}^\dagger_\alpha\left(\omega'\right) \hat{a}^\dagger_\beta\left(\omega\right) \hat{a}_\alpha\left(\omega\right) \hat{a}_\beta\left(\omega'\right) \right\rangle |C(\omega-\omega')|^2 \right).
\end{aligned} \tag{3.62}$$

In a realistic experiment, the coincidence rate is most conveniently measured as a function of the time delay τ between the two photons introduced by a delay line in the path of the photon with polarization α_1 as shown in Fig. 3.7. This is equivalent to adding a phase shift $i\omega_1\tau$ to the α_1-polarized photon, so that $\phi_{\text{Gauss}}(\omega_1,\omega_2) \rightarrow \phi_{\text{Gauss}}(\omega_1,\omega_2)\, e^{i\omega_1\tau}$ and similarly for the coherent state. Then, calculating the quantum

[6]By independent photons we mean two photons described by a separable state *and* well distinguishable in time. Therefore, two photons described by a separable state are not necessarily independent.

[7]Higher-order statistical moments of P_2 were studied in Ref. [10]; its correlation functions might also be of interest.

expectation values in the r.h.s. of Eq. (3.62) for the bi-Gaussian entangled state, we obtain

$$\overline{\langle : \hat{n}_i \hat{n}_j : \rangle}_{\text{Gauss}} = 2\overline{T}^2_{\alpha b} \left(1 + \delta_{ij} \iint_{-\infty}^{\infty} d\omega d\omega' \left| \phi_{\text{Gauss}} \left(\omega, \omega' \right) \right|^2 |C(\omega - \omega')|^2 \mathrm{e}^{-i(\omega-\omega')\tau} \right). \tag{3.63}$$

The same quantity for the two-mode coherent state is

$$\begin{aligned} \overline{\langle : \hat{n}_i \hat{n}_j : \rangle}_{\text{coh}} &= 4\overline{T}^2_{\alpha b} \left(1 + \delta_{ij} \iint_{-\infty}^{\infty} d\omega d\omega' \left| \alpha \left(\omega \right) \right|^2 \left| \alpha \left(\omega' \right) \right|^2 \right. \\ &\times \left. |C(\omega - \omega')|^2 \cos^2 \left(\left(\omega - \omega' \right) \tau / 2 \right) \right). \end{aligned} \tag{3.64}$$

In the multiple scattering regime, the quantities given by Eqs. (3.63) and (3.64) will be very small and one can doubt their interest for real experiments. Indeed, typically we have $\overline{T}_{\alpha b} \sim \ell / NL$ with $L/\ell \gtrsim 10$. The number of transverse modes for a slab of area $A = 1$ mm^2 will be $N = k^2 A / 2\pi \sim 10^7$ at optical frequencies, leading to a prefactor $\overline{T}^2_{\alpha b} \sim 10^{-16}$ in Eqs. (3.63) and (3.64). Nevertheless, photon coincidence measurements in transmission through a disordered medium were realized for coherent and quasi-chaotic states [143]. The measurement can be optimized by noting that Eqs. (3.63) and (3.64) does not depend on the particular choice of modes i and j but are only sensitive to the fact that $i = j$ or $i \neq j$. One can thus count photons in an arbitrary large number $M > 2$ of modes and then average over the results obtained for all pairs (i, j) of modes. Each mode should, however, be addressed individually, which will require M photodetectors. One can also think about more sophisticated experimental setups to detect photon coincidences without knowing the precise mode to which the photons belong, like the one exploiting the two-photon absorption [158]. From the theoretical point of view, we can avoid working with too small quantities by normalizing Eqs. (3.63) and (3.64) by $\overline{T}^2_{\alpha b}$. We thus define the normalized photocount coincidence rate R as

$$R_{ij} = \frac{1}{\overline{T}^2_{\alpha b}} \overline{P_2(i,j)} = \frac{1}{\overline{T}^2_{\alpha b}} \times \frac{\overline{\langle : \hat{n}_i \hat{n}_j : \rangle}}{1 + \delta_{ij}}. \tag{3.65}$$

An expression similar in structure to Eq. (3.63) was derived for the coincidence rate in Ref. [11], though for a slightly different entangled state. In addition, the authors of Ref. [11] have taken into account the lowest-order corrections to the Gaussian model for transmission coefficients $t_{i\alpha}$ that we discussed in Chapter 2, and found additional contributions to the coincidence rate. These contributions, however, turned out to be of order $1/g$, with $g = N\ell/L \gg 1$, and would be negligible under conditions of diffuse scattering that we consider here. In the absence of these terms, we find from Eqs. (3.63) and (3.64) that for $i \neq j$, $R_{\text{Gauss}} = 2$ and $R_{\text{coh}} = 4$ independent of any parameters. The latter result corresponds to the total absence of any correlation between photon numbers in two different modes $i \neq j$: $\overline{\langle : \hat{n}_i \hat{n}_j : \rangle} = 4\overline{T}^2_{\alpha b} = \overline{\langle \hat{n}_i \rangle}\ \overline{\langle \hat{n}_j \rangle}$, whereas the former indicates that there are negative correlations: $\overline{\langle : \hat{n}_i \hat{n}_j : \rangle} = 2\overline{T}^2_{\alpha b} < \overline{\langle \hat{n}_i \rangle}\ \overline{\langle \hat{n}_j \rangle}$. Negative correlations in transmission of non-classical light through disordered media were already predicted theoretically in Refs. [138, 141, 14] and observed experimentally in Ref. [142] for squeezed light. For $i \neq j$, the parameter-dependent corrections to

Eqs. (3.63) and (3.64) due to the non-Gaussian statistics of $t_{i\alpha}$ and correlations between them would be of order $1/g \ll 1$ [11]. This is much smaller than the variations of the coincidence rates by 50% or so for $i = j$. The latter should be therefore much easier to access experimentally. For this reason, in the rest of this section we will study the case $i = j$ and compute R_{ii} which describes the probability for two photons to be found in the same outgoing mode. We will omit the subscript 'ii' of R_{ii} to lighten the notation.

Bi-Gaussian state

Considering the model I for the frequency correlation function, we obtain from Eq. (3.63)

$$R_{\text{Gauss}}\,(t,w) \quad = \quad 1+\exp\left(\frac{1}{w^2}-\frac{t^2}{4}\right)\text{Re}\left[\exp\left(i\frac{t}{w}\right)\text{erfc}\left(\frac{1}{w}+i\frac{t}{2}\right)\right], \quad (3.66)$$

where the dimensionless variables are $t = b\tau$ and $w = \Omega_0/b$. The function erfc is the complementary error function defined by $\text{erfc}(x) = 1 - 2/\sqrt{\pi}\int_x^\infty dt\, \exp(-t^2)$.

For $\Omega_0 \gg b$, $t_{i\alpha}(\omega)$ can be assumed frequency-independent within the bandwidth b around $\overline{\omega}$ and Eq. (3.66) reduces to $R_{\text{Gauss}}\,(t,0) = 1 + \exp(-t^2/4)$, which is equivalent, up to a sign in front of the second term in the r.h.s, to the coincidence rate in the HOM interferometer studied in Sec. 3.3. Instead of a dip in the coincidence rate, we now find a peak, which is explained by the fact that we compute coincidences in the same outgoing mode and not in two different modes.

The minimum and the maximum values $R_{\text{Gauss}} = 1$ and 2 of the normalized coincidence rate in Eq. (3.66) can be understood without appealing to the entangled nature of the quantum state and turn out to be universal for all two-photon states. For $\tau b \gg 1$, the photons are well separated in time and are transmitted through the disordered medium independently. The probability for each photon to end up in a given outgoing mode i is equal to $\overline{T}_{\alpha b}$. The probability that both photons are measured in the same mode i is equal to the product of single-photon probabilities: $\overline{P_2(i,j)} = \overline{T}_{\alpha b}^2$, leading to $R_{\text{Gauss}} = 1$. In contrast, at $\tau = 0$ the two photons cannot be considered independent and the two-photon interference leads to a larger probability for them to be detected in the same mode, thus the coincidences have a peak. Because the information about the polarization is completely lost during the propagation through the disordered medium and because the two photons have the same spectrum the interference is perfectly constructive and R doubles with respect to the case of independent photons. We will show in Sec. 3.5.3 that *destructive* two-photon interference can lead to $R < 1$ and even to $R = 0$ for certain specially prepared states.

Let us now consider the case of arbitrary relation between the correlation frequency Ω_0 and b. In Fig. 3.8, we plot the coincidence rate for 3 different values of b/Ω_0. We observe that the increase of disorder–quantified by the increase of the parameter b/Ω_0–has two distinct consequences. First, we observe a lowering of the maximum coincidence rate in the absence of delay ($\tau = 0$). The disorder thus washes out the two-photon interferences. However, at the same time we see that the curve $R_{\text{Gauss}}(b\tau)$ broadens and the photon coincidence rate grows up at large $b\tau$. This is a consequence of the fluctuating time of flight of photons through the medium. Typically, the time of flight of a photon through a disordered medium fluctuates from very small values (ballistic propagation) to values exceeding $\Omega_{\text{Th}}^{-1} \sim \Omega_0^{-1}$ (diffusion). The medium can, therefore, partially compensate for the initial delay τ between the two photons and make them interfere even for $b\tau \gg 1$ at the price of a low coincidence rate however.

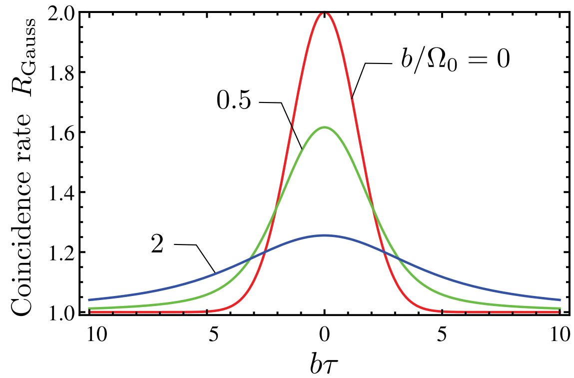

Figure 3.8: Photocount coincidence rate for two detectors in the same outgoing mode and the two-photon bi-Gaussian entangled state at the input of a disordered medium. Different values of b/Ω_0 correspond to different disorder strengths and/or sample thicknesses.

Concerning the entanglement, at a fixed disorder strength, the average coincidence rate appears to give the same information as the HOM interferometer, hence one cannot discriminate entangled from non-entangled states using transmission through a disordered medium. Indeed, at a low disorder, i.e., when $b/\Omega_0 \ll 1$, the width of the curves in Fig. 3.8 allows to access the value of b. We recall that for an entangled state, b is related to Δt_-, the relative time between the two photons at the output surface of the non-linear crystal but when the state is separable ($a = b$), b is related to the single-photon coherence time: $t_\text{c} = \sqrt{2}/b$. However, in the limit of strong disorder, the width depends on Ω_0 and it is no more possible to obtain information on the incident state. This regime allows to access information about the disordered medium. This property of the coincidence rate has been first noticed in Ref. [11].

Coherent state

Let us now compare these results with the one obtained for the coherent state defined by Eq. (3.55). From Eq. (3.64) and using the model I, we have

$$\begin{aligned} R_{\text{coh}}(t, w) &= 2 + \exp\left(\frac{2}{w^2}\right) \text{erfc}\left(\frac{\sqrt{2}}{w}\right) \\ &+ \exp\left(\frac{1}{2}\left(\frac{4}{w^2} - t^2\right)\right) \text{Re}\left[\exp\left(2i\frac{t}{w}\right) \text{erfc}\left(\frac{1}{\sqrt{2}}\left(\frac{2}{w} + it\right)\right)\right] \end{aligned} \tag{3.67}$$

where $t = \tau\Delta$ and $w = \Omega_0/\Delta$.

In Fig. 3.9, we show R_{coh} as a function of delay time τ for the realistic model II of the correlation function $C(\Delta\omega)$. Despite the fact that the coherent state exhibits neither entanglement, nor a well-defined photon number, the overall shape of the coincidence curve is still the same: it is a bell-shaped curve with the overall amplitude suppressed by disorder. However, R_{coh} reaches larger absolute values, up to $R_{\text{coh}} = 4$, in contrast to R_{Gauss} that is bounded by 2 from above.

The results for the coherent state can be rederived in a completely classical framework, by replacing the operators $\hat{a}$ and $\hat{a}^\dagger$ with complex numbers a and a^* and ignoring

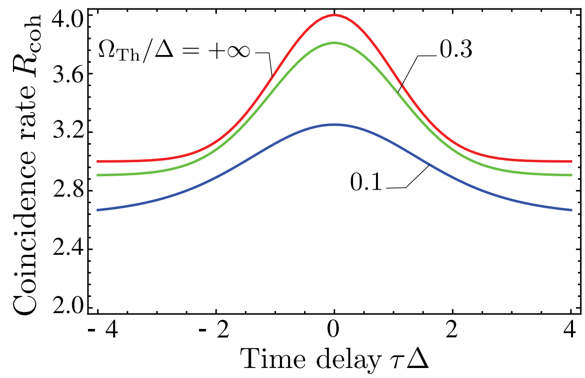

Figure 3.9: Same as Figs. 3.12 but for the coherent state (3.55) incident on the disordered medium. The delay time τ and the correlation frequency Ω_0 are in units of bandwidth Δ.

the commutation relations[8]. This provides a way to understand some of the aspects of Fig. 3.9 using the well-known facts from the theory of classical wave scattering [4, 1]. Indeed, we obtain from Eq. (3.65) that $R_{\rm coh} = 2\overline{I_{\Delta T}^2}/(\overline{I_{\Delta T}})^2$, where $I_{\Delta T}$ is the intensity of the transmitted wave, integrated over a time interval ΔT. When $\tau = 0$, the transmitted wave a_i is a superposition of independent waves $a_i^{(\alpha_1)}$ and $a_i^{(\alpha_2)}$ resulting from the transmission of incident waves with 'α_1' and 'α_2' polarizations, respectively. For weak disorder, both $a_i^{(\alpha_1)}$ and $a_i^{(\alpha_2)}$ (and hence a_i) have zero-mean circular Gaussian statistics. Because the intensity $I = |a_i|^2$, $\overline{I_{\Delta T}^2}/(\overline{I_{\Delta T}})^2 = 2$ is obtained for the monochromatic illumination ($\Delta \to 0$). This corresponds to the so-called large intensity fluctuations, well-known for classical speckle patterns [159]. The resulting maximum value of $R_{\rm coh}$ is 4, as can also be seen from Fig. 3.9. In contrast, when $|\tau|$ is large, the detections of signals due to the incident 'α_1' and 'α_2' waves are separated in time. The measured time-integrated intensity is a sum of two independent terms: $I_{\Delta T} = I_{\Delta T}^{(\alpha_1)} + I_{\Delta T}^{(\alpha_2)}$. This yields $\overline{I_{\Delta T}^2}/(\overline{I_{\Delta T}})^2 = 3/2$ and $R_{\rm coh} = 3$ for $\Delta \to 0$. When the spectral width Δ of the incident waves increases, the measured signals suffer from a partial averaging even for a single realization of disorder. In the limit of $\Delta \to \infty$, the intensity of transmitted light does not fluctuate and $R_{\rm coh} = 2$.

3.5 Two-photon speckle with a realistic type-II SPDC two-photon state

We now consider the more general type-II state given in Eqs. (3.2), (3.3) and (3.4). The main difference is that the two photons are distinguishable because without the extended phase matching the spectra of the two photons are different (see Sec. 3.2.1). It will appear to be a drawback for obtaining high visibility of two-photon speckles. However, this distinguishability will allow changing the symmetry of the state and obtaining a new type of non-classical interferences.

[8]This procedure is possible here because we computed a normal ordered observable. Otherwise, for the case of $\langle \hat{n}_i \hat{n}_j \rangle$ for example, the shot noise appears and the coherent state cannot be replace by a classical wave unless $\overline{\hat{n}_i} \gg 1$ which is obviously not the case here given that $\overline{T}_{\alpha b}$.

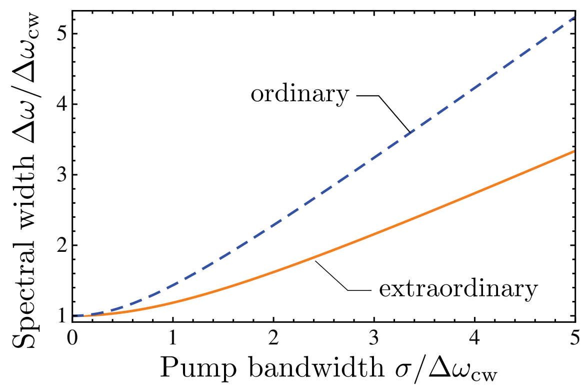

Figure 3.10: Spectral widths of the ordinary 'o' and extraordinary 'e' beams of photons in the type II state described by $\phi_{\mathrm{SPDC}}(\omega_1, \omega_2)$, as functions of the bandwidth of the pump beam σ, for typical parameters of a BBO non-linear crystal [152]. All quantities are normalized by the spectral width $\Delta\omega_{\mathrm{cw}}$ of the two beams in the monochromatic limit $\sigma = 0$.

3.5.1 Spectral distinguishability

In type-II phase matching, we have $h(\omega_1, \omega_2) = \mathrm{sinc}\left[\nu_{\mathrm{o}}(\omega_1 - \overline{\omega}) + \nu_{\mathrm{e}}(\omega_2 - \overline{\omega})\right]$ where $\nu_j = L_{\mathrm{crys}}\left(\partial k_j/\partial\omega|_{\omega=\overline{\omega}} - \partial k_{\mathrm{p}}/\partial\omega|_{\omega=2\overline{\omega}}\right)/2$, with $j = \mathrm{o}, \mathrm{e}$, quantify the phase mismatch between the down-converted photons 'o' and 'e' and the pump 'p' in the non-linear crystal, where 'o' and 'e' denote the ordinary and extraordinary polarization states, respectively. Due to the phase matching function h, the two-photon amplitude $\phi_{\mathrm{SPDC}}(\omega_1, \omega_2)$ is not symmetric with respect to the exchange of frequencies of ordinary and extraordinary photons: $\phi_{\mathrm{SPDC}}(\omega_1, \omega_2) \neq \phi_{\mathrm{SPDC}}(\omega_2, \omega_1)$. This property stems from the different dispersion relations for the two polarization states in the non-linear crystal and can, as we will see, have important consequences for the probability P_2 of simultaneous photon detection by two photodetectors because the two photons become more and more distinguishable as the bandwidth of the pump pulse σ is increased. We illustrate this in Fig. 3.10 where we show the spectral width $\Delta\omega_{\mathrm{e,o}}$, defined here as the full width of the spectrum at half-maximum height, of ordinary and extraordinary beams, normalized by their value $\Delta\omega_{\mathrm{cw}} = 2.78/|\eta_-|$ in the monochromatic limit $\sigma \to 0$. To be able to estimate this quantity analytically, we replace the square of the sinc function by a Gaussian[9] $\exp(-x^2/2.79)$ with the same width at half-maximum. We obtain

$$\frac{\Delta\omega_{\mathrm{o,e}}}{\Delta\omega_{\mathrm{cw}}} = \frac{2|\nu_{\mathrm{o,e}}|}{|\eta_-|}\sqrt{\ln(2)\left[\frac{2.79}{(\nu_{\mathrm{o,e}}\Delta\omega_{\mathrm{cw}})^2} + \left(\frac{\sigma}{\Delta\omega_{\mathrm{cw}}}\right)^2\right]}, \tag{3.68}$$

where $\eta_- = \nu_{\mathrm{o}} - \nu_{\mathrm{e}}$ gives the relative time of emission of the two-photon[10]. If the pump is monochromatic, $|\eta_-|$ has the meaning of coherence time of the two-photon state. We see from Eq. (3.68) and Fig. 3.10 that the spectral widths of the two beams become different when σ increases, making distinguishable the photons originating from different beams even after transmission through a disordered medium.

[9] Note that this Gaussian approximation is not at all the same than the one discussed in Sec. 3.2.1.
[10] η_- is equivalent to b in the bi-Gaussian approximation.

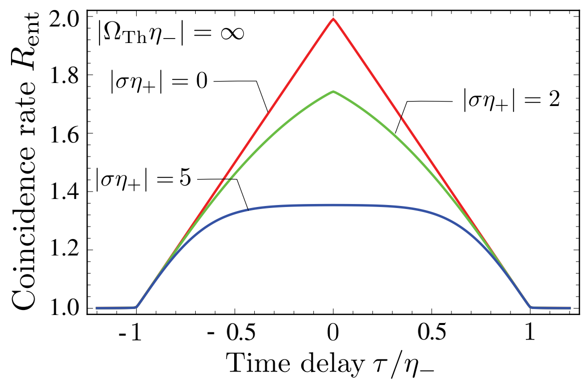

Figure 3.11: Photocount coincidence rate for two detectors in the same outgoing mode and the type II two-photon entangled state described by $\phi_{\mathrm{SPDC}}(\omega_1, \omega_2)$ at the input of a disordered medium with frequency-independent transmission coefficients $t_{\alpha i}$, as a function of delay τ between the two photons. Three curves correspond to different values of the parameter $s = \sigma\eta_+$ measuring the spectral width of the pulse that pumps the non-linear crystal where the photons are generated. An infinitely large value of Thouless frequency is assumed.

3.5.2 Coincidence rate

Because of asymmetry of $\phi_{\mathrm{SPDC}}(\omega_1, \omega_2)$, we have for the coincidence rate

$$\begin{aligned}\overline{\langle : \hat{n}_i \hat{n}_j : \rangle}_{\mathrm{SPDC}} &= 2\overline{T}^2_{\alpha b}\left(1 + \delta_{ij} \iint_{-\infty}^{\infty} d\omega d\omega' \phi^*_{\mathrm{SPDC}}\left(\omega, \omega'\right) \phi_{\mathrm{SPDC}}\left(\omega', \omega\right)\right. \\ &\times \left. |C(\omega - \omega')|^2 e^{-i(\omega-\omega')\tau}\right). \end{aligned} \tag{3.69}$$

Considering the exponential model I for the correlation function $C(\Delta\omega)$ of transmission coefficients, we obtain from Eq. (3.69):

$$\begin{aligned} &R_{\mathrm{ent}}(t, s, w) \\ &= 1 + \frac{1}{s\sqrt{\pi}} \int_{-1}^{1} dx\ f\left(t, w, x\right) \mathrm{erf}\left(\frac{s}{2}\left(1 - |x|\right)\right), \end{aligned} \tag{3.70}$$

where $f(t, w, x) = 2w/(4 + w^2 (x + t)^2)$ and the dimensionless variables are $t = \tau/\eta_-$, $s = \sigma\eta_+$ and $w = |\Omega_0\eta_-|$, with $\eta_\pm = \nu_{\mathrm{o}} \pm \nu_{\mathrm{e}}$. Here, erf denotes the error function defined by $\mathrm{erf}(x) = 2/\sqrt{\pi}\int_0^x dt\ \exp(-t^2)$.

For $\Omega_0 \gg 1/|\eta_-|$, $t_{i\alpha}(\omega)$ can be assumed frequency-independent within the bandwidth $1/|\eta_-|$ around $\bar{\omega}$ and Eq. (3.70) reduces to

$$R_{\mathrm{ent}}(t, s, \infty) = 1 + \frac{\sqrt{\pi}}{s}\begin{cases} \mathrm{erf}\left[\frac{s}{2}\left(1 - |t|\right)\right] & , |t| < 1 \\ 0 & , |t| \geq 1 \end{cases} \tag{3.71}$$

Exactly the same result is obtained for the model II in the limit of $|\Omega_{\mathrm{Th}}\eta_-| \to \infty$. Up to a sign in front of the second term in the r.h.s., Eq. (3.71) is equivalent to the coincidence rate in the HOM interferometer obtained in Ref. [37]. We show Eq. (3.71) in Fig. 3.11 for 3 values of s, corresponding to 3 different bandwidths σ of the pump pulse at fixed

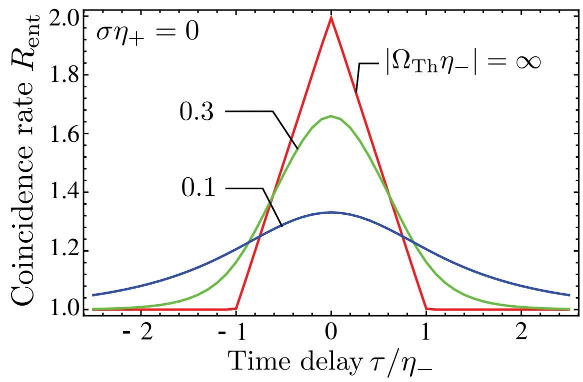

Figure 3.12: Photocount coincidence rate for two detectors in the same outgoing mode and the type II two-photon entangled state described by $\phi_{\mathrm{SPDC}}(\omega_1, \omega_2)$ incident on a disordered medium. The pump beam that generates the pair of photons in a non-linear crystal is assumed to be monochromatic ($\sigma = 0$); different values of $|\Omega_{\mathrm{Th}}\eta_-|$ correspond to different disorder strengths and/or sample thicknesses.

η_+. Increasing σ suppresses the two-photon interference effect in R_{ent}. This is due to the loss of indistinguishability of the two photons, which, in its turn, results from the fact that the two entangled photons do not have the same spectrum (see Fig. 3.10). As a consequence, the two-photon interference between them washes out with increase of σ. We do not discuss further the case of finite $\Omega_0\eta_-$ and $\Omega_{\mathrm{Th}}\eta_-$ because the physics is the same as for the bi-Gaussian state with the spectral distinguishability in addition. We just show in Fig 3.12 the coincidence rate obtained in this situation with the more realistic model II for the correlation function $C(\omega, \omega')$.

3.5.3 Symmetric and anti-symmetric entangled states

As we have shown in the previous section, the entangled state described by the function $\phi_{\mathrm{SPDC}}(\omega_1, \omega_2)$ defined by Eqs. (3.2), (3.3) and (3.4) leads to a coincidence rate R measured behind a random medium that is similar to that for a separable state. This might give an impression that entanglement adds no interesting physics to the optics of random media. This impression is, however, wrong. In order to demonstrate this, let us now consider a little bit more sophisticated entangled state, namely, the state given once again by Eq. (3.2) where we replace $\phi_{\mathrm{SPDC}}(\omega_1, \omega_2)$ by

$$\phi_\theta(\omega_1, \omega_2) = \mathcal{K}[\phi_{\mathrm{SPDC}}(\omega_1, \omega_2) + \mathrm{e}^{i\theta}\phi_{\mathrm{SPDC}}(\omega_2, \omega_1)], \tag{3.72}$$

with $\mathcal{K}$ being a normalization constant,

$$|\mathcal{K}|^2 = \frac{1}{2} \times \frac{1}{1 + \cos(\theta)\mathrm{erf}(\sigma\eta_+/2)\sqrt{\pi}/\sigma\eta_+}. \tag{3.73}$$

By properly adjusting the value of θ, we can make this state symmetric ($\theta = 0$) or antisymmetric ($\theta = \pi$) with respect to the exchange of the two photons. In other words, the state preserves its form with the same (symmetric) or opposite (antisymmetric) sign upon the exchange $\omega_1 \leftrightarrow \omega_2$ and can thus also be said to have bosonic or fermionic symmetry, respectively. An intermediate situation with $0 < \theta < \pi$ corresponds to

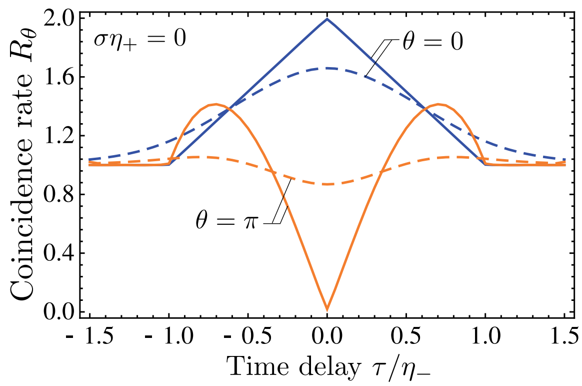

Figure 3.13: Photocount coincidence rate for two detectors in the same outgoing mode and the symmetric ($\theta = 0$, blue lines) and antisymmetric ($\theta = \pi$, orange lines) entangled states incident on a disordered medium. The pump is monochromatic and the disorder is weak ($|\Omega_{\mathrm{Th}}\eta_-| \to \infty$) for solid lines. $|\Omega_{\mathrm{Th}}\eta_-| = 0.3$ for dashed lines.

asymmetric states; $\theta = \pi/2$, for example, yields a state that leads to the same result for the average two-photon coincidence rate as the state (A.8) discussed in Sec. 3.5.2.

The states given by Eq. (3.72) can be prepared experimentally [160] and for $\theta = 0$, π have the advantage of conserving the perfect indistinguishability of the two photons whatever the bandwidth of the pump σ. This is in contrast to the entangled state considered in the previous section, in which the two photons become distinguishable as σ is increased because their spectra become different (see Fig. 3.10). As a result, Eq. (3.72) leads to a much weaker dependence of the coincidence rate on σ. In addition, the sign of the two-photon interference term can be inversed for the antisymmetric state ($\theta = \pi$), thus turning the constructive interference into the destructive one.

Because $\phi_\theta(\omega_1, \omega_2)$ is a linear combination of $\phi_{\mathrm{SPDC}}(\omega_1, \omega_2)$ and $\phi_{\mathrm{SPDC}}(\omega_2, \omega_1)$, the calculation of the coincidence rate for the former can be reduced to the analysis that was performed in Sec. 3.5.2. For the exponentially decaying correlation function $C(\Delta\omega)$ we obtain

$$\begin{aligned} R_\theta(t, s, w) &= 1 + 2\delta_{ij}|\mathcal{K}|^2 \int_{-1}^{1} dx f(t, w, x) \\ &\times \left[I(s, x) + \cos(\theta) J(s, x) \right], \end{aligned} \tag{3.74}$$

where $f(t, w, x)$ was defined in Sec. 3.5.2. The functions $I(s, x)$ and $J(s, x)$ are

$$I(s, x) = \frac{1}{s\sqrt{\pi}} \mathrm{erf}\left[\frac{s}{2}(1 - |x|)\right], \tag{3.75}$$

$$J(s, x) = \frac{1}{\pi}(1 - |x|) \exp\left(-\frac{s^2 x^2}{4}\right). \tag{3.76}$$

The striking difference between symmetric ($\theta = 0$) and antisymmetric ($\theta = \pi$) states is demonstrated in Fig. 3.13. We see that for a monochromatic pump ($\sigma = 0$) and weak disorder ($|\Omega_{\mathrm{Th}}\eta_-| \to \infty$), the symmetric state produces the same dependence of the coincidence rate on the delay time τ as the asymmetric state considered in Sec. 3.5.2. In contrast, the antisymmetric state ($\theta = \pi$) leads to a dip in the coincidence

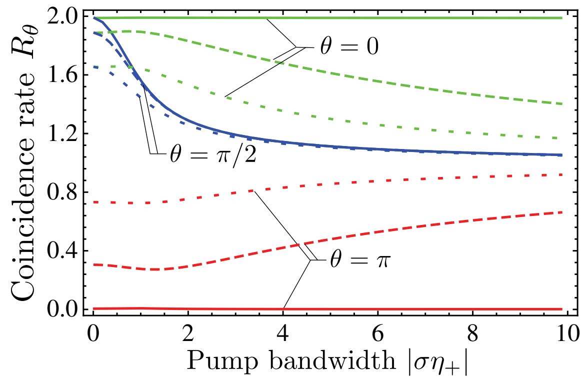

Figure 3.14: Photocount coincidence rate in the absence of time delay ($\tau = 0$) and for $|\Omega_{\text{Th}}\eta_-| \to \infty$ (solid lines), 1 (dashed lines) and 0.3 (dotted lines), as a function of the normalized bandwidth of the pump $|\sigma\eta_+|$.

rate at $\tau = 0$, instead of a peak. This is indeed reminiscent of the behavior of a pair of fermions that obey the Pauli principle and therefore avoid being in the same quantum state. Instead of an increase of coincidence rate observed for the state with the bosonic symmetry, the fermionic symmetry results in a complete suppression of coincidences, making it impossible to find two photons in the same outgoing mode. This effect is suppressed when the strength of disorder is increased (see the pair of lines corresponding to $|\Omega_{\text{Th}}\eta_-| = 0.3$ in Fig. 3.13), but the dip at $\tau = 0$ is still clearly visible.

The role of symmetry in the structure of the entangled state becomes obvious when we look at the evolution of $R_\theta(\tau)$ with the bandwidth σ of the pump. According to Fig. 3.10, increasing σ makes the spectra of the two photons different and thus makes the photons distinguishable. This suppresses two-photon interference effects and reduces the peak in $R_{\text{ent}}(\tau)$ (see Fig. 3.11). However, the situation is quite different for the symmetrized states that we study in the present section: in the states corresponding to $\theta = 0$ or π, the two photons remain indistinguishable independent of σ. The dependence of $R_\theta(\tau = 0)$ on $|\sigma\eta_+|$ shown in Fig. 3.14 illustrates this quite convincingly. At weak disorder ($|\Omega_{\text{Th}}\eta_-| \to \infty$), $R_\theta(\tau = 0)$ does not vary with σ, whereas at stronger disorder, increasing the bandwidth eventually suppresses interferences, though at considerably larger scales as compared to the asymmetric $\theta = \pi/2$ state.

To illustrate the positive impact of the symmetry of the state on the two-photon interference, in Fig. 3.15 we show the dependence of the photocount coincidence rate on the delay time for the symmetric state ($\theta = 0$) and the asymmetric state corresponding to $\theta = \pi/2$, at three different disorder strengths. For weak disorder ($|\Omega_{\text{Th}}\eta_-| \to \infty$), the difference is very important, although at stronger disorder the two results start to be closer, showing that disorder tends to reduce the role of symmetry. To quantify the impact of symmetry even further, in Fig. 3.16 we replot the solid lines corresponding to $\theta = 0$ and $|\sigma\eta_+| = 4$ and compare them with the result corresponding to the $\theta = \pi/2$ state at $|\sigma\eta_+| = 0$ (monochromatic pump). The curves of each of the 3 pairs, corresponding to different disorder strengths, are very close to each other. This illustrates that the symmetry of the state can compensate for the loss of two-photon interference due to the large bandwidth σ of the pump pulse.

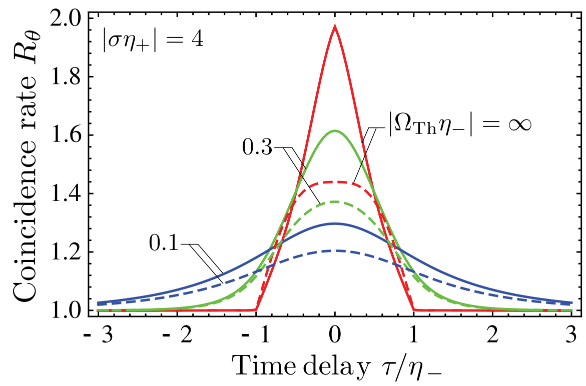

Figure 3.15: Comparison of photocount rates for states corresponding to $\theta = 0$ (symmetric state, solid lines) and $\pi/2$ (dashed lines), for a particular value of pump bandwidth $|\sigma\eta_+| = 4$.

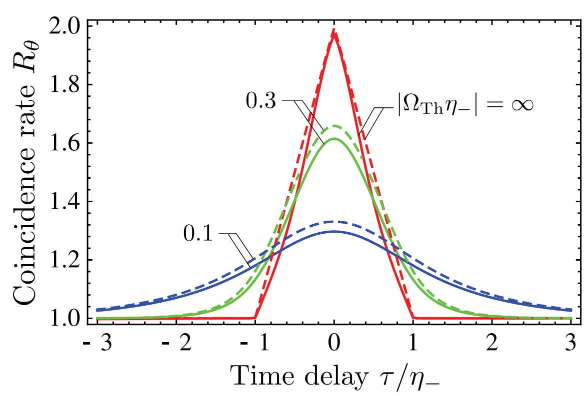

Figure 3.16: Comparison of photocount coincidence rates corresponding to $\theta = 0$, $|\sigma\eta_+| = 4$ (solid lines) and $\theta = \pi/2$, $|\sigma\eta_+| = 0$ (dashed lines).

3.5.4 Signs of non-classical light

Let us now clarify which properties of the coincidence rate R measured in transmission through a disordered medium result from the classical or non-classical nature of incident light. We adopt the following operational definition [161, 162]: we call light non-classical if its photocount statistics $p(n)$ cannot be obtained from the semi-classical Mandel's formula [40]

$$p(n) = \int_0^\infty \frac{I^n}{n!} \exp(-I) \mathcal{P}(I) dI \tag{3.77}$$

with $\mathcal{P}(I) \geq 0$ — the probability density of the classical variable (intensity) I. Obviously, the probability to detect 2 photons in a given outgoing mode i readily follows: $p(2) = \overline{I^2 \exp(-I)}/2 \simeq \overline{I^2}/2$. As before, the vertical line denotes averaging over realizations of disorder that in the present context is equivalent to averaging over the distribution $\mathcal{P}(I)$ and we made use of the fact that in transmission through a thick disordered medium, $\mathcal{P}(I)$ is appreciable only for $I \ll 1$. We see that Eq. (3.77) implies that the normalized photocount coincidence rate as defined by Eq. (3.65), is given by

$$R = \frac{p(2)}{\overline{T}_{\alpha b}^2} = 2\left(1 + \overline{\delta I^2}/\overline{I}^2\right), \tag{3.78}$$

where $\delta I = I - \overline{I}$ is the fluctuation of intensity and we used the fact that $\overline{I} = 2\overline{T}_{\alpha b}$ for the states considered in this work [see Eq. (3.60)].

In fact, we already used Eq. (3.78) to discuss the results obtained for the coherent state in Sec. 3.4.3 with $I = I_{\Delta T}$. $R = 2$ was obtained in the absence of intensity fluctuations ($\overline{\delta I^2} = 0$) and $R = 4$ — for $\overline{\delta I^2}/(\overline{I})^2 = 1$. We thus immediately conclude that the results for the coherent state can be described by Eq. (3.78) following from the Mandel's formula (3.77), confirming that, not surprisingly, this state remains classical after transmission through the medium. In contrast, we saw in Secs. 3.4.3 and 3.5.2 that two-photon entangled and separable states lead to $R < 2$. This would require $\overline{\delta I^2}/(\overline{I})^2 < 0$ in Eq. (3.78), which is impossible for any probability distribution $\mathcal{P}(I)$. Therefore, the results for two-photon states cannot be described by Eq. (3.77). This shows that these states remain non-classical upon transmission through a disordered medium.

Measurement of the absolute value of R in an experiment may be complicated because it requires proper normalization of the photocount number which is the raw output of the measuring device. The difference between classical and non-classical states of light also shows up in the contrast (or visibility) of the coincidence curve $R(\tau)$:

$$V = \frac{|R(0) - R(\infty)|}{R(0) + R(\infty)}. \tag{3.79}$$

This quantity is not sensitive to the normalization of R and may be easier to access experimentally. The maximum contrast is reached in the limit of $\Omega_{\mathrm{Th}} \to \infty$. For the asymmetric entangled state described by ϕ_{SPDC}, the symmetric entangled state (Eq. (3.72) with $\theta = 0$, and the bi-Gaussian two-photon state, the maximum contrast is $\max(V_{\mathrm{Gauss}}) = \max(V_{\mathrm{SPDC}}) = \max(V_{\theta=0}) = 1/3$, whereas for the coherent state we find $\max(V_{\mathrm{coh}}) = 1/7$. The largest contrast $\max(V_{\theta=\pi}) = 1$ is reached for the

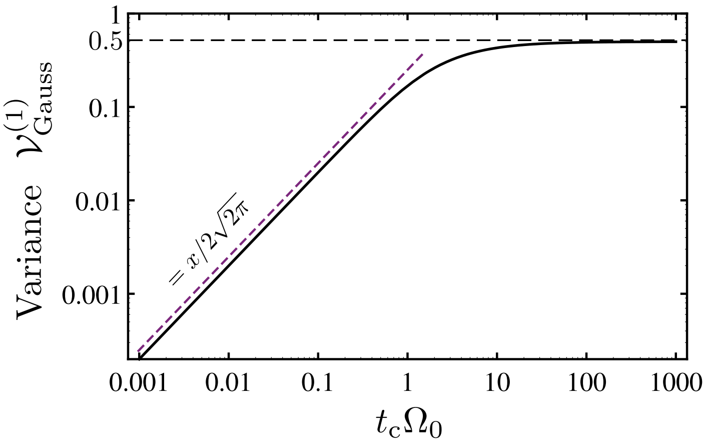

Figure 3.17: (Solid line) Visibility of the one-photon speckle pattern as a function of $t_c\Omega_0$ for the bi-Gaussian entangled two-photon state incident on a disordered medium. The horizontal dashed line shows the asymptotic limit of the variance when $t_c\Omega_0 \to \infty$. The purple dashed line corresponds to the limit of the variance for $t_c\Omega_0 \ll 1$.

antisymmetric entangled state (Eq. (3.72) with $\theta = \pi$). Therefore, the contrast of the two-photon speckle pattern is more than a factor of 2 larger for the non-classical light considered in this chapter than for the classical light, represented by the coherent state

3.6 Visibility of speckle patterns

3.6.1 Visibility of one-photon speckle patterns

Let us now consider the normalized variance $\overline{(\Delta\langle\hat{n}_i\rangle)^2}$ of the one-photon intensity defined by

$$\overline{(\Delta\langle\hat{n}_i\rangle)^2} = \frac{\overline{\langle\hat{n}_i\rangle^2}}{\overline{\langle\hat{n}_i\rangle}^2} - 1. \tag{3.80}$$

This quantity corresponds to the visibility of the one-photon speckle pattern $\overline{\mathcal{V}}^{(1)} = \overline{(\Delta\langle\hat{n}_i\rangle)^2}$. A maximal visibility equal to one implies large fluctuations of the intensity from one realization to another. In classical wave physics, this observable is associated with the so-called $C^{(1)}$ function introduced in Chapter 2 and related to the granularity of the speckle pattern.

As shown in Appendix C.2, the second moment of intensity is given by

$$\begin{aligned} \overline{\langle\hat{n}_i\rangle^2} \;\; = \;\; & \overline{T}^2_{\alpha b} \iint_{-\infty}^{\infty} d\omega d\omega' \sum_{\alpha,\beta} \left(\left\langle \hat{a}^\dagger_\alpha(\omega)\,\hat{a}_\alpha(\omega) \right\rangle \left\langle \hat{a}^\dagger_\beta(\omega')\,\hat{a}_\beta(\omega') \right\rangle + \right. \\ & \left. + \left\langle \hat{a}^\dagger_\beta(\omega)\,\hat{a}_\alpha(\omega) \right\rangle \left\langle \hat{a}_\alpha(\omega')\,\hat{a}_\beta(\omega') \right\rangle |C(\omega-\omega')|^2 \right). \end{aligned} \tag{3.81}$$

Bi-Gaussian state

Considering now a bi-Gaussian state and using the symmetry properties of its two-photon amplitude $\phi_{\text{Gauss}}(\omega_1, \omega_2) = \phi_{\text{Gauss}}(\omega_2, \omega_1)$, we write the visibility as

$$\overline{\mathcal{V}}^{(1)}_{\text{Gauss}} = \frac{1}{2} \iiiint_{-\infty}^{\infty} d\omega d\omega' d\Omega d\Omega' \left|\phi_{\text{Gauss}}(\omega, \omega')\right|^2 \left|\phi_{\text{Gauss}}(\Omega, \Omega')\right|^2 |C(\Omega - \omega)|^2. \tag{3.82}$$

From Eq. (3.82), one sees that the maximum of the visibility is equal to 1/2 and is obtained when $C(\Omega - \omega)$ does not vary significantly on the frequency scale of $\phi(\omega, \omega')$. It means that disorder does not discriminate the frequencies appearing in the two-photon spectrum, so that the state behaves as a monochromatic wave with a large coherence time. The value 1/2 of the maximum comes from the presence of two photons in two orthogonal polarization. Therefore, a partial averaging is performed due to the polarization diversity. For the type-I two-photon state involving only one polarization, the visibility would have been maximal and equal to one.

We now perform the integration in Eq. (3.82) using the model I for the correlation function $C(\Omega - \omega)$. Then, the visibility becomes

$$\overline{\mathcal{V}}^{(1)}_{\text{Gauss}}(w) = \frac{1}{2}\exp\left(\frac{2}{w^2}\right)\text{erfc}\left(\frac{\sqrt{2}}{w}\right), \tag{3.83}$$

where the dimensionless variable is $w = \Delta t_{\text{c}}\Omega_0$ with Δt_{c} the single-photon coherence time calculated in Sec. 3.2.2.

As shown in Fig. 3.17, the visibility reaches its maximum when $t_{\text{c}}\Omega_0$ tends to infinity meaning that the temporal extent of the state is much larger than the Thouless time, i.e., the average time the photons spend in the medium. When $t_{\text{c}}\Omega_0$ decreases the scattered state loses its time coherence both because the propagation in the disordered medium adds random phases to each frequency component and because the coherence of the incident light decreases.

As expected, the visibility of the one-photon speckle pattern does not allow to say if the state is entangled or not. However, it is interesting to note that in the case of a maximally entangled state the coherence time tends to zero. Hence, the one-photon speckle pattern disappears. The single-photon state being completely mixed, the resulting interference pattern can be seen as a sum of a large number of independent speckles leading to a completely blurred pattern with a vanishing visibility.

Coherent state

For a two-mode coherent state, using Eqs. (3.55) and (3.56), we obtain

$$\overline{\mathcal{V}}^{(1)}_{\text{coh}} = \iint_{-\infty}^{\infty} d\omega d\Omega \, |\alpha(\omega)|^2 |\alpha(\Omega)|^2 |C(\Omega - \omega)|^2, \tag{3.84}$$

and then

$$\overline{\mathcal{V}}^{(1)}_{\text{coh}}(w) = \exp\left(\frac{2}{w^2}\right)\text{erfc}\left(\frac{\sqrt{2}}{w}\right), \tag{3.85}$$

where $w = \Omega_0/\Delta$. Although it has two different polarizations, the coherent state allows for a visibility equal to one because its photon number is not conserved contrary to the two-photon state, i.e., measuring a photon does not give any information about the state. Except for the maximal value, the behavior is the same as for the two-photon state with $\Delta t_\mathrm{c} = 1/\Delta$. However, comparing Eq. (3.85) and $R_\mathrm{coh}(0, w)$ shows clearly that $\overline{\langle : \hat{n}_i \hat{n}_j : \rangle} = \overline{\langle \hat{n}_i \rangle \langle \hat{n}_i \rangle}$, whether $i \neq j$ or not, in agreement with the discussion at the end of Sec. 3.4.3.

3.6.2 Visibility of two-photon speckle patterns

The last quantity that we consider is the normalized variance $\overline{(\Delta \langle : \hat{n}_i \hat{n}_j : \rangle)^2}$ of the coincidence rate defined by

$$\overline{(\Delta \langle : \hat{n}_i \hat{n}_j : \rangle)^2} = \frac{\overline{\langle : \hat{n}_i \hat{n}_j : \rangle^2}}{\overline{\langle : \hat{n}_i \hat{n}_j : \rangle}^2} - 1. \tag{3.86}$$

From Sec. 3.4.3, we have $\overline{\langle : \hat{n}_i \hat{n}_j : \rangle} = 2\overline{T}_{\alpha b}^2$ for $i \neq j$. First introduced by Beenakker *et al.* in Ref. [10] the variance of the two-photon transmitted intensity corresponds to the visibility of the two-photon speckle pattern. In the following, we will use the notation $\mathcal{V}^{(2)} = \overline{(\Delta \langle : \hat{n}_i \hat{n}_j : \rangle)^2}$ and consider only the case $i \neq j$. The expression of the variance for an arbitrary state is given by Eq. (C.17) derived in Appendix C.3 and is quite lengthy. Therefore, we here consider the application of Eq. (C.17) to the coherent and bi-Gaussian states which yields

$$\begin{aligned} \mathcal{V}^{(2)}_\mathrm{Gauss} &= 2\,\mathcal{V}^{(1)}_\mathrm{Gauss} + \\ &+ \iiiint_{-\infty}^{\infty} d\omega d\omega' d\Omega d\Omega' \left|\phi_\mathrm{Gauss}(\omega, \omega')\right|^2 \left|\phi_\mathrm{Gauss}(\Omega, \Omega')\right|^2 \\ &\times |C(\Omega - \omega)|^2 |C(\Omega' - \omega')|^2, \end{aligned} \tag{3.87}$$

and

$$\begin{aligned} \mathcal{V}^{(2)}_\mathrm{coh} &= 2\,\mathcal{V}^{(1)}_\mathrm{coh} + \\ &+ \left(\iint_{-\infty}^{\infty} d\omega d\Omega \ \left|\alpha(\omega)\right|^2 \left|\alpha(\Omega)\right|^2 \left|C(\Omega - \omega)\right|^2 \right)^2 \\ &= 2\,\mathcal{V}^{(1)}_\mathrm{coh} + \left(\mathcal{V}^{(1)}_\mathrm{coh}\right)^2. \end{aligned} \tag{3.88}$$

The integrations in Eqs. (3.87) and (3.88) are easy to perform in the limiting case when the frequency scale of $C(\Omega - \omega)$ is large compared to that of $\phi_\mathrm{Gauss}(\omega, \omega')$ or $\alpha(\Omega)$, i.e., when light can be considered monochromatic. Putting $C(\Omega - \omega) = 1$ and reminding that in this situation $\mathcal{V}^{(1)}_\mathrm{Gauss} = 1/2$ and $\mathcal{V}^{(1)}_\mathrm{coh} = 1$, we obtain $\mathcal{V}^{(2)}_\mathrm{Gauss} = 2$ and $\mathcal{V}^{(2)}_\mathrm{coh} = 3$.

Bi-Gaussian state

After integration, Eq. (3.87) yields

$$\mathcal{V}^{(2)}_\mathrm{Gauss}(K, w) = 2\,\mathcal{V}^{(1)}_\mathrm{Gauss}\left(w/\sqrt{K}\right) + \frac{w}{\sqrt{K}} \int_{-\infty}^{\infty} dx \ g(x, K, w), \tag{3.89}$$

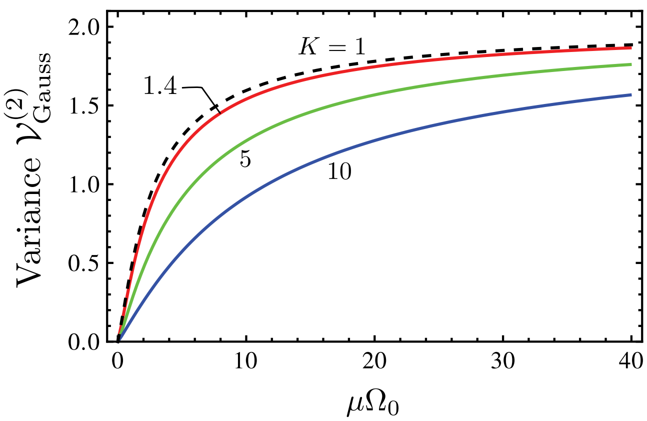

Figure 3.18: Visibility of the two-photon speckle pattern as a function of $\mu\Omega_0$ in transmission through a disordered medium for different amount of entanglement for the bi-Gaussian entangled two-photon state (solid lines) and for a separable state (dashed line).

where

$$g\left(x,K,w\right) = \frac{1}{2\sqrt{2\pi}}\exp\left(-2\left|x\right|\right)\exp\left(-\frac{x^2}{2}w^2K\right) \tag{3.90}$$
$$\times\left(\exp\left(\left(\frac{x}{\sqrt{2K}}w\sqrt{K^2-1}+\frac{\sqrt{2}}{w\sqrt{K}}\right)^2\right)\mathrm{erfc}\left(\frac{x}{\sqrt{2K}}w\sqrt{K^2-1}+\frac{\sqrt{2}}{w\sqrt{K}}\right)\right.$$
$$\left.+\exp\left(\left(-\frac{x}{\sqrt{2K}}w\sqrt{K^2-1}+\frac{\sqrt{2}}{w\sqrt{K}}\right)^2\right)\mathrm{erfc}\left(-\frac{x}{\sqrt{2K}}w\sqrt{K^2-1}+\frac{\sqrt{2}}{w\sqrt{K}}\right)\right),$$

with $w = \Omega_0\sqrt{2/ab}$ and K the Schmidt number of the incident state given by $K = (a^2+b^2)/2ab$. We expressed $\mathcal{V}^{(1)}_{\mathrm{Gauss}}$ as a function of $w/\sqrt{K}$ using the relation $\Delta t_{\mathrm{c}} = \mu/\sqrt{K}$ with $\mu = \sqrt{2/ab}$.

When the incident state is separable, $K = 1$ and the integration in Eq. (3.89) can be carried out leading to

$$\begin{aligned}\mathcal{V}^{(2)}_{\mathrm{Sep}}\left(w\right) &= 2\,\mathcal{V}^{(1)}_{\mathrm{Gauss}}\left(w\right)+\exp\left(\frac{4}{w^2}\right)\mathrm{erfc}^2\left(\frac{\sqrt{2}}{w}\right)\\ &= 2\,\mathcal{V}^{(1)}_{\mathrm{Gauss}}\left(w\right)+\left(2\mathcal{V}^{(1)}_{\mathrm{Gauss}}\left(w\right)\right)^2,\end{aligned} \tag{3.91}$$

where $w = \Omega_0\Delta t_{\mathrm{c}}$ because $a = b$.

When the state is entangled, i.e., when $K > 1$, $\mathcal{V}^{(2)}_{\mathrm{Gauss}}$ is no more a function of $\mathcal{V}^{(1)}_{\mathrm{Gauss}}$ only. We show in Fig. 3.18 the visibility of the two-photon speckle pattern as a function of $\mu\Omega_0$ for different amounts of entanglement. For a given amount of entanglement, $\mathcal{V}^{(2)}_{\mathrm{Gauss}}$ tends to zero with the strength of disorder. This behavior does not appear in the similar relation obtained by Beenakker *et al.* in Ref. [10] because the authors did not consider the non-stationary light and thus disregarded the effect of disorder on the temporal coherence of the transmitted light. Besides, when the amount of entanglement increases, $\mathcal{V}^{(2)}_{\text{Gauss}}$ decreases to zero for maximal entanglement. This comes from the fact that $\mathcal{V}^{(2)}_{\text{Gauss}}$ depends on the single-photon coherence time. Actually, Eq. (3.87) is related to the so-called complementarity between one- and two-photon interferences [145, 146]. However, the complementarity relation would imply that $\mathcal{V}^{(2)}_{\text{Gauss}}$ becomes maximal when $\mathcal{V}^{(1)}_{\text{Gauss}}$ is minimal and reciprocally, which is not the case here as we see. In the same way as in Ref. [145], to obtain a complementarity relation between $\mathcal{V}^{(1)}_{\text{Gauss}}$ and $\mathcal{V}^{(2)}_{\text{Gauss}}$, one has to suppress the part that comes from interferences of separable photons in $\mathcal{V}^{(2)}_{\text{Gauss}}$. Therefore, an increase of entanglement would decrease $\mathcal{V}^{(1)}_{\text{Gauss}}$ but increase $\mathcal{V}^{(2)}_{\text{Gauss}}$ and vice-versa.

Chapter 4

Statistics of bipartite entanglement in transmission through a random medium

In the previous chapter, we considered the possibility of characterizing the entanglement of a state via the interference pattern occurring after its transmission through a random medium. In the present chapter we address a related but different question. Given a quantum state incident on a random medium, what is the amount of entanglement in the transmitted state? Obviously the presence or not of entanglement in the incident state strongly orients the answer. In a certain way, the amount of entanglement in the incident state conditions the amount of entanglement in the transmitted state. Here again, we consider bipartite entanglement between particles, i.e., between two photons and not between modes. However, we deal with a different kind of entanglement than in Chapter 3 because we consider a high-dimensional entanglement in momentum [58], i.e., states with quantum correlations in the transverse component of the wave vector.

In order to quantify the entanglement, we perform the Schmidt decomposition of the transmitted state. Therefore, the main goal of this chapter is the study of the distribution of the Schmidt eigenvalues which become random quantities due to the multiple scattering of light in the disordered medium.

4.1 Schmidt decomposition and random matrices: an overview

Before studying in details the Schmidt eigenvalue distribution of scattered state it is instructive to consider what is called "entangled random pure bipartite states". Considering a system belonging to the Hilbert space $\mathcal{H}$ of dimension $N \times M$, entangled random pure states are randomly chosen states in $\mathcal{H}$, that is sampled according to the unitarily invariant Haar measure.[1] These states are then considered as the typical states belonging to $\mathcal{H}$. Therefore, it becomes particularly relevant to address the following question: What is the typical amount of entanglement in these states? Actually,

[1] The unitarily invariant Haar measure is the uniform measure over the unitary group. Hence, considering an arbitrary state $|\psi_0\rangle \in \mathcal{H}$, any random pure states can be written as $|\Psi\rangle = \hat{U}\,|\Psi_0\rangle$ where $\hat{U}$ is a unitary matrix chosen randomly in the unitary group. For instance, $\hat{U}$ can be the operator of evolution written as $\hat{U} = \mathrm{e}^{-i\hat{H}t/\hbar}$ with $\hat{H}$ the time independent Hamiltonian of the system considered.

this question is similar to asking what is the typical purity of a subsystem that is a part of a random pure bipartite state uniformly distributed over $\mathcal{H}$ (see Sec. 1.2).

At the end of the 80's, Lubkin addressed the latter question in the context of a subsystem of dimension M linked to a reservoir of dimension $N \gg M$ [163]. He studied the average purity $\mathcal{P}_1$ of the subsystem of interest and showed that $\mathcal{P}_1$ is almost minimal. Then, Page extended the work of Lubkin in the case where $N \geq M \gg 1$ [164] and, giving a theoretical estimation of the average entropy of the subsystem, showed that it is almost maximal too:

$$\overline{E} \sim \ln M - \frac{M}{2N}, \tag{4.1}$$

where $E_{\max} = \ln M$. Noting that for bipartite entangled states, the lower is the purity of the subsystem, the higher is the amount of entanglement, one can apply the above result to entangled random pure states. It suggests that maximally entangled state may be very probable, i.e., that random pure states are good candidates for having maximal entanglement. However, one needs to know the full probability density of the entropy to justify such a statement.

More recently, Facchi *et al.* applied the powerful methods of statistical physics to study the statistics of Schmidt eigenvalues of an entangled random pure state depending on a fictitious temperature [165]. They showed the presence of two phase transitions in the eigenvalue density when varying the temperature, i.e., when varying the amount of entanglement. In Ref. [118], Nadal *et al.* used a Coulomb gas method to study the random matrix ensemble of fixed trace Wishart matrices, where the fixed trace constraint is associated with the normalization of the state. This matrix ensemble is the one describing entangled random pure states.[2] With this method, in the limit of large matrices, i.e., for large subsystems, they calculated the distribution of the entropy of entanglement and found that maximally entangled states are far from being the most probable.

In the same context, other groups also studied the Schmidt eigenvalue density of random pure bipartite states for arbitrary dimensions of the subsystems [166, 167]. The starting point is the joint distribution of the Schmidt eigenvalues which is known for the fixed trace Wishart matrices. Then, by integrations of the joint distribution, they obtained the Schmidt eigenvalue density and average measures of entanglement like the entropy.

4.2 Distribution of the transmitted Schmidt eigenvalues in the diffusive regime

4.2.1 Model

Random medium

We consider a three-dimensional slab of elastically scattering random medium (no absorption and no gain) as shown in Fig. 4.1. The propagation happens in a multiple scattering diffusive regime so that $L \gg \ell \gg \lambda$, with λ the the central wavelength of the

[2]It means that for random pure bipartite states the Schmidt eigenvalue density is given by the Marchenko-Pastur law rescaled due to the normalization constraint.

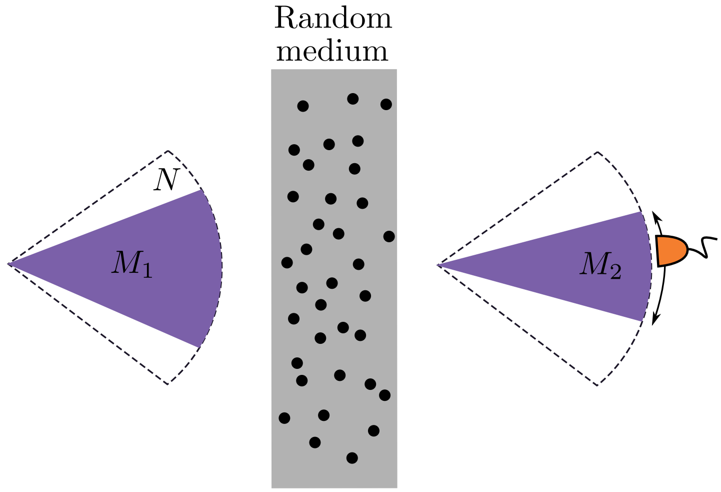

Figure 4.1: Sketch of a $3D$ disordered slab with the incoming and outgoing light described by the color cones where M_1 and M_2 are respectively the number of incoming and outgoing modes. The number of accessible outgoing modes M_2 is determined by the angular range of the detector denoted by the solid line double arrow. $2N$ is the total number of incoming and outgoing modes.

incoming quantum light. With $2N$ the total number of transverse modes[3] in the plane wave basis, the disorder media is described by a $2N \times 2N$ random scattering unitary matrix S defined by the input-output relations encountered in the previous chapters:

$$\hat{a}_i = \sum_{\alpha=1}^{2N} S_{i\alpha} \hat{a}_\alpha. \tag{4.2}$$

Then, using the unitarity properties of S ($S^\dagger = S^{-1}$), we have the following matricial relations:

$$\begin{aligned} \hat{a}^\dagger_{\text{out}} &= S^* \ \hat{a}^\dagger_{\text{in}}, \\ \hat{a}^\dagger_{\text{in}} &= S^T \ \hat{a}^\dagger_{\text{out}}, \end{aligned} \tag{4.3}$$

where $\hat{a}_{\text{out}}$ and $\hat{a}_{\text{in}}$ are $2N$ dimension vectors made up of annihilation operators $\hat{a}_i$ and $\hat{a}_\alpha$, respectively.

General two-photon state

Let us consider a very general two-photon state given in a certain basis (for instance, in the basis of plane waves) by

$$|\Psi\rangle = \frac{1}{\sqrt{2}} \sum_{\alpha,\beta=1}^{M_1} C_{\alpha\beta} \hat{a}^\dagger_\alpha \hat{a}^\dagger_\beta |0\rangle \ , \tag{4.4}$$

where the indices α, β refer to the modes of the light. The number of incoming modes M_1 is constraint by $M_1 < N$ (see. Fig. 4.1).

[3] We recall that a mode is the association of a polarization state and a wave vector.

Depending of the complex matrix C, which contains correlations between the two photons, the state (4.4) is *a priori* entangled. When the state is entangled, C cannot be factorized whereas for a separable state C can be written as $C = \mathbf{uv}$, with $\mathbf{u}$ a column vector and $\mathbf{v}$ a row vector. In contrast to the previous chapter, we do not treat the spectral structure of the incident light here and assume that light can be considered monochromatic. The normalization of the state (4.4) requires $\langle \Psi | \Psi \rangle = \mathrm{Tr}\left(C^\dagger C\right) = 1$.

Note that the state (4.4) implies two indistinguishable photons so that its entanglement has to be quantified following the procedure discussed in Sec. 1.3. Besides, the bosonic nature of the two-photon state constrains C to be symmetric so that $C = UDU^T$ where U is a $M_1 \times M_1$ unitary matrix and D a diagonal matrix that contains the singular values of C. Therefore the Schmidt decomposition of (4.4) is given by

$$|\Psi\rangle = \frac{1}{\sqrt{2}} \sum_{k=1}^{M_1} \sqrt{\lambda_k} \left(\hat{b}_k^\dagger\right)^2 |0\rangle \,, \tag{4.5}$$

where $\hat{b}_k^\dagger = \sum_\alpha U_{\alpha k} \hat{a}_\alpha^\dagger$. We recall that the Schmidt eigenvalues λ_k are the eigenvalues of the matrix $CC^\dagger$ so that for a maximally entangled state $\lambda_k = 1/\sqrt{M_1}$ for all $k \leq M_1$, and for a separable state $\lambda_k = 1/M_1$ for $k = 1$ and $\lambda_k = 0$ otherwise.

4.2.2 Transmitted state

We now derive the scattered state and give a matrix expression of this state that is convenient for performing the Schmidt decomposition. Substituting Eq. (4.2) into Eq. (4.4), we obtain

$$\begin{aligned} |\Psi\rangle &= \frac{1}{\sqrt{2}} \sum_{\alpha,\beta=1}^{M_1} C_{\alpha\beta} \left(\sum_{i=1}^{2N} S_{\alpha i}^T \hat{a}_i^\dagger \right) \left(\sum_{j}^{2N} S_{\beta j}^T \hat{a}_j^\dagger \right) |0\rangle \\ &= \sum_{i,j=1}^{2N} C_{ij}^{\mathrm{out}} \hat{a}_i^\dagger \hat{a}_j^\dagger \, |0\rangle \,, \end{aligned} \tag{4.6}$$

where

$$C_{ij}^{\mathrm{out}} = \sum_{\alpha,\beta=1}^{M_1} S_{i\alpha} C_{\alpha\beta} S_{\beta j}^T. \tag{4.7}$$

The matrix C^{out} is a $2N \times 2N$ random matrix that contains the correlations between the two scattered photons. It is worth noting that because the two matrices C and S do not have the same dimensions, it is not yet possible to express C^{out} as a matrix product. However by inserting a matching matrix P_1 in Eq. (4.7) we have

$$C^{\mathrm{out}} = S P_1 C P_1^T S^T, \tag{4.8}$$

where P_1 is a $2N \times M_1$ matrix made up of a $M_1 \times M_1$ identity matrix in the top and zeros in the bottom. Physically, P_1 expresses the fact that the expansion of the incident light in terms of incoming modes includes only a fraction of the total number of modes. This is necessarily the case when considering the transmission geometry.

In a typical experiment it is very difficult or even impossible to have access to all N outgoing modes and one detects $M_2 \ll N$ modes only. The results of measurements involving M_2 modes can be described by the projection of the state (4.6) on the corresponding subspace of modes. This projection is described by a $M_2 \times 2N$ matrix P_2 constructed in a way similar to P_1. Then, the projected state $|\widetilde{\Psi}\rangle$ is described by the truncated matrix $\widetilde{C}^{\text{out}}$ that we write as

$$\begin{aligned} \widetilde{C}^{\text{out}} &= \eta P_2 S P_1 C P_1^T S^T P_2^T \\ &= \eta P_2 S P_1 C \left(P_2 S P_1\right)^T , \end{aligned} \tag{4.9}$$

where the parameter η ensures the normalization of $\||\widetilde{\Psi}\rangle$. Because the number of incoming and outgoing modes that are under control satisfy M_1,$M_2 \leq N$, we define a $M_2 \times M_1$ truncated transmission matrix $\tilde{t}$ so that $\tilde{t} = P_2 S P_1$. When $M_1 = M_2 = N$, $\tilde{t}$ coincides the full transmission matrix t [10]. Therefore we have

$$\widetilde{C}^{\text{out}} = \eta\, \tilde{t} C \tilde{t}^{\,T}. \tag{4.10}$$

The Schmidt eigenvalues of the transmitted state are given by the eigenvalues of the random matrix $\widetilde{C}^{\text{out}}\widetilde{C}^{\text{out}\dagger}$. In our case the matrix $\widetilde{C}^{\text{out}}$ is random and hence the eigenvalues Λ_k should be characterized by their joint probability density $p_{\text{out}}(\{\Lambda\})$. If known, the latter gives access to statistical distributions of E_{out}, K_{out} and D_{out} that now become random quantities too. In what follows, we will compute only the eigenvalue density $p_{\text{out}}(\Lambda)$ that allows obtaining the average values of E_{out}, K_{out} and estimating the average value of D_{out}. Actually, contrary to fixed trace Whishard random matrices studied in Ref. [118, 166, 167], the joint probability distribution $p_{\text{out}}(\{\Lambda\})$ is not known so that the powerful Coulomb gas method used in Ref. [118] cannot be applied. Even if it would not be an easy task, it would be of great interest for comprehension to infer the joint probability $p_{\text{out}}(\{\Lambda\})$ in order to access more complex quantities than the average value of entanglement measures.

A few remarks about Eq. (4.10) are in order:

- When $M_1 = M_2 = 2N$, $\widetilde{C}^{\text{out}}\widetilde{C}^{\text{out}\dagger}$ is obtained from $CC^\dagger$ by a unitary transformation and hence their eigenvalues coincide. If now only $M_2 = 2N$, $\widetilde{C}^{\text{out}}\widetilde{C}^{\text{out}\dagger}$ is obtained from $P_1 CC^\dagger P_1^\dagger$ by a unitary transformation. Noting that $P_1 CC^\dagger P_1^\dagger$ and $CC^\dagger$ share the same set of eigenvalues, we see that the amount of entanglement does not change when $M_2 = 2N$ whatever the value of M_1, i.e., all the quantum correlations present in the incident state persist in the scattered state.

- The effect of the partial access to the outgoing modes in typical experiments on the distribution of transmission eigenvalues τ_n (see Sec. (2.3.4)) have been studied by Goetschy and Stone in Ref. [134]. Here, the idea is to describe the effect of this partial access on the distribution of Schmidt eigenvalues of the scattered state.

For practical reasons, we introduce the $M_2 \times M_2$ random matrix A such that $\eta^2 A = \widetilde{C}^{\text{out}}\widetilde{C}^{\text{out}\dagger}$. The state $|\widetilde{\Psi}\rangle$ is not normalized unless $\eta^2 = 1/\text{Tr}A$, which is equivalent to $\sum_k \Lambda_k = 1$ with Λ_k the Schmidt eigenvalues of $|\widetilde{\Psi}\rangle$. One sees that η depends on a particular realization of the scattering matrix and the choice of M_2 modes. The introduction of η corresponds to a post-selection procedure in an experiment. Only those measurements should be taken into account in which the two photons were effectively found in the M_2 detected modes. To simplify the further analysis, we will enforce the normalization requirement $\langle\widetilde{\Psi}|\widetilde{\Psi}\rangle = 1$ only on average, i.e. we will require

$$\overline{\langle\widetilde{\Psi}|\widetilde{\Psi}\rangle} = 1, \tag{4.11}$$

where the overbar denotes averaging over random realizations of the scattering matrix S. Therefore, we replace the normalization parameter η by an effective parameter $\overline{\eta}$ such that

$$\overline{\eta}^2 = \frac{1}{\overline{\mathrm{Tr}A}}. \tag{4.12}$$

Eq. (4.12) is equivalent to imposing $\overline{\sum_k \Lambda_k} = 1$ or $\overline{\Lambda} = 1/M_2$. The precise condition of validity of this approximation depends on the statistics of S but roughly speaking, it reduces to the requirement of a large number of modes $M_2 \gg 1$ provided that fluctuations of $|S_{i\alpha}|^2$ are not pathologically strong which is the case for weak disorder, far from the Anderson localization transition [4].

4.2.3 Link with the photocount coincidence rate

Let us briefly discuss the link between the Schmidt eigenvalues and the photocount coincidence rate introduced in Sec. 3.4.3. The photocount coincidence rate of two detectors counting photons in two outgoing modes α and β, studied in Refs. [10, 14, 12, 15, 11, 16], is simply

$$R_{ij} \propto \langle : \hat{n}_i \hat{n}_j : \rangle \propto |\widetilde{C}^{\mathrm{out}}_{ij}|^2, \tag{4.13}$$

where we remind that $\hat{n}_i = \hat{a}_i^\dagger \hat{a}_i$ is the photon number operator and $: \ldots :$ denotes normal ordering. R_{ij} is the random two-photon speckle [10] that, by analogy with the usual one-photon speckle $I_i = \langle \hat{n}_i \rangle$, should be characterized by its statistical properties. The probability distribution of R_{ij} was shown to bear signatures of entanglement of the incident light [10] but it is unclear whether it can be used to quantify the amount of entanglement in the scattered light. As we discussed above, for quantum states of the form (4.4), conventional entanglement measures (such as the von Neumann entropy E, the Schmidt number K and the quantum discord D introduced in Sec. 1.2.2) rely on eigenvalues Λ_k of the matrix $\widetilde{C}^{\mathrm{out}}\widetilde{C}^{\mathrm{out}\dagger}$ and not on the values of elements $\widetilde{C}^{\mathrm{out}}_{ij}$ of the matrix $\widetilde{C}^{\mathrm{out}}$. These eigenvalues are more difficult to access experimentally than coincidence rates; their measurement requires implementation of interferometric methods as it was done, for example, in Ref. [168] for photon pairs entangled in orbital angular momentum. However, the Schmidt number can also be determined without knowing the eigenvalues Λ_k by exploiting the link between the entanglement of the two-photon state and the degree of coherence of its one-photon components [169].

4.2.4 Density, resolvent, and $\mathcal{S}$-transform

The density of the eigenvalues Λ_k of a $N \times N$ Hermitian random matrix A is defined by

$$p(\Lambda) = \frac{1}{N} \overline{\sum_{k=1}^{N} \delta(\Lambda - \Lambda_k)}. \tag{4.14}$$

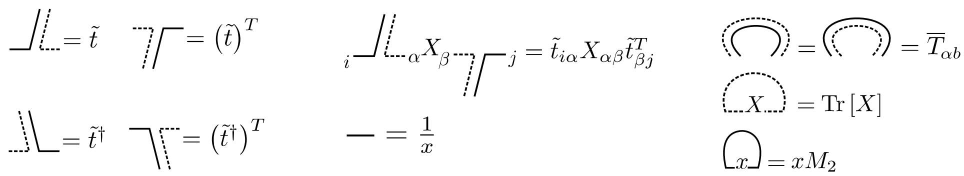

Figure 4.2: (a) Diagrammatic notations of the matrices $\tilde{t}$, $\tilde{t}^\dagger$ and their transposes. (b) Diagrams associated with the matrix product $\tilde{t}X\tilde{t}^\dagger$. (c) Diagrams corresponding to the pairwise contractions due to the average and loop diagrams associated with the tracing procedure.

In order to obtain $p\,(\Lambda)$ it is convenient to introduce the resolvent

$$g\,(z) \quad = \quad \frac{1}{N}\overline{\mathrm{Tr}\frac{1}{z-A}} = \frac{1}{N}\overline{\sum_{k=1}^{N}\frac{1}{z-\Lambda_k}}. \tag{4.15}$$

The density can then be reconstructed from the resolvent using the relation

$$p\,(\Lambda) = -\frac{1}{\pi}\lim_{\epsilon\to 0^+}\mathrm{Im}\;g\,(\Lambda + i\epsilon)\,. \tag{4.16}$$

Let us now introduce two other functions which are particularly useful in the random matrix theory. Consider $\chi\,(z)$ the solution of

$$\frac{1}{\chi\,(z)}g\left(\frac{1}{\chi\,(z)}\right) - 1 = z. \tag{4.17}$$

Then, the so-called $\mathcal{S}$-transform of the eigenvalue density of the matrix A [109] is given by

$$\mathcal{S}\,(z) = \frac{1+z}{z}\chi\,(z)\,. \tag{4.18}$$

Finally, we introduce the Blue function $\mathcal{B}\,(z)$ which is the functional inverse of the resolvent:

$$\mathcal{B}\,(z) = g^{-1}\,(z)\,. \tag{4.19}$$

4.2.5 Diagrammatic approach for the Gaussian transmission matrices

Diagrammatic expansion of the resolvent

In this section, we perform a diagrammatic expansion of the resolvent $g_A\,(z)$ of the matrix A defined in Sec. 4.2.4. We will take care of the normalization constraint (4.11) later. Using the definition of the resolvent given by Eq. (4.15), we can write

$$g_A\,(z) \quad = \quad \frac{1}{M_2}\overline{\mathrm{Tr}\left[\frac{1}{z} + \frac{1}{z}A\frac{1}{z} + \frac{1}{z}A\frac{1}{z}A\frac{1}{z} + \ldots\right]}. \tag{4.20}$$

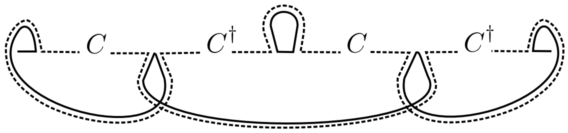

$$= \frac{\overline{T}_{\alpha b}^{4}}{z^3} M_2 \mathrm{Tr}[CC^{\dagger}(CC^{\dagger})^T]$$

Figure 4.3: Example of diagram appearing in the expansion of the resolvent and vanishing in the limit of large matrices.

To perform the averaging in Eq. (4.20), we consider a weakly disordered medium which, provided that M_1, $M_2 \leq g$ with g the dimensionless conductance, is characterized by a truncated transmission matrix $\tilde{t}$ with an eigenvalue distribution similar to the one of a random matrix with independent identically distributed complex entries following circular Gausian statistics [134]. In other words, $\tilde{t}$ can be considered as made up of independent complex elements having normally distributed independent real and imaginary parts with zero means and equal variances such that $\overline{\tilde{t}_{i\alpha}} = 0$ and $\overline{\tilde{t}_{i\alpha}\tilde{t}^{*}_{j\beta}} = \delta_{\alpha\beta}\delta_{ij}\overline{T}_{\alpha b}$, where $\overline{T}_{\alpha b}$ is the average intensity transmission coefficient independent the incoming and outgoing mode indices considered. Note that because $g = N\ell/L$, the multiple scattering implies M_1, $M_2 \ll N$. Besides, we consider here the limit of large matrices assuming that M_1, $M_2 \gg 1$.

Averaging in Eq. (4.20) can be performed using pairwise contractions following from the properties of Gaussian random variables. Instead of writing the full expression of the products of matrices involved in $\widetilde{C}^{\mathrm{out}}\widetilde{C}^{\mathrm{out}\dagger}$, the truncated transmission matrix is represented by diagrams depicted in Fig. 4.2.a so that the matrix products are written using the diagrams in Fig. 4.2.b. The diagrammatic expansion of the resolvent can be written as

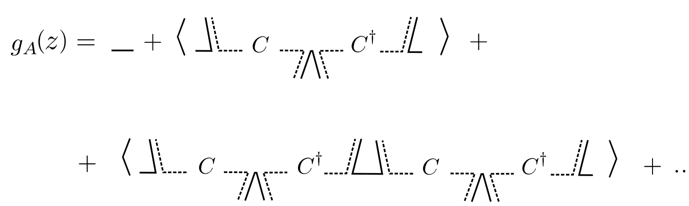

(4.21)

where the external trace and the prefactor $1/M_2$ that appears in the definition of the resolvent in Eq. (4.15) compensate each other as shown in Fig 4.2.c. When averaging, each pairwise contractions leads to a term $\overline{T}_{\alpha b}$ and each internal trace of matrices brings a factor M_2 or M_1 depending on the dimension of the corresponding matrix. The associated diagrams are depicted in Fig 4.2.c. We recall that $\overline{T}_{\alpha b} = \ell/NL \ll 1$ so that, in the limit of large matrices, the only diagrams that survive averaging are those with as many loops as contractions. They correspond to diagrams where plain and dashed lines do not cross and are called planar diagrams. In Fig. 4.3, we show an example of non-planar diagram that disappears in the limit N, M_1, $M_2 \gg 1$. Therefore, the beginning of the expansion of $g_A(z)$, when only the planar diagrams are kept, is given by

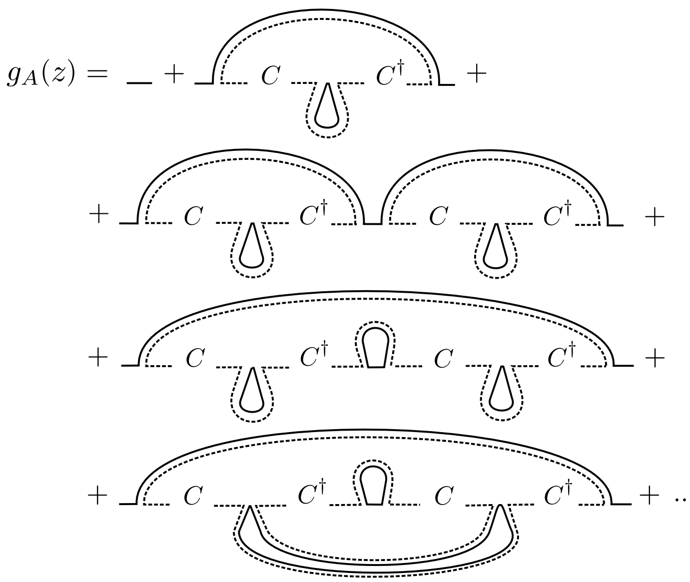

(4.22)

Self-consistent equation

In order to derive a self-consistent equation for the resolvent, we now introduce the self-energy $\sigma(z)$ defined by

$$g_A(z) = \frac{1}{z - \sigma(z)}, \tag{4.23}$$

so that, using the expansion $g_A(z) = \frac{1}{z} + \frac{1}{z}\sigma(z)\frac{1}{z} + \frac{1}{z}\sigma(z)\frac{1}{z}\sigma(z)\frac{1}{z} + ...$, the self-energy is the sum of all irreducible[4] terms in the diagrammatic expansion of $zg_A(z)z$. Then, the self energy can be written as

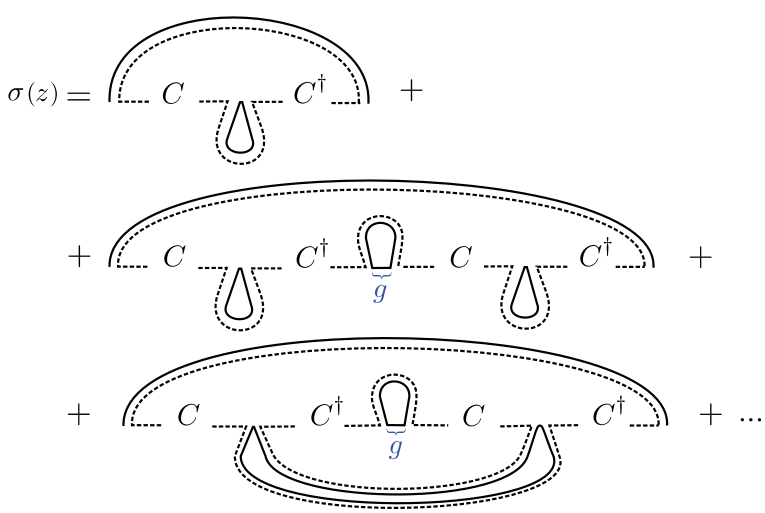

(4.24)

[4] Irreducible diagrams are those that cannot be factorized as products of simpler diagrams.

where we recognize terms contained in the beginning of the expansion of $g(z)$, as shown by the red braces in Eq. (4.24). Using the diagrammatic rules defined in Fig. 4.2 and after some combinatorics and algebra, we obtain

$$\sigma(z) = \frac{1}{M_2 g_A(z)} \mathrm{Tr}\left[\mathcal{F}(X,Y)\right] \tag{4.25}$$

with

$$\mathcal{F}(X,Y) = \frac{1 - X - XY - \sqrt{(1 - X - XY)^2 - 4X^2Y}}{2X} \tag{4.26}$$

and

$$X = \overline{T}_{\alpha b}^{2} M_2 \; g_A(z), \tag{4.27}$$
$$Y = M_2 \; CC^\dagger. \tag{4.28}$$

The function $\mathcal{F}(X,Y)$ is the generating function of the Narayana numbers

$$N(n,k) = \frac{1}{n}\binom{n}{k}\binom{k-1}{n}, \quad k \leq n, \tag{4.29}$$

and $N(0,0) = 1$. Then, using Eq. (4.23) we obtain a self-consistent equation for $g_A(z)$:

$$z = \frac{1}{g_A(z)}\left(1 + \frac{1}{M_2}\mathrm{Tr}\left[\mathcal{F}(X,Y)\right]\right). \tag{4.30}$$

From Eq. (4.30) one can obtain the resolvent $g_A(z)$ and then the eigenvalue density $p_A(\Lambda)$ of the matrix A. However, we are interested in the eigenvalue density of $\widetilde{C}^{\mathrm{out}}\widetilde{C}^{\mathrm{out}\dagger}$. The resolvent $g_{\mathrm{out}}(z)$ and the eigenvalue density $p_{\mathrm{out}}(z)$ of $\widetilde{C}^{\mathrm{out}}\widetilde{C}^{\mathrm{out}\dagger}$ are

$$g_{\mathrm{out}}(z) = \frac{1}{\eta^2}\; g\left(z/\eta^2\right), \tag{4.31}$$
$$p_{\mathrm{out}}(\Lambda) = \frac{1}{\eta^2}\; p\left(\Lambda/\eta^2\right). \tag{4.32}$$

In Sec. 4.3 we will apply Eqs. (4.30), (4.31) and (4.32) to different types of two-photon states, i.e., to different matrices C.

First and second moments

Let us use the diagrammatic approach to determine the first and second moments of the Schmidt eigenvalue density $p_{\mathrm{out}}(\Lambda)$ in the limit of large matrices. The moments are defined by

$$\overline{\Lambda^n} = \int_{-\infty}^{\infty} d\Lambda \; p_{\mathrm{out}}(\Lambda)\,\Lambda^n = \frac{\overline{\eta}^{2n}}{M_2}\overline{\mathrm{Tr}A^n}. \tag{4.33}$$

Because of the normalization constraint (4.11), the moments become

$$\overline{\Lambda^n} = \frac{1}{M_2}\frac{\overline{\mathrm{Tr}A^n}}{\overline{\mathrm{Tr}A}^n}. \tag{4.34}$$

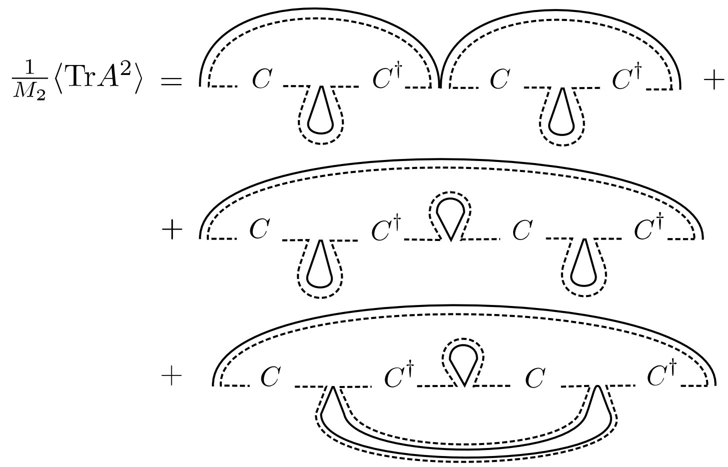

Figure 4.4: Sum of the diagrams contributing to the second moment $\overline{\Lambda^2}$ in the planar approximation associated with the limit of large matrices.

Noting that $\overline{\mathrm{Tr}A}/M_2$ is obtained from the first diagram on the r.h.s. of Eq. (4.24) and using $\mathrm{Tr}CC^\dagger = 1$, we have

$$\overline{\eta}^2 = 1/(M_2\overline{T}_{\alpha b})^2. \tag{4.35}$$

The second moment $\overline{\Lambda^2} = \frac{1}{M_2}\overline{\mathrm{Tr}A^2}/\overline{\mathrm{Tr}A}^2$ is obtained by summing the diagrams of Fig. 4.4 and reads

$$\overline{\Lambda^2} = \frac{2}{M_2^2} + \frac{1}{M_2}\mathrm{Tr}\left[CC^\dagger CC^\dagger\right]. \tag{4.36}$$

The first term on the r.h.s of Eq. (4.36) corresponds to the Gaussian term equal to $2\overline{\Lambda}^2$ whereas the second one can be shown to be related to the purity of the single-photon density matrix of the incident light. Hence, the second moment of the Schmidt eigenvalues of the transmitted state allows to accessing the amount of entanglement in the light.

4.2.6 Free probability approach

The free probability theory [170, 116] allows calculating statistical properties of a product of matrices from the statistical properties of multipliers. In particular, it states that the $\mathcal{S}$-transform of a matrix $C = AB$ is equal to the product of $\mathcal{S}$-transforms of A and B:

$$\mathcal{S}_{AB}(z) = \mathcal{S}_A(z)\mathcal{S}_B(z), \tag{4.37}$$

provided that the matrices A and B are asymptotically free.[5] Then, knowing the $\mathcal{S}$-transform of the multipliers A and B, one can derive the resolvent of the matrix AB using Eqs. (4.17) and (4.18). The notion of asymptotic freeness is an equivalent

[5]A similar property exists also for the sum of two random matrices which are asymptotically free, in terms of the so-called $\mathcal{R}$-transform [116].

of statistical independence for matrices; its rigorous definition can be found in Refs. [170, 109], for example.

To fully benefit from the power of the free probability theory, we restrict our study, as in the previous section, to large numbers of incoming and outgoing modes: M_1, $M_2 \gg 1$. From the definition of $\widetilde{C}^{\text{out}}$ in Eq. (4.10), we have

$$\begin{aligned}\mathcal{S}_{\widetilde{C}^{\text{out}}\widetilde{C}^{\text{out}\dagger}}(z) &= \frac{1}{\eta^2}\frac{z+1}{z+\beta}\mathcal{S}_{\tilde{t}^\dagger\tilde{t}C(\tilde{t}^\dagger\tilde{t})^T C^\dagger}(z/\beta) && (4.38)\\ &= \frac{1}{\eta^2}\frac{z+1}{z+\beta}\mathcal{S}_{\tilde{t}^\dagger\tilde{t}}(z/\beta)\,\mathcal{S}_{C(\tilde{t}^\dagger\tilde{t})^T C^\dagger}(z/\beta) && (4.39)\\ &= \frac{1}{\eta^2}\frac{z+1}{z+\beta}\mathcal{S}_{\tilde{t}^\dagger\tilde{t}}(z/\beta)\,\mathcal{S}_{CC^\dagger}(z/\beta)\,\mathcal{S}_{(\tilde{t}^\dagger\tilde{t})^T}(z/\beta)\,, && (4.40)\end{aligned}$$

where $\beta = M_1/M_2$. We use the scaling relation $\mathcal{S}_{\eta^2 A}(z) = 1/\eta^2\mathcal{S}_A(z)$ to obtain Eq. (4.38). Equation (4.39) follows from the assumption that $\tilde{t}^\dagger\tilde{t}$ and $C(\tilde{t}^\dagger\tilde{t})^T C^\dagger$ are asymptotically free. Finally, the obvious asymptotic freeness of $CC^\dagger$ and $(\tilde{t}^\dagger\tilde{t})^T$ leads to Eq. (4.40). Then, using $\mathcal{S}_{\tilde{t}^\dagger\tilde{t}}(z) = \mathcal{S}_{(\tilde{t}^\dagger\tilde{t})^T}(z)$, we obtain

$$\mathcal{S}_{\widetilde{C}^{\text{out}}\widetilde{C}^{\text{out}\dagger}}(z) = \frac{1}{\eta^2}\frac{z+1}{z+\beta}\mathcal{S}^2_{\tilde{t}^\dagger\tilde{t}}(z/\beta)\,\mathcal{S}_{CC^\dagger}(z/\beta)\,. \tag{4.41}$$

From Eq. (4.41) we see that given the knowledge of $\mathcal{S}_{\tilde{t}^\dagger\tilde{t}}(z)$ and $\mathcal{S}_{CC^\dagger}(z)$ we have access to $\mathcal{S}_{\widetilde{C}^{\text{out}}\widetilde{C}^{\text{out}\dagger}}(z)$ and so to the eigenvalue density of $\widetilde{C}^{\text{out}}\widetilde{C}^{\text{out}\dagger}$.

In the Gaussian regime, i.e., when M_1, $M_2 \leq g$, the truncated transmission matrix $\tilde{t}$ is statistically similar to a random matrix with uncorrelated Gaussian elements and then $\tilde{t}^\dagger\tilde{t}$ is similar to a Wishart random matrix introduced in Sec. 2.3.1. Therefore, from the properties of Wishart matrices, we have

$$\mathcal{S}_{\tilde{t}^\dagger\tilde{t}}(z) = \frac{1}{M_2\overline{T}_{\alpha b}}\frac{1}{1+\beta z}. \tag{4.42}$$

Eqs. (4.41) and (4.42) are all we need to obtain the Schmidt eigenvalue density given an arbitrary incident state defined by the $M_1 \times M_1$ matrix C with its $\mathcal{S}$-transform $\mathcal{S}_{CC^\dagger}(z)$ obeying

$$\frac{1}{M_1}\text{Tr}\left[\frac{1}{1+z\left(1-\mathcal{S}_{CC^\dagger}(z)\,CC^\dagger\right)}\right] = 1. \tag{4.43}$$

Contrary to the diagrammatic approach introduced in Sec. 4.2.5, the free probability theory allows to go beyond the Gaussian regime, i.e., to consider M_1, $M_2 > g$, and describes the situation when M_1, $M_2 \simeq N$. Indeed, in Ref. [134] Goetschy and Stone derived a self-consistent equation of $g_{\tilde{t}^\dagger\tilde{t}}(z)$, depending on the resolvent $g_{t^\dagger t}(z)$ that leads to the so-called bimodal distribution [108] and is given by

$$g_{t^\dagger t}(z) = \frac{1}{z} - \frac{\overline{T}}{z\sqrt{1-z}}\text{Arctanh}\left[\frac{\text{Tanh}\left(1/\overline{T}\right)}{\sqrt{1-z}}\right]. \tag{4.44}$$

Combining Eqs. (4.41), (4.18) and (4.17), and using (4.44) , we obtain after some algebra the following self-consistent equation for $g_{\text{out}}(z)$:

$$F(z)\,N(z)\,g_{t^\dagger t}\left(\frac{F(z)\,N^2(z)}{D(z)}\right) = D(z)\,, \tag{4.45}$$

where

$$F(z) = \left(\frac{\mathcal{S}_{CC^\dagger}\left(zg(z) - 1\right)g(z)}{xg(z) - 1} \right)^{\frac{1}{2}}, \tag{4.46}$$

$$N(z) = zm_1 g(z) + 1 - m_1, \tag{4.47}$$

$$D(z) = m_1 g(z)\left(zm_1 g(z) + m_2 - m_1\right). \tag{4.48}$$

with[6] $g_{\text{out}}(z) = \beta/\eta^2 g\left(z/\eta^2\right) + (1+\beta)/z$ and $m_{1,2} = M_{1,2}/N$.

4.3 Schmidt density for a maximally entangled incident state

We now assume that the incident state (4.4) is a maximally entangled state. It implies that the Schmidt eigenvalues are all equal to $1/M_1$. Therefore, we consider in the following the case of[7] $C = \mathbb{1}/\sqrt{M_1}$, where $\mathbb{1}$ is the $M_1 \times M_1$ identity matrix.

4.3.1 Eigenvalue density

Let us solve either Eqs. (4.30) and (4.31) obtained using the diagrammatic expansion or Eqs. (4.41), (4.42) and (4.43) obtained using the free probability theory with $C = \mathbb{1}/\sqrt{M_1}$. Both methods give the same result and lead to the following equation for the resolvent $g_{\text{out}}(z)$:

$$M_1\left(zg_{\text{out}}(z) - 1\right) = zg_{\text{out}}(z)^2\left(zg_{\text{out}}(z) - 1 + \beta\right). \tag{4.49}$$

Note that the average intensity transmission coefficient $\overline{T}_{\alpha b}$ does not appear any more in Eq. (4.49) because of the normalization constraint which implies that $\overline{\eta}^2 = 1/(\overline{T}_{\alpha b} M_2)^2$.

We solve the cubic equation (4.49) for $g_{\text{out}}(z)$ analytically (the resulting formulas are quite lengthy and we do not reproduce them here) and then find $p_{\text{out}}(\Lambda)$ from the imaginary part of the solution. The result is illustrated in Fig. 4.5 where $p_{\text{out}}(\Lambda)$ is shown for a fixed (large) value of $M_1 = 100$ and three different values of $M_2 = M_1/\beta$. When $M_2 < M_1$, $p_{\text{out}}(\Lambda)$ is a wide distribution that has little to do with $p_{\text{in}}(\lambda) = \delta(\lambda - 1/M_1)$ corresponding to the incident light and shown in Fig. 4.5 by a red arrow. A peak $(1-\beta)\delta(\Lambda)$ appearing in $p_{\text{out}}(\Lambda)$ for $M_2 > M_1$ corresponds to $M_2 - M_1$ zero eigenvalues that are due to the fact that the rank of the $M_2 \times M_2$ matrix $\tilde{C}^{\text{out}}\tilde{C}^{\text{out}\dagger}$ cannot exceed the rank of the $M_1 \times M_1$ matrix $CC^\dagger$. The remaining M_1 nonzero eigenvalues give rise to a peak in $p_{\text{out}}(\Lambda)$ around $\Lambda = 1/M_1$, as can be seen in Fig. 4.5.c. The distributions shown in Fig. 4.5 are similar (though not identical) to the familiar Marchenko-Pastur law describing the eigenvalue distribution of a product of a random matrix H with zero-mean complex independent identically distributed elements and its Hermitian conjugate $H^\dagger$ [109]. This is not surprising since the random matrix $\tilde{t}$

[6] $g(z)$ is an auxiliary function used to simplify the calculation; it corresponds to the resolvent of $\tilde{t}^\dagger\tilde{t}C\left(\tilde{t}^\dagger\tilde{t}\right)^T C^\dagger$.

[7] Note that it would be possible to consider a maximally entangled state with C which is not diagonal. However, it is convenient to assume that the basis used for the calculation is the Schmidt basis (i.e. the basis in which C is diagonal). The choice of the basis is without importance for the results of this chapter.

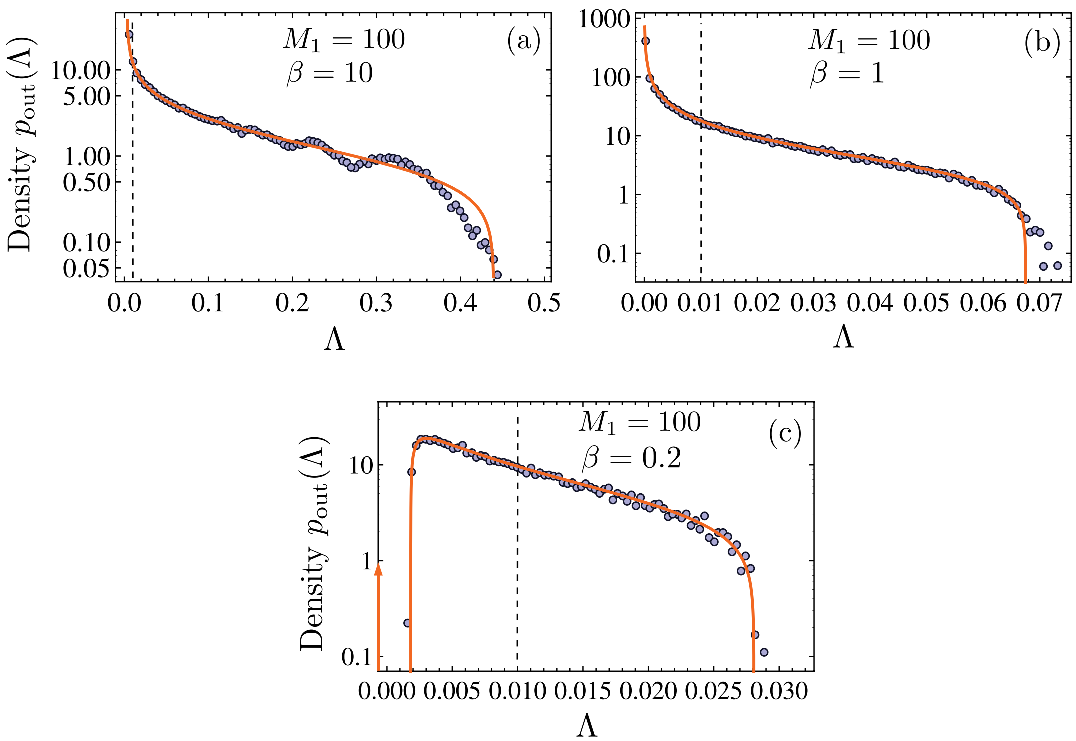

Figure 4.5: Eigenvalue densities $p_{\mathrm{out}}(\Lambda)$ obtained from Eq. (4.49) for $M_1 = 100$ and three different $\beta = M_1/M_2$ (lines) are compared to numerical simulations (symbols) in which the normalization condition $\langle\widetilde{\Psi}|\widetilde{\Psi}\rangle = \sum_k \Lambda_k = 1$ was imposed for each realization of the random scattering matrix S and not only on average as in our analytical approach. Discrepancy between analytical and numerical results at large Λ and oscillations of numerical results for $\beta = 10$ are finite-size effects due to the insufficiently large value of $M_2 = M_1/\beta$. For $\beta < 1$, $p_{\mathrm{out}}(\Lambda)$ contains a contribution $(1-\beta)\delta(\Lambda)$ shown in the figure by the orange arrow at $\lambda = 0$. Dashed vertical lines at $\Lambda = 1/M_1$ symbolize the eigenvalue distribution $p_{\mathrm{in}}(\Lambda) = \delta(1 - 1/M_1)$ corresponding to the incident light.

that we use to describe the transmission of light through the random medium has the same statistics as H.

Let us consider the first few moments of the eigenvalue density. The first moment does not depend on the incident state and $\overline{\Lambda} = 1/M_2$. Using Eq. (4.36) and $C = \mathbb{1}/\sqrt{M_1}$, we find that the second moment is

$$\overline{\Lambda^2} = \frac{2}{M_2^2} + \frac{1}{M_2 M_1}. \tag{4.50}$$

Therefore, in the limit $M_1/M_2 \gg 1$, only the Gaussian term remains, $\overline{\Lambda^2} \sim 2/M_2^2$. These two moments correspond to the first moments of the Marchenko-Pastur law with $c = 1$ and a rescaling of the density through the transformation $\overline{\Lambda} \to \overline{\Lambda}/M_2$ (see Eq. (2.39) in Sec. 2.3.1). Indeed, if we take the limit $\beta \gg 1$ in Eq. (4.49), we obtain

$$g_{\text{out}}(z) = \frac{M_2}{2z}\left(z - \sqrt{z\left(z - \frac{4}{M_2}\right)}\right), \quad \text{for } \beta \gg 1, \tag{4.51}$$

which corresponds to the rescaled Marchenko-Pastur law mentioned above.

4.3.2 Average entanglement measures

We now consider the average amount of entanglement contained in the scattered state. Average values of the von Neumann entropy $\overline{E}_{\text{out}}$, the Schmidt number $\overline{K}_{\text{out}}$ and the quantum discord $\overline{D}_{\text{out}}$ are calculated by averaging E_{out}, K_{out} and D_{out} (introduced in Sec. 1.2.2) over the distribution $p_{\text{out}}(\Lambda)$. For the entropy, the result can be written as $\overline{E}_{\text{out}} = E - \overline{\delta E}$ with $\overline{\delta E} > 0$ representing the average loss of entanglement entropy upon the transmission through the random medium. We find that at any given M_1, $\overline{\delta E}$ is a monotonously decreasing function of $1/\beta = M_2/M_1$ and that

$$\overline{\delta E} \simeq \begin{cases} \ln\beta + \frac{1}{2}, & \beta \gg 1 \\ \beta, & \beta \ll 1 \end{cases} \tag{4.52}$$

These asymptotic formulas are shown in Fig. 4.6.a by dashed lines together with the numerical average of δE using $p_{\text{out}}(\Lambda)$ following from Eq. (4.49) (lines) and the exact result obtained by numerically generating random realizations of matrices S and averaging over many realizations (symbols). An alternative way of writing the same result is

$$\overline{E}_{\text{out}} = \begin{cases} \ln M_2 - \frac{1}{2}, & M_2 \ll M_1 \\ E - M_1/M_2, & M_2 \gg M_1 \end{cases} \tag{4.53}$$

A simple analytical approximation for the average Schmidt number $\overline{K}_{\text{out}}$ can be obtained by replacing the average of inverse by the inverse of average in its formal definition. This is justified by the fact that $\sum_k \Lambda_k^2$ is a weakly fluctuating quantity for $M_2 \gg 1$ and the scattering matrix S having Gaussian statistics as described above. Hence the average of the inverse of $\sum_k \Lambda_k^2$ and the inverse of its average are not very different. Then

$$\begin{aligned} \overline{K}_{\text{out}} &= \overline{(\sum_k \Lambda_k^2)^{-1}} \approx \left(\overline{\sum_k \Lambda_k^2}\right)^{-1} = (M_2\overline{\Lambda^2})^{-1} \\ &= \frac{M_1}{1+2\beta}, \end{aligned} \tag{4.54}$$

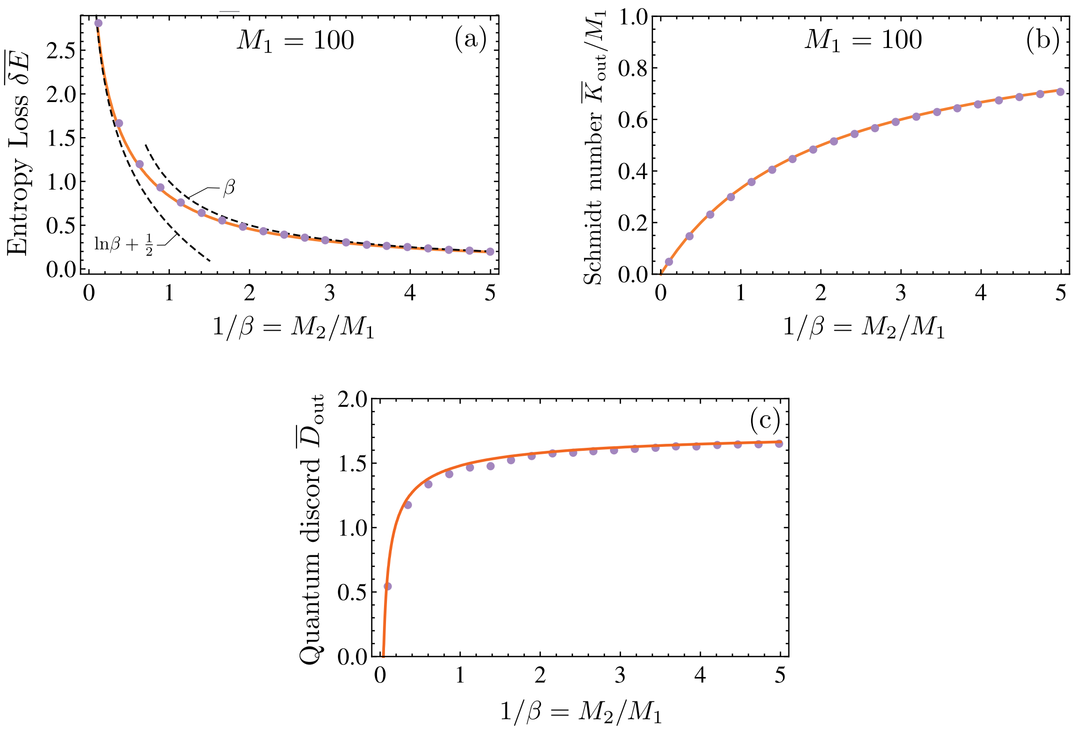

Figure 4.6: Entanglement of the maximally entangled two-photon state transmitted through a random medium. Average loss of entropy (a), the Schmidt number (b), and the geometric quantum discord (c) are shown as functions of $1/\beta = M_2/M_1$ for a fixed number $M_1 = 100$ of incoming modes. Lines are analytical results, symbols show results of exact numerical simulations, dashed lines are asymptotic formulas (4.52).

where $\langle \Lambda^2 \rangle = \beta(1+2\beta)/M_1^2$ is found from Eq. (4.36).

The average geometric quantum discord $\overline{D}_{\text{out}}$ of the scattered state can be estimated by replacing the average of the square root of $\Lambda_{\max}$ by the square root of the upper boundary λ_+ of the support of the eigenvalue density $p_{\text{out}}(\Lambda)$: $\overline{D}_{\text{out}} \simeq 2(1-\sqrt{\Lambda_+})$. Lower and upper boundaries of the support, Λ_- and Λ_+, can be found using the standard methods of random matrix theory from the condition $dg(z)/dz|_{z=\Lambda_\pm} \to \infty$ [109, 171], with $g_{\text{out}}(z)$ found from Eq. (4.49):

$$\Lambda_\pm = \frac{1}{M_1}\left[1+\frac{5\beta}{2}-\frac{\beta^2}{8} \pm \sqrt{8\beta}\left(1+\frac{\beta}{8}\right)^{3/2}\right]. \tag{4.55}$$

As we see from Fig. 4.6.c., this approximation yields satisfactory results although the agreement with exact numerical calculations is not as good as in Figs. 4.6.a and 4.6.b. This is not surprising because, in contrast to $\sum_k \Lambda_k^2$, $\Lambda_{\max}$ fluctuates significantly from one realization of disorder to another and hence the knowledge of its precise statistics is needed to obtain accurate results.

The condition M_1, $M_2 \gg 1$ ensures that $\overline{K}_{\text{out}}$ is always larger than 2. Therefore the transmitted photon pair remains entangled on average according to criterion of Ghirardi *et al.* [49] (see Sec. 1.3) although the entanglement is degraded because $\overline{E}_{\text{out}} < E = \ln M_1$, $\overline{K}_{\text{out}} < K = M_1$ and $\overline{D}_{\text{out}} < D$ (since $\Lambda_+ > 1/M_1$). For small $M_2 \ll M_1$, the transmitted state is close to a random entangled pure bipartite state [164]:

$$\overline{E}_{\text{out}} = \ln M_2 - \frac{1}{2}, \tag{4.56}$$

$$\overline{K}_{\text{out}} = M_{\text{out}}/2, \tag{4.57}$$

$$\overline{D}_{\text{out}} = 2 - 4/\sqrt{M_2}. \tag{4.58}$$

No memory about the number of modes in the incident light survives multiple scattering; the entanglement of the transmitted state is determined by the number of outgoing modes M_2. On the contrary, for large $M_2 \gg M_1$ the degree of entanglement of the transmitted state is close to that of the incoming light despite the multiple scattering:

$$\overline{E}_{\text{out}} \simeq E = \ln M_1, \tag{4.59}$$

$$\overline{K}_{\text{out}} \simeq K = M_1, \tag{4.60}$$

$$\overline{D}_{\text{out}} \simeq D = 2[1 - 1/\sqrt{M_1}]. \tag{4.61}$$

On the one hand, this is quite a surprising result that shows that entanglement is much less sensitive to disorder than one might expect, provided that sufficient information about the scattered wavefield is recovered (i.e. that M_2 is sufficiently large). On the other hand, one should remember that while the incident light is in the maximally entangled state, the degree of entanglement of transmitted light is much less than its maximum value allowed for a two-photon state involving M_2 modes. Therefore, while the absolute amount of entanglement is almost preserved when $M_2 \gg M_1$, its relative amount (with respect to the maximum possible amount given the number of modes) is significantly reduced. Nevertheless, it is interesting to note that the entanglement is degraded but never lost completely upon transmission of a maximally entangled state through a random medium.

4.3.3 Comparison with a separable incident state

If the initial state (4.4) is separable ($C_{ij} = 1/M_1$), we readily see from Eq. (4.6) that the state $|\widetilde{\Psi}\rangle$ is separable too. Thus, scattering in a random medium cannot entangle a photon pair that was initially in a separable state. Let us check whether this result is correctly captured by our Eq. (4.41). We proceed in the same way as for the maximally entangled state and obtain an equation which is similar but not identical to Eq. (4.49):

$$zg_{\text{out}}(z) - 1 = zg_{\text{out}}(z)^2 \left[zg_{\text{out}}(z) - 1 + \frac{1}{M_2} \right]. \tag{4.62}$$

A significant difference with respect to Eq. (4.49) appears already at this stage: Eq. (4.62) does not contain the number of incident modes M_1 but only the number of outgoing modes M_2. Solving this equation yields $p_{\text{out}}(\Lambda)$ that has two peaks: one at $\Lambda = 0$ and one around $\Lambda = 1$. The height and the width of the second peak depends on M_2 but its integral is always equal to $1/M_2$. This suggests that the nonzero width of the second peak (that also makes possible $p_{\text{out}}(\Lambda) > 0$ for unphysical $\Lambda > 1$) is an artifact of imposing the normalization condition $\langle\widetilde{\Psi}|\widetilde{\Psi}\rangle = 1$ only on average. In the limit of M_1, $M_2 \to \infty$, $p_{\text{out}}(\Lambda)$ converges to

$$p_{\text{out}}(\Lambda) = \left(1 - \frac{1}{M_2}\right)\delta(\Lambda) + \frac{1}{M_2}\delta(\Lambda - 1), \tag{4.63}$$

which is confirmed by numerical simulations to be the solution of the problem for any M_1, M_2. The resulting entropy is therefore $E_{\text{out}} = 0$, the Schmidt number is $K_{\text{out}} = 1$, and the quantum discord is $D_{\text{out}} = 0$. Therefore, Eq. (4.41) correctly captures the impossibility of entanglement creation upon transmission of a photon pair through a random medium. Note that this result is not in contradiction with Ref. [14] where multiple scattering was predicted to induce entanglement of *modes* that should be distinguished from the entanglement of *photons* that we study in this chapter.

4.3.4 Beyond the Gaussian regime

We finish our discussion of the transmission of the maximally entangled state by considering the situation when M_1, $M_2 \geq g$ so that the truncated transmission matrix is no more statistically equivalent to a random matrix with uncorrelated Gaussian distributed elements. To deal with this case, we solve the self-consistent equation (4.45) in order to obtain the resolvent $g_{\text{out}}(z)$. Besides, it follows from Eq. (4.43) that the $\mathcal{S}$-transform of the matrix $CC^\dagger$ is $\mathcal{S}_{CC^\dagger}(z) = M_1$. In order to compare our analytical results with numerical simulations, we consider here a waveguide geometry so that we can solve numerically the DMPK equation introduced in Chapter 2.

In Fig 4.7, we show the eigenvalue density $p_{\text{out}}(\Lambda)$ for different values of β. The first important thing to note is the fact that there is no evident sign in $p_{\text{out}}(\Lambda)$ of the bimodal distribution obeyed by the transmission eigenvalues τ_n when $m_1 = m_2 = 1$ (see Sec. 2.3.3). Besides, we see that the numerical results show strong oscillations even for the case of $m_2 = m_1 = 1$. Contrary to the oscillations observed before in Fig. 4.5.a, this effect does not come from the finite dimensions of the matrices C and $\widetilde{C}^{\text{out}}$. The origin of these oscillations is more subtle and comes from the finite value of the dimensionless conductance g used in the Monte-Carlo simulation. As discussed in Chapter 2, g gives

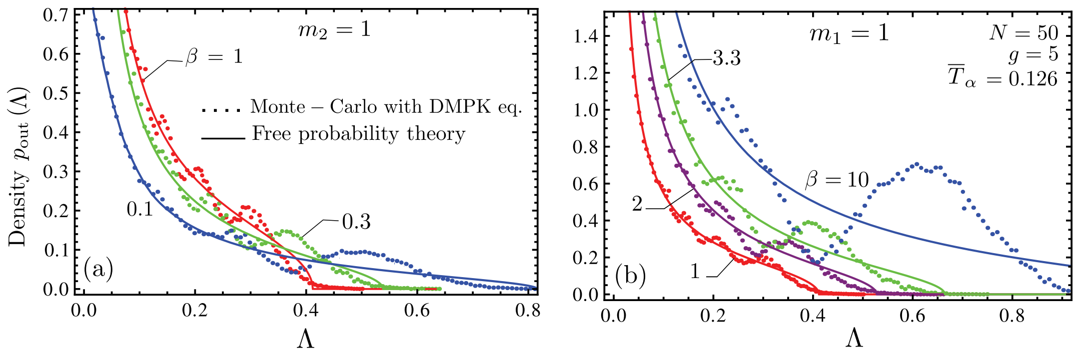

Figure 4.7: Eigenvalue densities $p_{\text{out}}(\Lambda)$ beyond the Gaussian regime obtained from Eq. (4.45) for a maximally entangled incident state (lines) for different values of $\beta = M_1/M_2$ and (a) $m_2 = M_2/N = 1$, (b) $m_1 = M_1/N = 1$. Here, $g = 5$, $\overline{T}_\alpha = 0.126$ and $N = 50$. Analytical results are compared to numerical simulations (dots) in which the normalization condition $\langle\widetilde{\Psi}|\widetilde{\Psi}\rangle = \sum_k \Lambda_k = 1$ was imposed for each realization of the random scattering matrix S and not only on average as in our analytical approach. The numerical simulation is a Monte-Carlo simulation [125] in which several realizations of truncated transmission matrices are generated by solving the DMPK equation introduced in Sec. 2.3.3. The oscillations of numerical results are coming both from finite-size effects (M_1, M_2 finite) and from the finite value of the effective number of transmission channels, i.e., the finite value of conductance g.

the effective number of transmission channels that contribute to transmission, i.e., the number of "open" channels characterized by a transmission eigenvalue $\tau_n \sim 1$. In other words, the dimensionless conductance gives the rank of the matrix $t^\dagger t$. Then, even if M_1 and M_2 are large, the rank of the matrix $\widetilde{C}^{\text{out}}\widetilde{C}^{\text{out}\dagger}$ can not be much larger than one if $g \sim 1$ as it is the case in Fig. 4.7.

Based on the above discussion, let us address yet another question to conclude this chapter. How does the amount of entanglement of the scattered state change when one enters the regime of Anderson localization? We again consider a waveguide geometry and assume for simplicity that $m_1 = m_2 = 1$ with $N \gg 1$. Besides, we still consider a maximally entangled state incident on the disordered medium, therefore the rank of the matrix C is given by $M_1 \gg 1$. Therefore, the rank of $\widetilde{C}^{\text{out}}\widetilde{C}^{\text{out}\dagger}$, and thus the number of Schmidt eigenvalues of the scattered state, are only constrained by the dimensionless conductance g. The first conclusion is that, when g is larger than one, the average amount of entanglement is bounded, so that $\overline{E}_{\text{out}} \leq \ln g$. When entering the localized regime, $g < 1$. In this regime, g is no more associated with the effective number of channels. However, when getting deeper in the localized regime one reaches the single-channel regime of transport [172]. In this regime $t^\dagger t$ possesses only one eigenvalue. Therefore, the rank of $\widetilde{C}^{\text{out}}\widetilde{C}^{\text{out}\dagger}$ is necessarily equal to one and hence, whether the incident state is highly entangled or not, the scattered state is necessarily separable.[8] However, a detail study of this crossover has not been realized yet and remained to be done in the future.

[8]Note that this picture is valid only when the entanglement is in momentum or spatial degrees of freedom.

Conclusion and perspectives

In this thesis, we have addressed the following two main questions:

- Which signs of non-classicality of the incident light can be obtained from a two-photon speckle pattern?
- What is the amount of entanglement contained in a scattered two-photon state?

Before giving answers to the above questions, in the first chapter, we have introduced the basic mathematical tools used in quantum optics and considered the notion of quantum entanglement between two subsystems. The end of the first chapter was an occasion to discuss the entanglement between identical particles and to show that it is an actively debated subject in the recent literature. In the second chapter, we have introduced the basis of the statistical approach to the multiple scattering of light.

Regarding the first question, in Chapter 3, we have discussed quantum and classical aspects of two-photon interference in light transmitted through a disordered medium. We have first considered a bi-Gaussian two-photon state and then a more realistic type-II SPDC state of light. Both describe a light pulse of finite bandwidth and containing two orthogonally polarized photons, of which one can be delayed by an arbitrary time τ. We have shown that a disordered media can be seen as a multi-port beam splitter which reproduces HOM interferences. By comparing the rates $R(\tau)$ of coincident photon counting in the same outgoing mode in transmission through a disordered medium for different quantum states of the incident light (bi-Gaussian, SPDC and coherent state), we have demonstrated that disorder strongly impacts the interference pattern through the time coherence of the scattered state. Moreover, if no additional information about the incident pulse is available, it is barely possible to see any sign of entanglement in $R(\tau)$ for a typical two-photon entangled state generated by the collinear type-II SPDC. Almost identical $R(\tau)$ curves can be obtained for the SPDC and separable two-photon states, provided that the bandwidth of the latter is adjusted. However, the result obtained for the coherent state is different, which highlights the second important factor that plays a role in the two-photon interference: the quantum nature of light. Here it is manifest in the fact that the number of photons is well-defined in the entangled and separable two-photon states, whereas it is not a good quantum number in the coherent state. The third important aspect is the entanglement between the two incident photons that allows one to control the symmetry of the two-photon state. Symmetric and antisymmetric states that can be prepared in this way lead to coincidence rates $R(\tau)$ that do not decrease with the pump bandwidth as fast as for the standard SPDC-generated entangled state. In addition, the antisymmetric state allows one to model fermionic behavior and to change the constructive two-photon interference into a destructive one. As a result, the peak of $R(\tau)$ observed for the state with the bosonic symmetry (i.e., for the symmetric state), as well as for the states with no particular symmetry, at $\tau = 0$, turns into a deep for the state with the fermionic symmetry (i.e., for the antisymmetric state). In the last section of Chapter 3, we derived the visibilities of the one- and two-photon speckle patterns $\mathcal{V}^{(1)}$ and $\mathcal{V}^{(2)}$ and showed their strong dependence on the single-photon coherence time which is absent in the result of Ref. [10] where the spectral properties of the incident light were disregarded. This dependence shows that the knowledge of the two visibilities as defined in Chapter 3 and in Ref [10], even if sensitive to entanglement, does not allow to distinguish an entangled from a separable state.

In Chapter 4, in order to answer the second of the two main questions, we have considered the impact of multiple scattering in a weakly disordered random medium in combination with the subsequent selection of only a fraction of outgoing modes on the high-dimensional entanglement of a photon pair. To this aim, we have introduced a new theoretical approach that combines both the random S-matrix approach and the Schmidt decomposition of the scattered state. Instead of the photocount coincidence rate that can be expressed through the absolute value square of an element of the matrix $\widetilde{C}^{\text{out}}$ describing the state, we have calculated the eigenvalue density of the matrix $\widetilde{C}^{\text{out}}\widetilde{C}^{\text{out}\dagger}$ and its global properties (the von Neumann entropy, the Schmidt number and the geometric quantum discord) that provide quantitative measures of entanglement in the scattered light. As could be expected, the entanglement does not change if all scattered light is collected. In a more realistic situation, when only a small fraction of outgoing modes is accessible, an initially maximally entangled photon pair remains entangled but the amount of entanglement is reduced. To recover the amount of entanglement of the incident state, one has to access a number of outgoing modes exceeding significantly the number of incoming modes over which the incident light is expanded. Besides, our derivation confirms that a pair of photons in a separable state does not gain any entanglement when transmitted through a random medium. Finally, we have discussed the fact that entanglement in momentum will necessarily decrease after the transmission through a random medium, for a fixed amount of entanglement in the incident state, with the decrease of the dimensionless conductance, until entanglement vanishes completely in the single-channel regime.

The work presented in this thesis opens a number of new interesting questions. Some of these questions have been partially addressed by the author but not presented in this manuscript and will be tackled in the near future in order to get a better understanding of the propagation of entangled two-photon states in random media. Concerning the two-photon speckle pattern, a detailed study of the complementarity between the visibilities of one- and two-photon speckle patterns would allow understanding genuine two-photon interferences, i.e., interferences that truly require entanglement of the two-photon state. Another interesting perspective concerns the study of the focusing of non-classical light behind a disordered medium. A first step into this direction will be the calculation of the coincidence photocount rate obtained with an incident $N00N$-state $|\Psi\rangle_{N00N} = \frac{1}{\sqrt{2N!}}(\hat{a}_\alpha^{\dagger N} + \mathrm{e}^{i\theta}\hat{a}_\beta^{\dagger N})\,|0\rangle$ in order to see how the symmetry of the state, which depends on the parameter θ, impacts the coincidence rate. Finally, the study of the coherent backscattering with two-photon states of light has to our knowledge never been addressed.

Regarding the quite recent field dealing with the quantification of entanglement of light transmitted through a random medium, we have already begun considering the case of more general incident states. Indeed, maximally entangled and separable states are two extreme cases and in most experimental schemes in quantum optics the SPDC states are the most "popular". Besides, when considering maximally entangled states, one cannot always separate the effects due to the size of the matrix C from those coming from the finite value of its rank which is associated with the amount of entanglement. The extension of this work to more general state would allow checking if the diagrammatic and the free probability theories are equivalent for all incident states. Therefore, the application of the formalism introduced in the last chapter to the case of SPDC states is of great interest for both theory and experiment. In addition to the study of the crossover from the diffusive to the localized regime discussed in Sec. 4.3.4, it would be helpful to develop a more general diagrammatic approach that would rely on the SVD of the transmission matrix t. It would imply performing a diagrammatic expansion with unitary random matrices instead of random matrices with independent entries. Finally, one might be interested in the capacity of quantum information transfer through a random medium. This capacity is expected to depend on both the fraction of accessible modes and the strength of disorder.

Appendices

Appendix A

Derivation of the two-photon SPDC state

In this appendix, we present a derivation of the two-photon SPDC state. We consider here a Type II SPDC process where the non-linear crystal is pumped by a broadband pump. Besides, for the simplicity of the derivation, we deal with a collinear propagation of the two photons along the direction of propagation of the pump beam, i.e., they do not have transverse momentum. Note that the case of the Type I SPDC state, with or without collinearity and monochromatic pump is derived in a similar way. Using the interaction picture, the final state $|\Psi(t)\rangle$ can be written as

$$|\Psi(t)\rangle = \exp\left[\frac{1}{\mathrm{i}\hbar}\int_{t_0}^{t} dt' \hat{H}_{\mathrm{I}}(t')\right]|\Psi(t_0)\rangle\,, \tag{A.1}$$

with $\hat{H}_{\mathrm{I}}(t)$ the interaction Hamiltonian given by

$$\hat{H}_{\mathrm{I}}(t) = \int_V d^3\mathbf{r}\ \chi^{(2)}\hat{E}_p^{(+)}(\mathbf{r},t)\,\hat{E}_o^{(-)}(\mathbf{r},t)\,\hat{E}_e^{(-)}(\mathbf{r},t) + \mathrm{H.c.} \tag{A.2}$$

where $\chi^{(2)}$ is the second order non-linear susceptibility and is assumed to be frequency independent. H.c. stands for Hermitian conjugate. For a collinear propagation along the z-axis, the electric field takes the form

$$\hat{E}_i^{(+)}(z,t) = \int d\omega_i A(\omega_i)\,\hat{a}_i(\omega_i)\,\mathrm{e}^{\mathrm{i}(k_i(\omega_i)z-\omega_i t)}, \tag{A.3}$$

with $A(\omega) = \mathrm{i}\sqrt{\frac{\hbar\omega}{2\epsilon_0 n^2(\omega)}}$ a slowly varying function of ω.

The weak efficiency of this non-linear process necessitates an intense pump field, consequently the pump can be described by a classical field:

$$E_p(z,t) = \widetilde{\alpha}(t)\,\mathrm{e}^{\mathrm{i}k_p(\omega_p)z}. \tag{A.4}$$

Considering the pulse behavior of the pump, the interaction in the non-linear crystal is very short in time then the limits of integration in Eq. (A.1) can be extended to infinity. Thus we have

$$\begin{aligned}\int_{t_0}^{t} dt' \hat{H}_I\left(t'\right) &= \chi^{(2)}\left[A^*\left(\overline{\omega}_p\right)\right]^2 \int_{-\infty}^{\infty} d\omega_o d\omega_e \hat{a}_o^{\dagger}\left(\omega_o\right)\hat{a}_e^{\dagger}\left(\omega_e\right) \times \\ & \int_{-\infty}^{\infty} dt' \widetilde{\alpha}\left(t'\right) \exp\left[i\left(\omega_o+\omega_e\right)t'\right] \times \\ & \int_{-L_c/2}^{L_c/2} dz \exp\left\{-i\left[k_o\left(\omega_o\right)+k_e\left(\omega_e\right)-k_p\left(\omega_p\right)\right]z\right\} + \text{H.c.}, \quad \text{(A.5)}\end{aligned}$$

where L_c is the length of the non-linear crystal and $\overline{\omega}_p$ the central frequency of the pump. Introducing the Fourier transform $\widetilde{\alpha}\left(t\right)$

$$\alpha\left(\omega\right) = \frac{1}{\sqrt{2\pi}} \int_{-\infty}^{\infty} dt \widetilde{\alpha}\left(t\right) e^{i\omega t},$$

and performing the time integration yields

$$\int_{t_0}^{t} dt' \hat{H}_I\left(t'\right) = \sqrt{2\pi}\chi^{(2)}\left[A^*\left(\overline{\omega}_p\right)\right]^2 \frac{L_c}{2} \int_{-\infty}^{\infty} d\omega_o d\omega_e \alpha\left(\omega_o+\omega_e\right) h\left(\omega_o,\omega_e\right) \hat{a}_o^{\dagger}\left(\omega_o\right)\hat{a}_e^{\dagger}\left(\omega_e\right), \tag{A.6}$$

where

$$h\left(\omega_o,\omega_e\right) = \text{sinc}\left\{\frac{L}{2}\left[k_o\left(\omega_o\right)+k_e\left(\omega_o\right)-k_p\left(\omega_p\right)\right]\right\}. \tag{A.7}$$

Since the interaction is weak, Eq. (A.1) can be approximated by taking the first two terms of the expansion of the interaction operator so that

$$\left|\psi\left(t\right)\right\rangle \simeq \left|\psi\left(t_0\right)\right\rangle + \frac{1}{i\hbar}\int_{t_0}^{t} dt' \hat{H}_I\left(t'\right)\left|\psi\left(t_0\right)\right\rangle.$$

Finally, dropping out the first term corresponding to the initial state — $\left|\psi\left(t_0\right)\right\rangle = \left|0\right\rangle$ for a spontaneous down-conversion — we obtain the two-photon state

$$\left|\psi\right\rangle = \int_{-\infty}^{\infty} d\omega_o \int_{-\infty}^{\infty} d\omega_e\ \phi\left(\omega_o,\omega_e\right)\hat{a}_o^{\dagger}\left(\omega_o\right)\hat{a}_e^{\dagger}\left(\omega_e\right)\left|0\right\rangle \tag{A.8}$$

where $\phi\left(\omega_o,\omega_e\right) = K\alpha\left(\omega_o+\omega_e\right)h\left(\omega_o,\omega_e\right)$ and $K = \frac{L_c}{2}\sqrt{2\pi}\chi^{(2)}\left[A^*\left(\overline{\omega}_p\right)\right]^2/\text{i}\hbar$.

Appendix **B**

Photon number correlation versus coincidence rate

In this Appendix, we establish a relation between the photon number correlation function $C_{ij} = \langle \hat{n}_i \hat{n}_j \rangle$ and the probability $P_2(i,j)$ to detect a photon in each of the modes i and j. Let us first assume $i \neq j$. Denote the state of the field *before* detection of photons by $|\psi\rangle$ and assume that $\{|\psi_n\rangle\}$ is an orthonormal basis composed of all possible, orthogonal states in which the field can be found *after* the two photons are detected. The probability density to detect a photon from the mode i at a time t_1 and a photon from the mode j afterwards, at a time $t_2 > t_1$, is then [40]

$$\begin{aligned} P_2(i,j;t_1,t_2) &= \sum_n |\langle \psi_n| \hat{a}_j(t_2)\hat{a}_i(t_1) |\psi\rangle|^2 \\ &= \sum_n \langle \psi| \hat{a}_i^\dagger(t_1)\hat{a}_j^\dagger(t_2) |\psi_n\rangle \; \langle \psi_n| \hat{a}_j(t_2)\hat{a}_i(t_1) |\psi\rangle \\ &= \langle \psi| \hat{a}_i^\dagger(t_1)\hat{a}_j^\dagger(t_2)\hat{a}_j(t_2)\hat{a}_i(t_1) |\psi\rangle \\ &= \langle : \hat{n}_i(t_1)\hat{n}_j(t_2) : \rangle, \end{aligned} \tag{B.1}$$

where the operator $\hat{a}_i(t)$ corresponds to the detection of a photon in the mode i at a time t [40] and we made use of the closure relation $\sum_n |\psi_n\rangle \langle\psi_n| = 1$; the colons $: \cdots :$ denote normal ordering of operators.

The probability that the two photons are detected at any times $t_1 < t_2$ during a sampling time ΔT is obtained by integrating Eq. (B.1) over times:

$$P_2^{t_1<t_2}(i,j) = \int_{-\Delta T/2}^{\Delta T/2} dt_1 \int_{t_1}^{\Delta T/2} dt_2 P_2(i,j;t_1,t_2). \tag{B.2}$$

Finally, the probability $P_2(i,j)$ of detecting the two photons in arbitrary order is equal to the sum of $P_2^{t_1<t_2}(i,j)$ given by Eq. (B.2) and $P_2^{t_1>t_2}(i,j)$ given by Eq. (B.2) with the integration over t_2 running from $-\Delta T/2$ to t_1:

$$\begin{aligned} P_2(i,j) &= P_2^{t_1<t_2}(i,j) + P_2^{t_1>t_2}(i,j) \\ &= \int_{-\Delta T/2}^{\Delta T/2} dt_1 \int_{t_1}^{\Delta T/2} dt_2 P_2(i,j;t_1,t_2) \\ &+ \int_{-\Delta T/2}^{\Delta T/2} dt_1 \int_{-\Delta T/2}^{t_1} dt_2 P_2(i,j;t_1,t_2) \\ &= \int_{-\Delta T/2}^{\Delta T/2} dt_1 \int_{-\Delta T/2}^{\Delta T/2} dt_2 P_2(i,j;t_1,t_2) \\ &= \langle : \hat{n}_i \hat{n}_j : \rangle = \langle \hat{n}_i \hat{n}_j \rangle. \end{aligned} \tag{B.3}$$

We therefore conclude that for $i \neq j$, $P_2(i,j)$ and C_{ij} are exactly equal.

Assume now that $i = j$. We have

$$P_2(i,i;t_1,t_2) = \langle : \hat{n}_i(t_1)\hat{n}_i(t_2) : \rangle \tag{B.4}$$

and

$$\begin{aligned} P_2(i,i) &= \int_{-\Delta T/2}^{\Delta T/2} dt_1 \int_{t_1}^{\Delta T/2} dt_2 P_2(i,i;t_1,t_2) \\ &= \frac{1}{2}\langle : \hat{n}_i^2 : \rangle = \frac{1}{2}\left(\langle \hat{n}_i^2 \rangle - \langle \hat{n}_i \rangle\right). \end{aligned} \tag{B.5}$$

The difference with respect to the case $i \neq j$ comes from the fact that the two photons now belong to the same mode and hence are indistinguishable. The two cases $t_1 < t_2$ and $t_1 > t_2$ cannot be distinguished anymore and there is only one [instead of two in Eq. (B.3)] contribution to P_2. Equations (B.3) and (B.5) lead to Eq. (3.61) of the main text.

The importance of the additional prefactor $\frac{1}{2}$ in Eq. (B.5) as compared to Eq. (B.3) can be understood if we consider two identical one-photon wave packets incident at the same input port of a symmetric beam splitter having two outgoing modes $i, j = 1$ (transmission) or 2 (reflection). Assume that the wave packets are well separated in time so that they interact with the beam splitter independently and each photon can be transmitted or reflected with a probability $P_1(1) = P_1(2) = \frac{1}{2}$. On the one hand, the calculation of joint probabilities readily yields $P_2(1,1) = P_2(2,2) = \frac{1}{4}$ and $P_2(1,2) = \frac{1}{2}$. On the other hand, we find $\langle : \hat{n}_1^2 : \rangle = \langle : \hat{n}_2^2 : \rangle = \langle : \hat{n}_1\hat{n}_2 : \rangle = \frac{1}{2}$. We thus see that although $P_2(1,2) = \langle : \hat{n}_1\hat{n}_2 : \rangle$, an additional factor $\frac{1}{2}$ is necessary to link $P_2(1,1)$ and $\langle : \hat{n}_1^2 : \rangle$: $P_2(1,1) = \frac{1}{2}\langle : \hat{n}_1^2 : \rangle$. The difference between the cases $i = j$ and $i \neq j$ comes from the fact that two different processes can lead to detecting one photon in the mode 1 and the other — in the mode 2: either the first photon is transmitted and the second is reflected or vice versa. The (equal) probabilities of these two processes add up to give $P_2(1,2)$. However, a unique process leads to finding both photons in the mode 1 (or 2): both photons should be transmitted (or reflected).

Appendix C

Average expectation values of one and two-photon observables in transmission

C.1 Calculation of normally ordered photon number correlation functions

In this Appendix, we derive Eq. (3.62) of the main text. Consider first the case of $\tau = 0$, i.e. the case when there is no time delay between the two photon beams. We have

$$\langle : \hat{n}_i \hat{n}_j : \rangle = \iint_{-\Delta T/2}^{\Delta T/2} dt_1 dt_2 \; \langle : \hat{n}_i(t) \hat{n}_j(t') : \rangle, \tag{C.1}$$

where

$$\begin{aligned} \langle : \hat{n}_i(t) \hat{n}_j(t') : \rangle &= \langle \psi | \, \hat{a}_i^\dagger (t) \, \hat{a}_j^\dagger \left(t'\right) \hat{a}_i (t) \, \hat{a}_j \left(t'\right) | \psi \rangle \\ &= |\hat{a}_i (t) \, \hat{a}_j \left(t'\right) | \psi \rangle \, |^2. \end{aligned} \tag{C.2}$$

Representing $\hat{a}_i(t)$ through its Fourier transform $\hat{a}_i(\omega)$, $\hat{a}_i(t) = (1/\sqrt{2\pi}) \int_{-\infty}^{+\infty} d\omega \hat{a}_i(\omega) e^{-i\omega t}$, we obtain

$$\hat{a}_j(t') \hat{a}_i(t) | \psi \rangle \;=\; \frac{1}{2\pi} \iint_{-\infty}^{\infty} d\omega d\omega' \; \mathrm{e}^{-i(\omega t + \omega' t')} \hat{a}_i(\omega) \hat{a}_j(\omega') | \psi \rangle \; . \tag{C.3}$$

Using the input-output relation (3.57), we now express $\hat{a}_j(\omega)$ and $\hat{a}_i(\omega)$ through $\hat{a}_\alpha(\omega)$ by considering only the transmission so that

$$\begin{aligned} \hat{a}_j(t') \hat{a}_i(t) | \psi \rangle \;&=\; \frac{1}{2\pi} \iint_{-\infty}^{\infty} d\omega d\omega' \; \mathrm{e}^{-i(\omega t + \omega' t')} \\ &\times \; \sum_{\alpha\beta}^{N} t_{i\alpha} (\omega) \, t_{j\beta} \left(\omega'\right) \hat{a}_\alpha(\omega) \hat{a}_\beta(\omega') | \psi \rangle \; . \end{aligned} \tag{C.4}$$

We now assume that the sampling time ΔT during which the photons are counted is much longer than all other time scales of the problem. This allows us to take the limit

$\Delta T \to \infty$ in Eq. (C.1) and to use the integral relation $\int_{-\infty}^{\infty} dt\ e^{-i(\omega-\Omega)t} = 2\pi\delta(\omega-\Omega)$. We then obtain

$$\begin{aligned}\langle : \hat{n}_i \hat{n}_j : \rangle &= \iint_{-\infty}^{\infty} d\omega d\omega' \sum_{\alpha\beta\alpha'\beta'}^{N} t_{i\alpha}(\omega)\, t_{j\beta}(\omega')\, t^*_{i\alpha'}(\omega)\, t^*_{j\beta'}(\omega') \\ &\times \langle \hat{a}^\dagger_{\beta'}(\omega')\hat{a}^\dagger_{\alpha'}(\omega)\hat{a}_\alpha(\omega)\hat{a}_\beta(\omega')\rangle, \end{aligned} \qquad \text{(C.5)}$$

which can be applied for incident light in any quantum state.

Before averaging over the realizations of disorder, let us consider Eq. (C.5) for different types of states. For an incident two-photon state with each photon in a different polarization state (α_1 or α_2), the expectation value in Eq. (C.5) leads to four possibilities corresponding to the following constraints on the set of indices $\{\alpha, \beta, \alpha', \beta'\}$:

$$\begin{cases} \delta_{\alpha\alpha_1}\delta_{\beta\alpha_2}\delta_{\alpha'\alpha_1}\delta_{\beta'\alpha_2} \\ \delta_{\alpha\alpha_2}\delta_{\beta\alpha_1}\delta_{\alpha'\alpha_1}\delta_{\beta'\alpha_2} \\ \delta_{\alpha\alpha_1}\delta_{\beta\alpha_2}\delta_{\alpha'\alpha_2}\delta_{\beta'\alpha_1} \\ \delta_{\alpha\alpha_2}\delta_{\beta\alpha_1}\delta_{\alpha'\alpha_2}\delta_{\beta'\alpha_1} \end{cases}$$

Then for the bi-Gaussian state, using the symmetry of the two-photon amplitude, we obtain

$$\begin{aligned}\langle : \hat{n}_i \hat{n}_j : \rangle &= \iint_{-\infty}^{\infty} d\omega d\omega' \left|\phi_{\text{Gauss}}(\omega,\omega')\right|^2 \qquad \text{(C.6)} \\ &\times \left(t_{i\alpha_1}(\omega)\, t^*_{i\alpha_1}(\omega)\, t_{j\alpha_2}(\omega')\, t^*_{j\alpha_2}(\omega') + t_{i\alpha_2}(\omega)\, t^*_{i\alpha_2}(\omega)\, t_{j\alpha_1}(\omega')\, t^*_{j\alpha_1}(\omega')\right. \\ &+ \left. t_{i\alpha_1}(\omega)\, t^*_{i\alpha_2}(\omega)\, t_{j\alpha_2}(\omega')\, t^*_{j\alpha_1}(\omega') + t_{i\alpha_2}(\omega)\, t^*_{i\alpha_1}(\omega)\, t_{j\alpha_1}(\omega')\, t^*_{j\alpha_2}(\omega')\right).\end{aligned}$$

When $\alpha_1 \neq \alpha_2$, whether $\phi_{\text{Gauss}}(\omega,\omega')$ is separable or not, it is not possible to express $\langle : \hat{n}_i \hat{n}_j : \rangle$ as a product of one-photon terms.

We now average Eq. (C.5) over the realizations of disorder. As discussed in Chapter 2, owing to the Gaussian statistics of the transmission coefficients, we have

$$\overline{t_{i\alpha}(\omega)\, t_{j\beta}(\omega')\, t^*_{i\alpha'}(\omega)\, t^*_{j\beta'}(\omega')} = \overline{T}^2_{\alpha b}\left(\delta_{\alpha\alpha'}\delta_{\beta\beta'} + \delta_{ij}\delta_{\alpha\beta'}\delta_{\beta\alpha'}\left|C(\omega-\omega')\right|^2\right). \qquad \text{(C.7)}$$

Then

$$\begin{aligned}\overline{\langle : \hat{n}_i \hat{n}_j : \rangle} &= \overline{T}_{\alpha b} \iint_{-\infty}^{\infty} d\omega d\omega' \sum_{\alpha\beta}^{N} \left(\langle \hat{a}^\dagger_\beta(\omega')\hat{a}^\dagger_\alpha(\omega)\hat{a}_\alpha(\omega)\hat{a}_\beta(\omega')\rangle\right. \\ &+ \left.\delta_{ij}\langle \hat{a}^\dagger_\alpha(\omega')\hat{a}^\dagger_\beta(\omega)\hat{a}_\alpha(\omega)\hat{a}_\beta(\omega')\rangle \left|C(\omega-\omega')\right|^2\right). \end{aligned} \qquad \text{(C.8)}$$

C.2 Derivation of $\overline{\langle \hat{n}_i \rangle \langle \hat{n}_j \rangle}$

In order to obtain the variance of the one-photon intensity used in Sec. 3.6.1, we derive in this appendix an expression of the observable $\overline{\langle \hat{n}_i \rangle \langle \hat{n}_j \rangle}$. Assuming that the sampling time is much larger than all other time scales of the problem, we have

$$\overline{\langle \hat{n}_i \rangle \langle \hat{n}_j \rangle} = \iint_{-\infty}^{\infty} dt dt' \times \overline{\left\langle \hat{a}^\dagger_i(t)\, \hat{a}_i(t)\right\rangle \left\langle \hat{a}^\dagger_j(t')\, \hat{a}_j(t')\right\rangle}. \qquad \text{(C.9)}$$

From the Fourier transform $\hat{a}_i(t) = (1/\sqrt{2\pi})\int_{-\infty}^{+\infty} d\omega \hat{a}_i(\omega)e^{-i\omega t}$ and the input-output relation (3.57), the average over realizations of disorder of the integrand of Eq. (C.9) is given by

$$\overline{\left\langle \hat{a}_i^\dagger(t)\,\hat{a}_i(t)\right\rangle\left\langle \hat{a}_j^\dagger(t')\,\hat{a}_j(t')\right\rangle} = \frac{1}{4\pi^2}\iiiint_{-\infty}^{\infty} d\omega d\omega' d\Omega d\Omega' \mathrm{e}^{-i((\omega-\Omega)t+(\omega'-\Omega')t')} \times$$
$$\times \sum_{\alpha\beta\alpha'\beta'}^{N} \overline{t_{i\alpha}(\omega)\,t_{j\alpha'}(\omega')\,t_{i\beta}^*(\Omega)\,t_{j\beta'}^*(\Omega')}\left\langle \hat{a}_\beta^\dagger(\Omega)\,\hat{a}_\alpha(\omega)\right\rangle\left\langle \hat{a}_{\beta'}^\dagger(\Omega')\,\hat{a}_{\alpha'}(\omega')\right\rangle. \quad \text{(C.10)}$$

The we insert Eq. (C.10) into Eq. (C.13) and perform the time integration using the relation $\int_{-\infty}^{\infty} dt e^{-i(\omega-\Omega)t} = 2\pi\delta(\omega-\Omega)$, so that

$$\begin{aligned}\overline{\langle\hat{n}_i\rangle\langle\hat{n}_j\rangle} &= \iint_{-\infty}^{\infty} d\omega d\omega' \sum_{\alpha\beta\alpha'\beta'}^{N} \overline{t_{i\alpha}(\omega)\,t_{j\alpha'}(\omega')\,t_{i\beta}^*(\omega)\,t_{j\beta'}^*(\omega')} \times \\ &\quad\times\left\langle \hat{a}_\beta^\dagger(\omega)\,\hat{a}_\alpha(\omega)\right\rangle\left\langle \hat{a}_{\beta'}^\dagger(\omega')\,\hat{a}_{\alpha'}(\omega')\right\rangle. \end{aligned} \quad \text{(C.11)}$$

We now average over the realizations of disorder as in Appendix C.1 and obtain

$$\begin{aligned}\overline{\langle\hat{n}_i\rangle\langle\hat{n}_j\rangle} &= \overline{T}_{\alpha b}^2\iint_{-\infty}^{\infty} d\omega d\omega' \sum_{\alpha\beta}^{N}\Big(\left\langle \hat{a}_\alpha^\dagger(\omega)\,\hat{a}_\alpha(\omega)\right\rangle\left\langle \hat{a}_\beta^\dagger(\omega')\,\hat{a}_\beta(\omega')\right\rangle \times \\ &\quad\times\delta_{ij}\left\langle \hat{a}_\beta^\dagger(\omega)\,\hat{a}_\alpha(\omega)\right\rangle\left\langle \hat{a}_\alpha^\dagger(\omega')\,\hat{a}_\beta(\omega')\right\rangle\left|C(\omega-\omega')\right|^2\Big). \end{aligned} \quad \text{(C.12)}$$

Taking $i = j$ leads to the second moment of intensity needed to obtain its variance. Note that Eq. (C.12) is valid for any quantum state.

C.3 Derivation of $\overline{\langle:\hat{n}_i\hat{n}_j:\rangle^2}$ for $i \neq j$

We derive here the second moment of $\langle:\hat{n}_i\hat{n}_j:\rangle$. Assuming large sampling time and $i \neq j$, $\overline{\langle:\hat{n}_i\hat{n}_j:\rangle^2}$ is given by

$$\begin{aligned}\overline{\langle:\hat{n}_i\hat{n}_j:\rangle^2} &= \iiiint_{-\infty}^{\infty} dt dt' dT dT' \times \\ &\quad\times \overline{\left\langle \hat{a}_i^\dagger(t)\,\hat{a}_j^\dagger(t')\,\hat{a}_j(t')\,\hat{a}_i(t)\right\rangle\left\langle \hat{a}_i^\dagger(T)\,\hat{a}_j^\dagger(T')\,\hat{a}_j(T')\,\hat{a}_i(T)\right\rangle}. \end{aligned} \quad \text{(C.13)}$$

Let us consider the first quantum expectation value appearing in the r.h.s of Eq. (C.13). Using the relation $\hat{a}_i(t) = (1/\sqrt{2\pi})\int_{-\infty}^{+\infty} d\omega\ \hat{a}_i(\omega)e^{-i\omega t}$ and the input-output relation (3.57) we have

$$\left\langle \hat{a}_i^\dagger(t)\,\hat{a}_j^\dagger(t')\,\hat{a}_j(t')\,\hat{a}_i(t)\right\rangle = \frac{1}{4\pi^2}\iiiint_{-\infty}^{\infty} d\omega d\omega' d\Omega d\Omega'\ \mathrm{e}^{-i((\omega-\Omega)t+(\omega'-\Omega')t')} \times$$
$$\times \sum_{\alpha\beta\alpha'\beta'}^{N} t_{i\alpha}(\omega)\,t_{j\alpha'}(\omega')\,t_{i\beta}^*(\Omega)\,t_{j\beta'}^*(\Omega')\left\langle \hat{a}_\beta^\dagger(\Omega)\,\hat{a}_{\beta'}^\dagger(\Omega')\,\hat{a}_{\alpha'}(\omega')\,\hat{a}_\alpha(\omega)\right\rangle, \quad \text{(C.14)}$$

and similarly for the second quantum expectation value in the r.h.s of Eq. (C.13). Inserting the product of two expectation values into Eq. (C.13) and using the relation $\int_{-\infty}^{\infty} dt\ e^{-i(\omega-\Omega)t} = 2\pi\delta(\omega-\Omega)$, the second moment becomes

$$\begin{aligned}\overline{\langle : \hat{n}_i \hat{n}_j : \rangle^2} \quad &= \quad \iiiint_{-\infty}^{\infty} d\omega d\omega' d\Omega d\Omega' \sum_{\alpha\beta\alpha'\beta'\gamma\delta\gamma'\delta'}^{N} \times \\ &\times \quad \overline{t_{i\alpha}(\omega)\, t_{j\alpha'}(\omega')\, t^*_{i\beta}(\omega)\, t^*_{j\beta'}(\omega')\, t_{i\gamma}(\Omega)\, t_{j\gamma'}(\Omega')\, t^*_{i\delta}(\Omega)\, t^*_{j\delta'}(\Omega')} \times \\ &\times \quad \left\langle \hat{a}^\dagger_\beta(\omega)\, \hat{a}^\dagger_{\beta'}(\omega')\, \hat{a}_{\alpha'}(\omega')\, \hat{a}_\alpha(\omega) \right\rangle \left\langle \hat{a}^\dagger_\delta(\Omega)\, \hat{a}^\dagger_{\delta'}(\Omega')\, \hat{a}_{\gamma'}(\Omega')\, \hat{a}_\gamma(\Omega) \right\rangle .\end{aligned} \tag{C.15}$$

Averaging over the realizations of disorder in Eq. (C.15) leads to 24 terms. However, because we are considering the case of $i \neq j$, only 4 terms are different from zero. Using the Gaussian statistics of the transmission coefficients we obtain

$$\begin{aligned}&\overline{t_{i\alpha}(\omega)\, t_{j\alpha'}(\omega')\, t^*_{i\beta}(\omega)\, t^*_{j\beta'}(\omega')\, t_{i\gamma}(\Omega)\, t_{j\gamma'}(\Omega')\, t^*_{i\delta}(\Omega)\, t^*_{j\delta'}(\Omega')} = \\ &= \overline{t_{i\alpha}(\omega)\, t_{i\gamma}(\Omega)\, t^*_{i\beta}(\omega)\, t^*_{i\delta}(\Omega)}\ \ \overline{t_{j\alpha'}(\omega')\, t_{j\gamma'}(\Omega')\, t^*_{j\beta'}(\omega')\, t^*_{j\delta'}(\Omega')} = \\ &= \overline{T}^4_{\alpha b} \left(\delta_{\alpha\beta}\delta_{\gamma\delta} + \delta_{\alpha\delta}\delta_{\gamma\beta} \left| C(\omega-\Omega) \right|^2 \right) \left(\delta_{\alpha'\beta'}\delta_{\gamma'\delta'} + \delta_{\alpha'\delta'}\delta_{\gamma'\beta'} \left| C(\omega'-\Omega') \right|^2 \right) .\end{aligned} \tag{C.16}$$

Substituting Eq. (C.16) into Eq. (C.15) yields

$$\begin{aligned}&\overline{\langle : \hat{n}_i \hat{n}_j : \rangle^2} = \overline{T}^4_{\alpha b} \iiiint_{-\infty}^{\infty} d\omega d\omega' d\Omega d\Omega' \sum_{\alpha\beta\alpha'\beta'}^{N} \times \\ &\times \Big(\left\langle \hat{a}^\dagger_\alpha(\omega)\, \hat{a}^\dagger_{\alpha'}(\omega')\, \hat{a}_{\alpha'}(\omega')\, \hat{a}_\alpha(\omega) \right\rangle \left\langle \hat{a}^\dagger_\beta(\Omega)\, \hat{a}^\dagger_{\beta'}(\Omega')\, \hat{a}_{\beta'}(\Omega')\, \hat{a}_\beta(\Omega) \right\rangle + \\ &+ \left\langle \hat{a}^\dagger_\beta(\omega)\, \hat{a}^\dagger_{\alpha'}(\omega')\, \hat{a}_{\alpha'}(\omega')\, \hat{a}_\alpha(\omega) \right\rangle \left\langle \hat{a}^\dagger_\alpha(\Omega)\, \hat{a}^\dagger_{\beta'}(\Omega')\, \hat{a}_{\beta'}(\Omega')\, \hat{a}_\beta(\Omega) \right\rangle \times \\ &\times \left| C(\omega-\Omega) \right|^2 + \\ &+ \left\langle \hat{a}^\dagger_\alpha(\omega)\, \hat{a}^\dagger_{\beta'}(\omega')\, \hat{a}_{\alpha'}(\omega')\, \hat{a}_\alpha(\omega) \right\rangle \left\langle \hat{a}^\dagger_\beta(\Omega)\, \hat{a}^\dagger_{\alpha'}(\Omega')\, \hat{a}_{\beta'}(\Omega')\, \hat{a}_\beta(\Omega) \right\rangle \times \\ &\times \left| C(\omega'-\Omega') \right|^2 + \\ &+ \left\langle \hat{a}^\dagger_\beta(\omega)\, \hat{a}^\dagger_{\beta'}(\omega')\, \hat{a}_{\alpha'}(\omega')\, \hat{a}_\alpha(\omega) \right\rangle \left\langle \hat{a}^\dagger_\alpha(\Omega)\, \hat{a}^\dagger_{\alpha'}(\Omega')\, \hat{a}_{\beta'}(\Omega')\, \hat{a}_\beta(\Omega) \right\rangle \times \\ &\times \left| C(\omega-\Omega) \right|^2 \left| C(\omega'-\Omega') \right|^2 \Big) .\end{aligned} \tag{C.17}$$

Eq. (C.17) is valid for all quantum states in transmission through a disordered medium. In Sec. 3.6.2, we apply it both for a bi-Gaussian two-photon state and for a two-mode coherent state.

Bibliography

[1] M. C. W. van Rossum and Th. M. Nieuwenhuizen, *Multiple scattering of classical waves: microscopy, mesoscopy, and diffusion*, Rev. Mod. Phys. **71**, 313 (1999).

[2] D. S. Wiersma, M. P. van Alba, and A. Lagendijk, *Random laser?*, Nature **373**, 203 (1995).

[3] P. W. Anderson, *Absence of Diffusion in Certain Random Lattices*, Phys. Rev. **109**, 1492 (1958).

[4] E. Akkermans and G. Montambaux. *Mesoscopic physics of electrons and photons.* Cambridge University Press, 2007.

[5] *Quantum optics*, Nat. Photonics **3**, 669 (2009).

[6] P. G. Kwiat, K. Mattle, H. Weinfurter, A. Zeilinger, A. V. Sergienko, and Y. Shih, *New high-intensity source of polarization-entangled photon pairs*, Phys. Rev. Lett. **75**, 4337 (1995).

[7] A. J. Shields, *Semiconductor quantum light sources*, Nat. Photonics **1**, 215 (2007).

[8] M. Nielsen and I. L. Chuang. *Quantum Computation and Quantum Information.* Cambridge University Press, 2000.

[9] C. W. J. Beenakker, *Thermal Radiation and Amplified Spontaneous Emission from a Random Medium*, Phys. Rev. Lett. **81**, 1829 (1998).

[10] C. W. J. Beenakker, J. W. F. Venderbos, and M. P. van Exter, *Two-photon speckle as a probe of multi-dimensional entanglement*, Phys. Rev. Lett. **102**, 193601 (2009).

[11] N. Cherroret and A. Buchleitner, *Entanglement and thouless times from coincidence measurements across disordered media*, Phys. Rev. A **83**, 033827 (2011).

[12] W. H. Peeters, J. J. D. Moerman, and M. P. van Exter, *Observation of two-photon speckle patterns*, Phys. Rev. Lett. **104**, 173601 (2010).

[13] M. P. van Exter, J. Woudenberg, H. Di Lorenzo Pires, and W. H. Peeters, *Bosonic, fermionic, and anyonic symmetry in two-photon random scattering*, Phys. Rev. A **85**, 033823 (2012).

[14] J. R. Ott, N. Mortensen, and P. Lodahl, *Quantum interference and entanglement induced by multiple scattering of light*, Phys. Rev. Lett. **105**, 090501 (2010).

[15] Y. Lahini, Y. Bromberg, D. N. Christodoulides, and Y. Silberberg, *Quantum Correlations in Two-Particle Anderson Localization*, Phys. Rev. Lett. **105**, 163905 (2010).

[16] V. A. Markel and J. C. Schotland, *Radiative transport for two-photon light*, Phys. Rev. A **90**, 033815 (2014).

[17] C. K. Hong, Z. Y. Ou, and L. Mandel, *Measurement of subpicosecond time intervals between two photons by interference*, Phys. Rev. Lett. **59**, 2044 (1987).

[18] R. Ghosh and L. Mandel, *Observation of nonclassical effects in the interference of two photons*, Phys. Rev. Lett. **59**, 1903 (1987).

[19] D. Bouwmeester, J.-W. Pan, K. Mattle, M. Eibl, H. Weinfurter, and A. Zeilinger, *Experimental quantum teleportation*, Nature **390**, 575 (1997).

[20] S. L. Braunstein and H. J. Kimble, *Teleportation of continuous quantum variables*, Phys. Rev. Lett. **80**, 869 (1998).

[21] C. Cohen-Tannoudji, J. Dupont-Roc, and G. Grynberg. *Photons and Atomes-Introduction to Quantum Electrodynamics*. Wiley Science Paper Series, New York, 1992.

[22] K. J. Blow, R. Loudon, S. J. D. Phoenix, and T. J. Shepherd, *Continuum fields in quantum optics*, Phys. Rev. A **42**, 4102 (1990).

[23] D. Kleppner, *Inhibited Spontaneous Emission*, Phys. Rev. Lett. **47**, 233 (1981).

[24] P. Goy, J. M. Raimond, M. Gross, and S. Haroche, *Observation of Cavity-Enhanced Single-Atom Spontaneous Emission*, Phys. Rev. Lett. **50**, 1903 (1983).

[25] B. J. Dalton, Stephen M. Barnett, and P. L. Knight, *Quasi mode theory of macroscopic canonical quantization in quantum optics and cavity quantum electrodynamics*, J. Mod. Opt. **46**, 1315 (1999).

[26] S. M. Dutra and G. Nienhuis, *Quantized mode of a leaky cavity*, Phys. Rev. A **62**, 063805 (2000).

[27] G. Hackenbroich, C. Viviescas, and F. Haake, *Field Quantization for Chaotic Resonators with Overlapping Modes*, Phys. Rev. Lett. **89**, 083902 (2002).

[28] C. Viviescas and G. Hackenbroich, *Field quantization for open optical cavities*, Phys. Rev. A **67**, 013805 (2003).

[29] N. Killoran, M. Cramer, and M. B. Plenio, *Extracting entanglement from identical particles*, Phys. Rev. Lett. **112**, 150501 (2014).

[30] R. J. Glauber, *The Quantum Theory of Optical Coherence*, Phys. Rev. **130**, 2529 (1963).

[31] R. J. Glauber, *Coherent and Incoherent States of the Radiation Field*, Phys. Rev. **131**, 2766 (1963).

[32] W.-M. Zhang, D. H. Feng, and R. Gilmore, *Coherent states: Theory and some applications*, Rev. Mod. Phys. **62**, 867 (1990).

[33] M. H. Rubin, D. N. Klyshko, Y. H. Shih, and A. V. Sergienko, *Theory of two-photon entanglement in type-II optical parametric down-conversion*, Phys. Rev. A **50**, 5122 (1994).

[34] D. V. Strekalov, A. V. Sergienko, D. N. Klyshko, and Y. H. Shih, *Observation of Two-Photon "Ghost" Interference and Diffraction*, Phys. Rev. Lett. **74**, 3600 (1995).

[35] T. S. Humble and W. P. Grice, *Spectral effects in quantum teleportation*, Phys. Rev. A **75**, 022307 (2007).

[36] A. V. Belinsky and D. N. Klyshko, *Two-photon wave packets*, Laser Physics **4**, 663 (1994).

[37] W. P. Grice and I. A. Walmsley, *Spectral information and distinguishability in type-II down-conversion with a broadband pump*, Phys. Rev. A **56**, 1627 (1997).

[38] Z-Y. Ou. *Multi-photon quantum interference*. Springer, 2007.

[39] S. P. Walborn, C. H. Monken, S. Pádua, and P. H. Souto Ribeiro, *Spatial correlations in parametric down-conversion*, Physics Reports **495**, 87 (2010).

[40] L. Mandel and E. Wolf. *Optical coherence and quantum optics*. Cambridge University Press, 1995.

[41] M. O. Scully and M. S. Zubairy. *Quantum Optics*. Cambridge University Press, 1997.

[42] E. C. G. Sudarshan, *Equivalence of Semiclassical and Quantum Mechanical Descriptions of Statistical Light Beams*, Phys. Rev. Lett. **10**, 277 (1963).

[43] M. V. Fedorov, M. A. Efremov, A. E. Kazakov, K. W. Chan, C. K. Law, and J. H. Eberly, *Spontaneous emission of a photon: Wave-packet structures and atom-photon entanglement*, Phys. Rev. A **72**, 032110 (2005).

[44] C. W. J. Beenakker, C. Emary, M. Kindermann, and J. L. van Velsen, *Proposal for Production and Detection of Entangled Electron-Hole Pairs in a Degenerate Electron Gas*, Phys. Rev. Lett. **91**, 147901 (2003).

[45] A. P. Hines, R. H. McKenzie, and G. J. Milburn, *Entanglement of two-mode Bose-Einstein condensates*, Phys. Rev. A **67**, 013609 (2003).

[46] D. Bruß, N. Datta, A. Ekert, L. C. Kwek, and C. Macchiavello, *Multipartite entanglement in quantum spin chains*, Phys. Rev. A **72**, 014301 (2005).

[47] H. Haffner, *Scalable multiparticle entanglement of trapped ions*, Nature **438**, 643–646 (2005).

[48] R. Horodecki, P. Horodecki, M. Horodecki, and K. Horodecki, *Quantum entanglement*, Rev. Mod. Phys. **81**, 865 (2009).

[49] G. Ghirardi and L. Marinatto, *General criterion for the entanglement of two indistinguishable particles*, Phys. Rev. A **70**, 012109 (2004).

[50] G. C. Ghirardi and L. Marinatto, *Identical particles and entanglement*, Opt. Spec. **99**, 386 (2005).

[51] A. Einstein, B. Podolsky, and N. Rosen, *Can Quantum-Mechanical Description of Physical Reality Be Considered Complete ?*, Phys. Rev. **47**, 777 (1925).

[52] J. Bell. *Speakable and Unspeakable in Quantum Machanics*. Cambridge University Press, 1987.

[53] J. S. Bell, *On the Einstein Podolsky Rosen paradox*, Physics **1**, 195 (1964).

[54] A. Aspect, P. Grangier, and G. Roger, *Experimental Tests of Realistic Local Theories via Bell's Theorem*, Phys. Rev. Lett. **47**, 460 (1981).

[55] R. F. Werner, *Quantum states with Einstein-Podolsky-Rosen correlations admitting a hidden-variable model*, Phys. Rev. A **40**, 4277 (1989).

[56] N. Gisin, *Bell's inequality holds for all non-product states*, Physics Letters A **154**, 201 (1991).

[57] A. Ekert and P.L. Knight, *Entangled quantum systems and the Schmidt decomposition*, American Journal of Physics **63**, 415 (1995).

[58] C. K. Law and J. H. Eberly, *Analysis and Interpretation of High Transverse Entanglement in Optical Parametric Down Conversion*, Phys. Rev. Lett. **92**, 127903 (2004).

[59] C. K. Law, I. A. Walmsley, and J. H. Eberly, *Continuous Frequency Entanglement: Effective Finite Hilbert Space and Entropy Control*, Phys. Rev. Lett. **84**, 5304 (2000).

[60] M. Horodecki, P. Horodecki, and R. Horodecki, *Limits for entanglement measures*, Phys. Rev. Lett. **84**, 2014 (2000).

[61] W. K. Wootters, *Entanglement of Formation of an Arbitrary State of Two Qubits*, Phys. Rev. Lett. **80**, 2245 (1998).

[62] T.-C. Wei and P. M. Goldbart, *Geometric measure of entanglement and applications to bipartite and multipartite quantum states*, Phys. Rev. A **68**, 042307 (2003).

[63] D. Spehner and M. Orszag, *Geometric quantum discord with Bures distance*, New Journal of Physics **15**, 103001 (2013).

[64] S. J. van Enk, *Entanglement of electromagnetic fields*, Phys. Rev. A **67**, 022303 (2003).

[65] M. S. Kim, W. Son, V. Bužek, and P. L. Knight, *Entanglement by a beam splitter: Nonclassicality as a prerequisite for entanglement*, Phys. Rev. A **65**, 032323 (2002).

[66] H. Cable and J. P. Dowling, *Efficient Generation of Large Number-Path Entanglement Using Only Linear Optics and Feed-Forward*, Phys. Rev. Lett. **99**, 163604 (2007).

[67] A. N. Boto, P. Kok, D. S. Abrams, S. L. Braunstein, C. P. Williams, and J. P. Dowling, *Quantum Interferometric Optical Lithography: Exploiting Entanglement to Beat the Diffraction Limit*, Phys. Rev. Lett. **85**, 2733 (2000).

[68] C. F. Wildfeuer, Austin P. Lund, and J. P. Dowling, *Strong violations of Bell-type inequalities for path-entangled number states*, Phys. Rev. A **76**, 052101 (2007).

[69] A. Peres. *Quantum theory: concepts and methods.* Springer, 1995.

[70] J. R. Gittings and A. J. Fisher, *Describing mixed spin-space entanglement of pure states of indistinguishable particles using an occupation-number basis*, Phys. Rev. A **66**, 032305 (2002).

[71] H. M. Wiseman and J. A. Vaccaro, *Entanglement of indistinguishable particles shared between two parties*, Phys. Rev. Lett. **91**, 097902 (2003).

[72] E. Schrödinger, *Discussion of Probability Relations between Separated Systems*, Mathematical Proceedings of the Cambridge Philosophical Society **31**, 555 (1935).

[73] D. Bohm and Y. Aharonov, *Discussion of Experimental Proof for the Paradox of Einstein, Rosen, and Podolsky*, Phys. Rev. **108**, 1070 (1957).

[74] S. Bose and D. Home, *Duality in Entanglement Enabling a Test of Quantum Indistinguishability Unaffected by Interactions*, Phys. Rev. Lett. **110**, 140404 (2013).

[75] M. Genovese and C. Novero, *Double entanglement and quantum cryptography*, Eur. Phys. J. D-At., Mol., Opt. Plas. Phys. **21**, 109 (2002).

[76] P. G. Kwiat, *Hyper-entangled states*, J. Mod. Opt. **44**, 2173 (1997).

[77] J. T. Barreiro, N. K. Langford, N. A. Peters, and P. G. Kwiat, *Generation of hyperentangled photon pairs*, Phys. Rev. Lett. **95**, 260501 (2005).

[78] W. Gao, C.-Y. Lu, X.-C. Yao, P. Xu, O. Gühne, A. Goebel, Y.-A. Chen, C.-Z. Peng, Z.-B. Chen, and J.-W. Pan, *Experimental demonstration of a hyper-entangled ten-qubit Schrödinger cat state*, Nat. Phys. **6**, 331 (2010).

[79] F. Benatti, R. Floreanini, and K. Titimbo, *Entanglement of identical particles*, Open Syst. Info. Dyn. **21** (2014).

[80] J. Schliemann, J. Ig. Cirac, M. Kuś, M. Lewenstein, and D. Loss, *Quantum correlations in two-fermion systems*, Phys. Rev. A **64**, 022303 (2001).

[81] K. Eckert, J. Schliemann, D. Bruß, and M. Lewenstein, *Quantum Correlations in Systems of Indistinguishable Particles*, Annals of Physics **299**, 88 (2002).

[82] B. C. Sanders, S. D. Bartlett, T. Rudolph, and P. L. Knight, *Photon-number superselection and the entangled coherent-state representation*, Phys. Rev. A **68**, 042329 (2003).

[83] S. D. Bartlett and H. M. Wiseman, *Entanglement constrained by superselection rules*, Phys. Rev. Lett. **91**, 097903 (2003).

[84] N. Schuch, F. Verstraete, and J. I. Cirac, *Quantum entanglement theory in the presence of superselection rules*, Phys. Rev. A **70**, 042310 (2004).

[85] Gerald G., Michael H., and Yaakov S. W., *Use of maximally entangled N-photon states for practical quantum interferometry*, J. Opt. Soc. Am. B **25**, 1336 (2008).

[86] F. Benatti, R. Floreanini, and U. Marzolino, *Sub-shot-noise quantum metrology with entangled identical particles*, Annals of Physics **325**, 924 (2010).

[87] A. P. Balachandran, T. R. Govindarajan, A. R. de Queiroz, and A. F. Reyes-Lega, *Entanglement and Particle Identity: A Unifying Approach*, Phys. Rev. Lett. **110**, 080503 (2013).

[88] P. Zanardi, *Virtual quantum subsystems*, Phys. Rev. Lett. **87**, 077901 (2001).

[89] S. M. Tan, D. F. Walls, and M. J. Collett, *Nonlocality of a single photon*, Phys. Rev. Lett. **66**, 252 (1991).

[90] D. M. Greenberger, M. A. Horne, and A. Zeilinger, *Nonlocality of a single photon?*, Phys. Rev. Lett. **75**, 2064 (1995).

[91] S. J. van Enk, *Single-particle entanglement*, Phys. Rev. A **72**, 064306 (2005).

[92] A. Drezet, *Comment on "Single-particle entanglement"*, Phys. Rev. A **74**, 026301 (2006).

[93] J. Dunningham and V. Vedral, *Nonlocality of a Single Particle*, Phys. Rev. Lett. **99**, 180404 (2007).

[94] H.-W. Lee and J. Kim, *Quantum teleportation and Bell's inequality using single-particle entanglement*, Phys. Rev. A **63**, 012305 (2000).

[95] B. Hessmo, P.l Usachev, H. Heydari, and G. Björk, *Experimental demonstration of single photon nonlocality*, Phys. Rev. Lett. **92**, 180401 (2004).

[96] M. Pawłowski and M. Czachor, *Degree of entanglement as a physically ill-posed problem: The case of entanglement with vacuum*, Phys. Rev. A **73**, 042111 (2006).

[97] S. J. Jones and H. M. Wiseman, *Nonlocality of a single photon: Paths to an Einstein-Podolsky-Rosen-steering experiment*, Phys. Rev. A **84**, 012110 (2011).

[98] G. Björk, A.e Laghaout, and U. L. Andersen, *Deterministic teleportation using single-photon entanglement as a resource*, Phys. Rev. A **85**, 022316 (2012).

[99] J. W. Goodman. *Speckle phenomena in optics: theory and applications*, volume 1. 2007.

[100] J. W. Goodman. Statistical properties of laser speckle patterns. In *Laser speckle and related phenomena*, pages 9–75. Springer, 1975.

[101] A. Kozmat and C. R. Christensent, *Effects of speckle on resolution*, JOSA **66**, 1257 (1976).

[102] D. J. Pine, D. A. Weitz, P. M. Chaikin, and E. Herbolzheimer, *Diffusing wave spectroscopy*, Phys. Rev. Lett. **60**, 1134 (1988).

[103] F. Scheffold, S. E. Skipetrov, S. Romer, and P. Schurtenberger, *Diffusing-wave spectroscopy of nonergodic media*, Phys. Rev. E **63**, 061404 (2001).

[104] A. Labeyrie, *Attainment of diffraction limited resolution in large telescopes by Fourier analysing speckle patterns in star images*, Astron. Astrophys **6**, 85 (1970).

[105] A. K. Dunn, H. Bolay, M. A. Moskowitz, and D. A. Boas, *Dynamic imaging of cerebral blood flow using laser speckle*, J. Cer. Blood Flow & Meta. **21**, 195 (2001).

[106] P. Zakharov, A. C. Völker, M. T. Wyss, F. Haiss, N. Calcinaghi, C. Zunzunegui, A. Buck, F. Scheffold, and B. Weber, *Dynamic laser speckle imaging of cerebral blood flow*, Opt. Exp. **17**, 13904 (2009).

[107] E. P. Wigner. *On the statistical distribution of the widths and spacings of nuclear resonance levels*, volume 47. 1951.

[108] C. W. J. Beenakker, *Random-matrix theory of quantum transport*, Rev. Mod. Phys. **69**, 731 (1997).

[109] A. M. Tulino ans S. Verdu. *Random Matrix Theory and Wireless Communications.* Now Publishers, Delft, 2004.

[110] L. Laloux, P. Cizeau, M. Potters, and J.-P. Bouchaud, *Random matrix theory and financial correlations*, Int. J. Theor. App. Fin. **3**, 391 (2000).

[111] A. D. Stone, P. A. Mello, K. A. Muttalib, J. L. Pichard, and B. L. Al'tshuler. *Mesoscopic phenomena in solids.* North-Holland, Amsterdam, 1991.

[112] A. V. Andreev, O. Agam, B. D. Simons, and B. L. Altshuler, *Quantum chaos, irreversible classical dynamics, and random matrix theory*, Phys. Rev. Lett. **76**, 3947 (1996).

[113] A. Aubry and A. Derode, *Random matrix theory applied to acoustic backscattering and imaging in complex media*, Phys. Rev. Lett. **102**, 084301 (2009).

[114] O. Bohigas, M.-J. Giannoni, and C. Schmit, *Characterization of chaotic quantum spectra and universality of level fluctuation laws*, Phys. Rev. Lett. **52**, 1 (1984).

[115] H. U. Baranger and P. A. Mello, *Mesoscopic transport through chaotic cavities: A random S-matrix theory approach*, Phys. Rev. Lett. **73**, 142 (1994).

[116] A. Goetschy. *Light in disordered atomic systems: Euclidean matrix theory of random lasing.* (PhD Thesis), 2011.

[117] I. M. Johnstone, *On the distribution of the largest eigenvalue in principal components analysis*, Annals Stat. pages 295–327 (2001).

[118] C. Nadal, S. N. Majumdar, and M. Vergassola, *Phase transitions in the distribution of bipartite entanglement of a random pure state*, Phys. Rev. Lett. **104**, 110501 (2010).

[119] V. A. Marchenko and L. A. Pastur, *Distribution of eigenvalues for some sets of random matrices*, Mat. Sb. (N.S.) **72**, 507 (1967).

[120] O. N. Dorokhov, *Transmission coefficient and the localization length of an electron in N bound disordered chains*, JETP Lett. **36**, 318 (1982).

[121] P. A. Mello, P. Pereyra, and N. Kumar, *Macroscopic approach to multichannel disordered conductors*, Annals Phys. **181**, 290 (1988).

[122] V. A. Gopar, K. A. Muttalib, and P. Wölfle, *Conductance distribution in disordered quantum wires: Crossover between the metallic and insulating regimes*, Phys. Rev. B **66**, 174204 (2002).

[123] C. W. J. Beenakker and B. Rejaei, *Nonlogarithmic repulsion of transmission eigenvalues in a disordered wire*, Phys. Rev. Lett. **71**, 3689 (1993).

[124] C. W. J. Beenakker and B. Rajaei, *Exact solution for the distribution of transmission eigenvalues in a disordered wire and comparison with random-matrix theory*, Phys. Rev. B **49**, 7499 (1994).

[125] L. S. Froufe-Pérez, P. García-Mochales, P. A. Serena, P. A. Mello, and J. J. Sáenz, *Conductance distributions in quasi-one-dimensional disordered wires*, Phys. Rev. Lett. **89**, 246403 (2002).

[126] F. G. Tricomi. *Integral equations*, volume 5. Courier Dover Publications, 1985.

[127] T. A. Brody, J. Flores, J. B. French, P. A. Mello, A. Pandey, and S. S. M. Wong, *Random-matrix physics: spectrum and strength fluctuations*, Rev. Mod. Phys. **53**, 385 (1981).

[128] K. A. Muttalib, J.-L. Pichard, and A. D. Stone, *Random-Matrix Theory and universal statistics for disordered quantum conductors*, Phys. Rev. Lett. **59**, 2475 (1987).

[129] Y. V. Nazarov, *Limits of universality in disordered conductors*, Phys. Rev. Lett. **73**, 134 (1994).

[130] R. Landauer, *Spatial Variation of Currents and Fields Due to Localized Scatterers in Metallic Conduction*, IBM J. Res. Dev. **1**, 223 (1957).

[131] E. Kogan and M. Kaveh, *Random-matrix-theory approach to the intensity distributions of waves propagating in a random medium*, Phys. Rev. B **52**, R3813 (1995).

[132] E. Kogan, M. Kaveh, R. Baumgartner, and R. Berkovits, *Statistics of waves propagating in a random medium*, Phys. Rev. B **48**, 9404 (1993).

[133] S. A. Van Langen, P. W. Brouwer, and C. W. J. Beenakker, *Nonperturbative calculation of the probability distribution of plane-wave transmission through a disordered waveguide*, Phys. Rev. E **53**, R1344 (1996).

[134] A. Goetschy and A. D. Stone, *Filtering Random Matrices: The Effect of Incomplete Channel Control in Multiple Scattering*, Phys. Rev. Lett. **111**, 063901 (2013).

[135] S. M. Popoff, G. Lerosey, R. Carminati, M. Fink, A. C. Boccara, and S. Gigan, *Measuring the transmission matrix in optics: an approach to the study and control of light propagation in disordered media*, Phys. Rev. Lett. **104**, 100601 (2010).

[136] M. Patra and C. W. J. Beenakker, *Propagation of squeezed radiation through amplifying or absorbing random media*, Phys. Rev. A **61**, 063805 (2000).

[137] J. Tworzydło and C. W. J Beenakker, *Quantum optical communication rates through an amplifying random medium*, Phys. Rev. Lett. **89**, 043902 (2002).

[138] P. Lodhal, A. P. Mosk, and A. Lagendijk, *Spatial quantum correlations in multiple scattered light*, Phys. Rev. Lett. **95**, 173901 (2005).

[139] P. Lodahl and A. Lagendijk. Transport of quantum noise through random media, 2005.

[140] S. Balog, P. Zakharov, F. Scheffold, and S. E. Skipetrov, *Photocount statistics in mesoscopic optics*, Phys. Rev. Lett. **97**, 103901 (2006).

[141] S. E. Skipetrov, *Quantum theory of dynamic multiple light scattering in fluctuating disordered media*, Phys. Rev. A **75**, 053808 (2007).

[142] S. Smolka, A. Huck, U. L. Andersen, A. Lagendijk, and P. Lodahl, *Observation of spatial quantum correlations induced by multiple scattering of nonclassical light*, Phys. Rev. Lett. **102**, 193901 (2009).

[143] S. Smolka, O. L. Muskens, A. Lagendijk, and P. Lodahl, *Angle-resolved photon-coincidence measurements in a multiple-scattering medium*, Phys. Rev. A **83**, 043819 (2011).

[144] H. Di Lorenzo Pires, J. Woudenberg, and M. P. van Exter, *Statistical properties of two-photon speckles*, Phys. Rev. A **85**, 033807 (2012).

[145] G. Jaeger, M. A. Horne, and A. Shimony, *Complementarity of one-particle and two-particle interference*, Phys. Rev. A **48**, 1023 (1993).

[146] A. F. Abouraddy, M. B. Nasr, B. E. A. Saleh, A. V. Sergienko, and M. C. Teich, *Demonstration of the complementarity of one- and two-photon interference*, Phys. Rev. A **63**, 063803 (2001).

[147] S. L. Braunstein and P. Van Loock, *Quantum information with continuous variables*, Rev. Mod. Phys. **77**, 513 (2005).

[148] O. Kuzucu, M. Fiorentino, M. A. Albota, F. N. C. Wong, and F. X. Kärtner, *Two-Photon Coincident-Frequency Entanglement via Extended Phase Matching*, Phys. Rev. Lett. **94**, 083601 (2005).

[149] V. Giovannetti, L. Maccone, J. H. Shapiro, and F. N. C. Wong, *Generating Entangled Two-Photon States with Coincident Frequencies*, Phys. Rev. Lett. **88**, 183602 (2002).

[150] M. V. Fedorov, Yu M. Mikhailova, and P. A. Volkov, *Gaussian modelling and Schmidt modes of SPDC biphoton states*, J. Phys. B: At. Mol. Op. Phys. **42**, 175503 (2009).

[151] S. Mancini, V. Giovannetti, D. Vitali, and P. Tombesi, *Entangling macroscopic oscillators exploiting radiation pressure*, Phys. Rev. Lett. **88**, 120401 (2002).

[152] W. P. Grice, A. B. U'ren, and I. A. Walmsley, *Eliminating frequency and space-time correlations in multiphoton states*, Phys. Rev. A **64**, 063815 (2001).

[153] T. E. Keller and M. H. Rubin, *Theory of two-photon entanglement for spontaneous parametric down-conversion driven by a narrow pump pulse*, Phys. Rev. A **56**, 1534 (1997).

[154] R. S. Bennink, S. J. Bentley, R. W. Boyd, and J. C. Howell, *Quantum and classical coincidence imaging*, Phys. Rev. Lett. **92**, 033601 (2004).

[155] J. C. Howell, R. S. Bennink, S. J. Bentley, and R. W. Boyd, *Realization of the Einstein-Podolsky-Rosen paradox using momentum-and position-entangled photons from spontaneous parametric down conversion*, Phys. Rev. Lett. **92**, 210403 (2004).

[156] M. D'Angelo, Y. Kim, S. P. Kulik, and Y. Shih, *Identifying entanglement using quantum ghost interference and imaging*, Phys. Rev. Lett. **92**, 233601 (2004).

[157] P. Sebbah, R. Pnini, and A. Z. Genack, *Field and intensity correlation in random media*, Phys. Rev. E **62**, 7348 (2000).

[158] F. Boitier, A. Godard, E. Rosencher, and C. Fabre, *Measuring photon bunching at ultrashort timescale by two-photon absorption in semiconductors*, Nat. Phys. **5**, 267 (2009).

[159] B. Shapiro, *Large Intensity Fluctuations for Wave Propagation in Random Media*, Phys. Rev. Lett. **57**, 2168 (1986).

[160] D. Branning, W. P. Grice, R. Erdmann, and I. A. Walmsley, *Engineering the indistinguishability and entanglement of two photons*, Phys. Rev. Lett. **83**, 955 (1999).

[161] D. N. Klyshko, *The nonclassical light*, Physics-Uspekhi **39**, 573 (1996).

[162] D. N. Klyshko, *Observable signs of nonclassical light*, Phys. Lett. A **213**, 7 (1996).

[163] E. Lubkin, *Entropy of an n system from its correlation with a k reservoir*, N. Math. Phys. **19**, 1028 (1978).

[164] D. N. Page, *Average entropy of a subsystem*, Phys. Rev. Lett. **71**, 1291 (1993).

[165] P. Facchi, U. Marzolino, G. Parisi, S. Pascazio, and A. Scardicchio, *Phase Transitions of Bipartite Entanglement*, Phys. Rev. Lett. **101**, 050502 (2008).

[166] P. Vivo, *Entangled random pure states with orthogonal symmetry: exact results*, J. Phys. A: Math. Theor. **43**, 405206 (2010).

[167] S. Kumar and A. Pandey, *Entanglement in random pure states: spectral density and average von Neumann entropy*, J. Phys. A: Math. Theor. **44**, 445301 (2011).

[168] H. Di Lorenzo Pires, H. C. B. Florijn, and M. P. van Exter, *Measurement of the Spiral Spectrum of Entangled Two-Photon States*, Phys. Rev. Lett. **104**, 020505 (2010).

[169] H. Di Lorenzo Pires, C. H. Monken, and M. P. van Exter, *Direct measurement of transverse-mode entanglement in two-photon states*, Phys. Rev. A **80**, 022307 (2009).

[170] D. V. Voiculescu, K. J. Dykema, and A. Nica. *Free random variables.* American Mathematical Society, 1992.

[171] A. Zee, *Law of addition in random matrix theory*, Nucl. Phys. B **474**, 726 (1996).

[172] A. Pena, A. Girschik, F. Libisch, S. Rotter, and A. A. Chabanov, *The single-channel regime of transport through random media*, Nat. Com. **5** (2014).